The role of paleogeography in Asian monsoon evolution: a review and new insights from climate modelling

D. Tardif, A.-C. Sarr, F. Fluteau, W. Banfield, C. T. Bolton, Y. Donnadieu, Guillaume Dupont-Nivet, M. Kaya, J.-B. Ladant, G. Le Hir, et al.

Asynchronous apparition of the Asian monsoons features since the late Eocene and associated paleogeographic and climatic drivers

D. Tardif[1,2], A-C. Sarr[1], F. Fluteau[2], W. Banfield[1], C. Bolton[1], Y. Donnadieu[1], G. Dupont-Nivet[3,4], M. Kaya[1], J-B. Ladant[5], G. Le Hir[2], A. Licht[1], Q. Pillot[1], F. Poblete[6], P. Sepulchre[5], A. Toumoulin[1]

[1]Aix Marseille Univ, CNRS, IRD, INRAE, CEREGE, Aix-en-Provence, France
[2]Université Paris Cité, Institut de physique du globe de Paris, CNRS, F-75005 Paris, France
[3]Géosciences Rennes, UMR CNRS 6118, Univ Rennes, Rennes, France
[4]Institute of Geosciences, Potsdam University, Potsdam, Germany
[5]Laboratoire des Sciences du Climat et de l'Environnement, LSCE/IPSL, CEA-CNRS-UVSQ, Université Paris-Saclay, 91191 Gif-sur-Yvette, France
[6]Departamento de Geología, Facultad de Ciencias Físicas y Matematicas, Universidad de Chile, Chile

Key Points:

- Asian monsoons modern characteristics appeared sequentially during the Cenozoic, driven by distinct paleogeographic and climatic forcings.
- Model results depict seasonal precipitation in parts of Southern and Eastern Asia since the Paleogene.
- The Paratethys Sea retreat and the Arabian Platform emergence, by greatly increasing continentality, are instrumental for the development of surface temperature gradients between Asia and the Indian Ocean which reinforces the advection of moist air towards Asia in summer.
- Iran-Zagros and East African landforms contribute to channel and enhance the Somali Jet that brings moisture to Southeastern Asia in summer, while the Himalayan-Tibetan plateau uplift induces heavy orographic precipitation.
- Mongolian landforms uplift is the main driver for the Siberian high pressure settlement in winter. It results in a broad reinforcement of East Asian Monsoon precipitation seasonality, as it strongly reduces winter precipitation. It also induces aridification of current Gobi desert region.
- Tian Shan and Pamir uplifts, by intercepting and deviating westerly moisture flux, concur to force the summer northern Jet Stream migration in Tibet and Eastern China. This triggers local orographic precipitation, increased winter precipitation in India (weaker South Asian Monsoon), and increased summer precipitation in Northeastern China (stronger East Asian monsoon). It enhances global aridification of Gobi, Taklamakan and Northeastern Tibet regions.

Corresponding author: Delphine Tardif, `delphine.tardif@hotmail.fr`

Corresponding author: Anta-Clarisse Sarr, `anta.clarisse.sarr@gmail.com`

Abstract

Modern Asian monsoons are triggered by complex interactions between the atmosphere, Asian and African orography and the surrounding oceans, resulting in a highly seasonal climate characterized by typical regional features. Although long considered as a Neogene phenomenon, recent evidence for monsoon-like seasonality as early as in the Paleogene Greenhouse, has come to challenge this paradigm. The occurrence of monsoons in a climatic and paleogeographic context very different from the present-day question our understanding of the drivers underpinning this peculiar atmospheric phenomenon, in particular with regards to its dependence to paleogeography. In this study, we take advantage of the wealth of new studies to tentatively draw an up-to-date portrait of the Asian tectonic and paleoenvironmental evolution through the Cenozoic and of the questions that remain to be answered. We then simulate the evolution of the Asian monsoon subsystems by investigating seasonal trends of 20 paleoclimate simulations spanning the late Eocene to latest Miocene (40-6 Ma). At odds with the traditional view of a monsoonal evolution driven mainly by the Himalayan-Tibetan uplift, this study confirms the findings of previous works stating the importance of peripheral landforms on the different Asian monsoons subsystems. Eastern African and Anatolian-Iranian topography, as well as the Arabian Peninsula emergence all concur to shape the South Asian summer Monsoon. Additionally, we suggest that continentality, together with Mongolia, Tian Shan and Pamir orographic evolution, and pCO_2 decrease, played important parts in the settlement of the East Asian Monsoon and in the aridification of inland Asia.

1 Introduction

The South and East Asian monsoons are highly seasonal climatic phenomenons, that today conditions the livelihood of billions of people. During summer, moisture-loaded winds blowing from the Indian Ocean (Fig. 1) trigger important nutrients-rich upwellings and lead to heavy precipitation over Southeastern Asia, allowing for widespread agriculture and fisheries. In winter, the reversal in wind direction induces advection of cold, dry and dust-loaded air masses from Siberia over Eastern and Southern Asia (Fig. 1). The spectacular extension and intensity of the Asian monsoons, combined to the highly dynamic tectonic context of the region, have triggered a lot of interest from the scientific community, in order to understand potential links between orography, land-sea distribution, global climate and the monsoon.

While monsoons have long been viewed as an atmospheric phenomenon intimately intertwined with the Himalayan-Tibetan plateau uplift history (Molnar et al., 1993; Zhisheng et al., 2001; Tada et al., 2016; X. Liu, Guo, et al., 2015) and rooted in the Neogene, first with records of strong upwellings initiating in the Arabian Sea at ∼8 Ma (Kroon et al., 1991), then with evidence for massive dust deposition in the Chinese Loess Plateau since ∼22 Ma (Guo et al., 2002), a wealth of recent studies has come to challenge this paradigm. Indeed, aeolian dust deposits in the Xining basin (northeastern China, see Fig. 1 for localities mentioned in the text), as well as paleoflora and isotopic measurement in fossils indicating a seasonal climate in Myanmar (Licht et al., 2014) and in the Yunnan region (South China) (Sorrel et al., 2017; Fang et al., 2021; Zheng et al., 2022) have been interpreted as pieces of evidence for an active monsoon as early as in the late Eocene. Proposing a monsoonal onset in the Paleogene, in a warmer, ice-free climate, during the early stage of the Tibetan plateau uplift and with much lower continentality due to higher sea level and to the presence of the Paratethys Sea in the west (see the late Eocene paleogeography in Fig. 3a), radically questions our understanding of the forcings of the monsoons.

Climate modeling provides a unique opportunity to understand the part played by each potential forcing on the resulting climate. Overall, such studies, and independently of the model used (complexity, resolution) or the simulation protocol (i.e., derived from modern geography or with realistic paleogeography), have tended to highlight that paleogeography

out-compete global pCO_2 variations or far-field ice-sheets effects when it comes to the SAM and EAM settlement and intensification over multi-million years time scales (Farnsworth et al., 2019; J.-Y. Lee et al., 2015; Zoura et al., 2019; Roe et al., 2016; Thomson et al., 2021). In a second time, sensitivity experiments of increasing complexity and precision, have helped disentangle the effect of the Himalaya-Tibet (and its sub units) uplift from that of peripheral landforms uplifts, such as the Tian Shan ranges, the Iranian-Anatolian orogen, eastern African domes, Mongolia landforms (H. Tang et al., 2013; Acosta & Huber, 2020; R. Zhang et al., 2017), and from the effect of land-sea distribution changes (Fluteau et al., 1999; Z. Zhang et al., 2007). While modeling studies provide mechanistic basis to apprehend potential leverages for monsoon and aridity modulation, it remains paramount to dispose of robust constraints on the paleogeography and paleoclimate evolution, and on the relative chronology of these events. The past decades have been rich in both modeling and field studies, for example with marine cores that were extended back to the late Paleogene (W. Ding et al., 2021; S. Ali et al., 2021; Betzler et al., 2016; Beasley et al., 2021), and increased coverage in well-dated paleoclimate indicators, which offer new constraints on Cenozoic tectonic and paleoclimate.

In this contribution, and building upon previous work (Sarr et al., 2022; Tardif et al., 2020; Barbolini et al., 2020), we aim at providing a comprehensive picture of large-scale wind circulation, precipitation seasonality and aridity evolution in continental Asia from the late Eocene to the late Miocene, using realistic paleoclimate simulations. In the following parts, we first describe in more depth the Asian monsoon subsystems characteristics (section 2), and propose an up-to-date overview of the Asian monsoon history as understood through proxy and models studies, and of remaining outstanding issues (section 3, Fig. 2). The main paleogeographic events that affected the regions surrounding the Indian Ocean together with continental Asia during the Cenozoic are presented (section 4), along with the past continental configurations that have been used (Fig.3). Other boundary conditions and simulations spin-up are then introduced, as well as criteria retained to track the Asian monsoons evolution throughout the different simulations (section 5). Our results are then presented and discussed in the light of actual knowledge.

2 Modern Asian Monsoon subsystems characteristics

The Asian monsoon is subdivided into two regional subsystems: the South Asian Monsoon, spreading roughly from Pakistan to Myanmar, and the East Asian Monsoon, from Myanmar to Japan. We hereafter refer to them as SAM and EAM respectively, SASM and EASM are used for the summer monsoon season while SAWM and EAWM refer to the winter monsoon season. These regional monsoons present specific climatic characteristics and have long been studied by distinct communities, although regions situated in the Southeastern Asian Peninsula can present mixed attributes of both subsystems and may be referred to as "transition area" in the literature (R. Spicer et al., 2017).

2.1 Summer season

The SASM is associated with intense orographic precipitation over the Himalayan foothills as well as over smaller mountains ranges like the Ghats in western India and the Indo-Burman Ranges in Myanmar (Fig. SI 14 a,b). In these regions, summer precipitation account for nearly 80% of the total annual precipitation and are responsible for massive fresh-water discharge in the Bay of Bengal, *via* the Ganga, Brahmaputra and Ayeyarwady Rivers and in the Arabian Sea *via* the Indus River. Precipitation is supplied by moisture-loaded air masses from the Inter Tropical Convergence Zone (ITCZ), which is steered towards the Asian continent during summer, as a consequence of the wide low pressure belt develop-ing from Arabia to eastern China (Fig. SI 14 d). This typical pressure pattern is driven by the establishment of a surface temperature gradient between the Indian Ocean and the overheated Asian continent and the Arabian Peninsula (up to 40°C, Fig. SI 14 d).

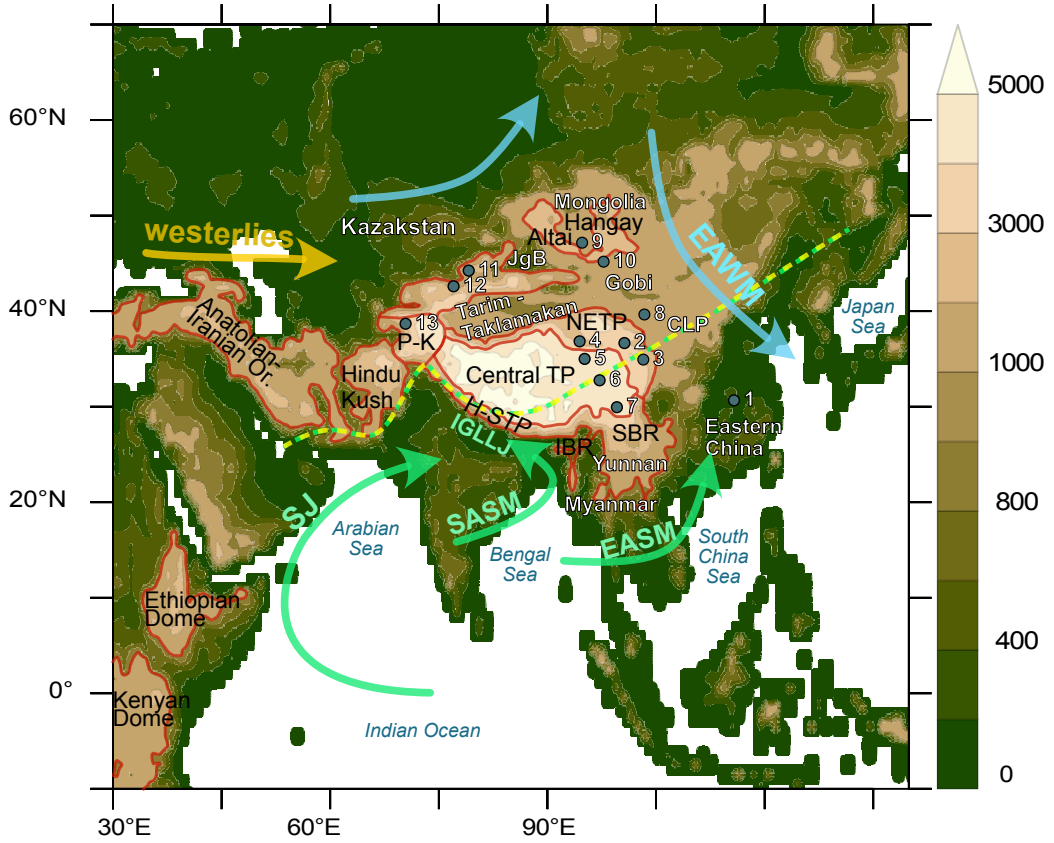

Figure 1. Modern geography and topography (in m), with main seasonal winds: Westerlies (yellow arrow), East Asian Winter monsoon (blue arrow) and Summer monsoons (green arrows) ; Somali Jet (SJ), Indo-Gangetic-Low Level Jet (IGLLJ). Dotted green/yellow line indicate the modern limit between the westerlies and the monsoonal regions. Main landforms units (in black) and main geographical regions (in white) mentioned in the text, with the following abbreviations: H-STP - Himalayas and Southern Tibetan Plateau, NETP - Northeastern Tibetan Plateau, IBR - Indo Burman Ranges, SBR - Sino Burman Ranges, ML - Mongolian Landforms, CLP - Chinese Loess Plateau, JgB - Junggar Basin. Smaller basins and localities mentionned in the text are numbered as follow: (1) Jianghan B., (2) Xining B., (3) Linzhou B., (4) Qaidam, (5) Hoh Xil B., (6) Nangqian B., (7) Markam B., (8) Bayanhot B., (9) Valley of Lakes, (10) Taatsin Gol, (11) Ili B., (12) Issyk Kul B., (13) Tajik B.

Characteristic low-level wind patterns are associated with the SASM, represented by the Findlater Jet (Findlater, 1969) (or Somali Jet (H.-H. Wei & Bordoni, 2016)), which crosses the equator alongshore East Africa and blows towards the Indian subcontinent (Fig. SI 14 d). This powerful trans-equatorial jet triggers strong surface oceanic currents, flowing up the East African and Arabian coasts, then circumventing India from West to East. These currents generate strong upwellings in the Arabian Sea and the Bay of Bengal (Schott & McCreary, 2001), favoring broad phytoplankton productivity blooms from July to September (Lévy et al., 2007). Over the Bay of Bengal, the Somali Jet splits into two distinct branches (Fig. SI 14 d), one pursuing its northeastern flow towards southeastern and eastern Asia (from Myanmar to China), and the Indo-Gangetic Low Level Jet (Acosta & Huber, 2017), bifurcating towards northwestern India and the Himalayan foothills.

The EASM is characterized by a band of strong convective precipitation stretching from Myanmar to Japan along eastern China, also called the Meiyu-Bayu front. This high-precipitation zone is fed by warm moist air, advected from the Bay of Bengal and nearby Indo-Pacific Warm Pool (IPWP) (Fig. SI 14 d). The Meiyu-Bayu front results from the ascension of these moist winds over the Jet Stream in the subtropics (Kong et al., 2017; Molnar et al., 2010; Sampe & Xie, 2010). The progressive northward migration of the front during spring and early summer is likely influenced by the seasonal displacement of the Jet Stream relative to the Tibetan Plateau (TP): it is located south of the TP at ∼25°N in winter, and progressively migrates to its northern edge in summer. The EASM, observed up to ∼40°N, is an extra-tropical phenomenon, and is therefore regularly questioned as being a "real" monsoon (Molnar et al., 2010; R. A. Spicer et al., 2016).

2.2 Winter season

Boreal winter is marked by a generally dry climate over most of the Asian continent. North of ∼20°N, Eastern Asia is swept by northwestern winds bringing cold air and dusts from inland Asia, while south of ∼20°N, northeastern winds carry moisture from the Pacific Warm Pool, leading to monsoonal precipitation over Indonesia and northern Australia (Fig. SI 14 f). The Indian subcontinent experiences a more complex wind pattern, as the westerly winds in the North are channeled by the Zagros and Himalaya-Tibetan orography and then deviated into northeasterly winds over the Arabian Sea, towards the eastern African coast (Fig. SI 14 f). These peculiar winds lead to the formation of upwellings in the Bay of Bengal and the Arabian Sea, allowing phytoplankton productivity blooms to occur in winter as well (Lévy et al., 2007). This typical winter wind circulation (Fig. SI 14 f) is controlled by the pressure gradients forming between the Siberian High and the surrounding Aleutian Low (over the North Pacific) to the East and the low pressure center settled over the Maritime Continent to the South (L. Wang & Chen, 2014). The spectacular extent and strength of the Siberian High in boreal winter is a consequence of a strong radiative cooling of the lower troposphere over snow-covered Asia (Jeong et al., 2011; Cohen et al., 2001; Jhun & Lee, 2004).

2.3 Summary: what traces leave the monsoons ?

Asian climate is under the crossed influence of the dry East Asian winter monsoon and of three moisture sources, the westerlies and the East and South Asian summer monsoon (Fig. 1). Nowadays, the boundary between regions receiving most of their annual precipitation via the monsoons or via the westerlies is clearly bounded by the Himalayas in the South, while it fluctuates in the East over China (Chen et al., 2021), crossing Eastern Tibet and the Chinese Loess Plateau (Fig. 1). This boundary however likely evolved in the past, especially during the Paleogene when the orography and land-sea distribution were substantially different from today (no Himalayas, less extent Tibetan Plateau, presence of the Paratethys epicontinental Sea until the EOT) (X. Liu, Guo, et al., 2015) (see section 4). Tracking the monsoons back in time can be done thanks to a variety of paleoclimatic archives recording either their winds (intensity, direction) or precipitation (amount, seasonality) (P. Wang et al., 2005; Zhisheng et al., 2015; Tada et al., 2016). Markers of aridification on the other hand, such as increased proportion of xerophytic or halophytic plants or aeolian deposits (dusts, loesses) in the fossil record are often interpreted as evidence for the presence of a winter monsoon. The next section depicts the evolution of the Asian climate throughout the Cenozoic based on these different paleoclimate indicators.

3 Increasingly old testimonies of paleo-monsoons through times

The classical view for the Asian paleoenvironment evolution throughout the Cenozoic usually proposes a transition from a Paleogene "zonal climatic pattern" to a Neogene "monsoonal climatic pattern" (Guo et al., 2008; X. Sun & Wang, 2005; Jia et al., 2003). The

zonal pattern is described as a widespread arid to semi-arid band stretching across China and bracketed in its southern and northern borders by two humid belts, while the monsoonal pattern hosts a core of pronounced aridity in inland Asia, surrounded by monsoonal (seasonally wet) climate on its southern and eastern edges. This view is mostly based on paleoclimate indicators compilations (pollen, fossils and lithological arguments, e.g. from Boucot et al. (2013)) used to infer either humid conditions (coal, indicators of forested environments, large mammals, etc.) or arid ones (evaporites, desert and shrub environment, etc.). Recent evidence for highly seasonal climate in India, Myanmar and China as early as in the Eocene, at least 20 Myr earlier than previously thought, nevertheless challenge this paradigm. This section aims at presenting in the most comprehensive way the broad paleoenvironmental changes inferred from paleoclimate indicators in Asia from the Eocene to the early Pliocene, which are tentatively gathered in Fig. 2 (upper part). Localities and basins mentioned throughout the text are localized in Fig. 1.

3.1 Eocene to Oligocene paleoenvironment evolution

3.1.1 A progressive increase in summer monsoon indices from the Eocene to the Oligocene

Oldest testimonies of strongly seasonal precipitation in Southern Asia come from early Eocene floras situated in northwestern India (Shukla et al., 2014; Bhatia, Khan, et al., 2021) and from mid-late Eocene (40 Ma) floras and isotopic measurements in freshwater gastropod shells and mammals tooth enamel found in Myanmar (Licht et al., 2014; H. Huang et al., 2021). Both regions were however located further South at their respective period of deposition (between the equator and ∼10°N, Shukla et al. (2014); Westerweel et al. (2019)) and their seasonality is therefore mainly interpreted within the scope of a pronounced ITCZ seasonal migration rather than monsoonal climate.

Further east, in the Yunnan region (Southwestern China), today submitted to a mixture of Southern and Eastern Asian summer monsoon, a shift from arid/semi-arid to humid environment is recorded during the late Eocene and interpreted as the onset of the Asian monsoon at that time (Sorrel et al., 2017; Fang et al., 2021; Zheng et al., 2022). Such climate transition is inferred by the presence of coal layers, a change in the pollen record from xerophytic to mixed forest, change in lithology interpreted as lake and swamps expansion, together with the presence of fossils of freshwater fishes, gastropods and large mammals. While the precise date for this paleoenvironmental change is still debated between ∼41 Ma (Fang et al., 2021), ∼36 Ma (Zheng et al., 2022) and ∼35.5 Ma (Sorrel et al., 2017), it nevertheless predates the Eocene-Oligocene Transition (∼34 Ma). Proposed driving mechanisms to explain this regional climate shift usually involve either the crossing of a Tibetan Plateau elevation threshold (Zheng et al., 2022), a response to the Paratethys Sea retreat in the west, that would have allowed the penetration of more moisture from the east (Fang et al., 2021), or a response to the global climate cooling initiated after the Middle Eocene Climate Optimum (MECO) and subsequent sea surface temperature patterns reorganization (Sorrel et al., 2017).

Signs for the presence of an Eocene East Asian summer monsoon are also debated. In eastern China, Eocene paleovegetation mostly point to warm, humid and weakly seasonal evergreen forested environments on the coast (R. A. Spicer et al., 2016; X. Ma et al., 2012; Pound & Salzmann, 2017), except for northeastern middle-late Eocene Chinese floras retrieved from the coal deposits of the Huadian basin, that already seem to indicate adaptation to highly seasonal climate (Meng et al., 2018). Further inland, toward the eastern edge of the TP, these paleoenvironments gradually translate into sub-humid and/or seasonally dry conditions, as attested by various basin displaying alternating mudstone and evaporite deposits (D. Wang et al., 2013; Abels et al., 2011). Highly resolved deposits from the Jianghan basin, spanning the mid Eocene to early Oligocene (∼40-34 Ma), together with modeling studies (Tardif et al., 2021), have shown that the penetration of moisture into east-

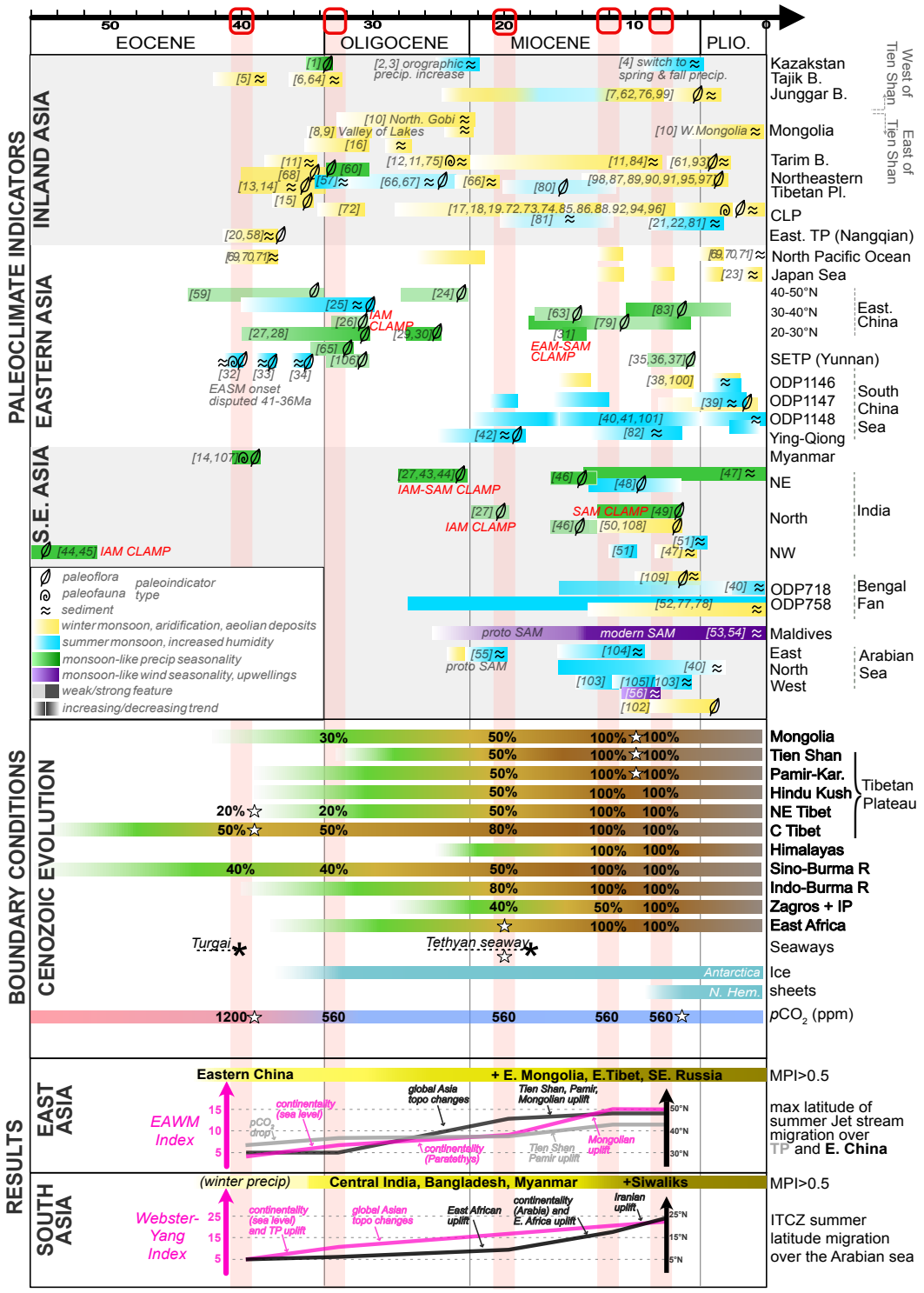

Figure 2. **upper** Paleoclimate tendencies recorded in inland, eastern and southern Asia. Bibliographic references in brackets are listed in SI Table 3 ; **center** Evolution of main landforms, seaways, ice sheets and pCO_2 during the Cenozoic overlain with values used in our reference simulations (elevations expressed in % of modern). White stars indicate parameters that where tested with sensitivity experiments ; **bottom** Overview of the main monsoon indicators evolution obtained in this study. We used the following abbreviations: NETP (SETP) - Northeastern (Southeastern) Tibetan Plateau, CLP - Chinese Loess Plateau.

ern China in the late Eocene was likely strongly modulated by orbital forcing. This may indicate that this Paleogene wet/dry zonal climatic pattern previously introduced (Guo et al., 2008; X. Sun & Wang, 2005) was already periodically disturbed in the late Eocene, and may have prefigured a more stable and widespread monsoon-like precipitation seasonality settlement in the Oligocene.

Indeed, after the global cooling and aridification occurring at the Eocene-Oligocene Transition, pieces of evidence for monsoon-like precipitation seasonality of variable intensity become more widespread in floras from both China (X. Ma et al., 2012; Herman et al., 2017; Vornlocher et al., 2021; J. Ren et al., 2021; Miao, 2013; Ling et al., 2021; S. Li et al., 2018; C. Huang & Hinnov, 2019; H. Tang et al., 2020) and India (Bhatia, Khan, et al., 2021; R. Spicer et al., 2017; Srivastava et al., 2012). Additionally, oceanographic records from adjacent seas (Bay of Bengal and South China Sea) that were recently extended back to the late Paleogene, have been used to track the SAM and EAM evolution from the middle Oligocene onward. Drilling from the Ying-Qiong Basin in the South China Sea, spanning the late Oligocene to early Miocene (25-18 Ma), record an increase in terrigenous organic matter influx, together with increased tropical-subtropical angiosperm pollen proportion, which are interpreted as signs of increasing East Asian summer monsoon during this period (W. Ding et al., 2021). In the Bay of Bengal (ODP 758), measurements of clays radiogenic isotopic composition, indicating undisturbed weathering patterns over the last 27 Ma, are interpreted as signs of stable South Asian summer monsoon activity since at least the late Oligocene (S. Ali et al., 2021).

3.1.2 Late Eocene aridification in response to the Paratethys Sea retreat and global climate cooling

Markers of arid to sub-humid climate are already widespread in inland Asia in the Eocene with, for example, many sites displaying pollen assemblages characteristics of steppe-desert environments such as in the Xining, Hoh Xil, Qaidam and Tarim basins (Q. Yuan et al., 2020; Miao, Wu, et al., 2016; X. Ma et al., 2012). During the mid-late Eocene (∼40-34 Ma), inland Asia records an evolution toward drier conditions, as suggested by increased proportions of xerophytic plants such as *Nitraria* and *Ephedra* in Xining, Hoh Xil, Qaidam (Northeastern Tibet), Nangqian (central-eastern Tibet) and Tarim basins (Q. Yuan et al., 2020; Barbolini et al., 2020; Hoorn et al., 2012; Miao, Wu, et al., 2016), δ^{18}O measurements from ostracod shells in the Tarim basin (Bougeois et al., 2018), clumped isotopes from pedogenic carbonates in the Xining basin (Page et al., 2019), compound-specific hydrogen isotope analyses (δ^{2}H) applied to sedimentary leaf wax *n-alkanes* in the Qaidam basin (Wu et al., 2021) and by lipid biomarkers and compound-specific carbon isotopic compositions from bulk sediments in the Nangqian basin (J. Wei et al., 2022). The presence of detrital material attributed to Asian dusts is also recorded in sediments from Central North Pacific (GPC3 and ODP site 1215) since ∼40 Ma (Pettke et al., 2002; D. Rea et al., 1985; Ziegler et al., 2007).

This late Eocene aridification stage is mostly interpreted as resulting from the reduced westerly moisture input during the two successive Paratethys Sea regression phases from the Tarim and the Tajik basins, recorded between ∼41-37 Ma (Carrapa et al., 2015; J. Sun et al., 2020, 2022; Bougeois et al., 2018; Bosboom et al., 2014b; Kaya et al., 2019). Highly resolved sediment deposits, such as those of the Xining basin (northeastern Tibet) display good correlation between wetter evaporite layers and Paratethys Sea transgressions phases into the Tajik and Tarim basins, and between arid mudstone intervals and regression phases. This confirms the key role played by the westerlies and the Paratethys Sea as a major moisture source for inland Asia in the Eocene, even over long distances (Meijer et al., 2019; Bosboom et al., 2014a). Additionally, a strong obliquity cyclicity is imprinted on the Xining evaporite/mudflat layers in the late Eocene (40-34 Ma), coeval with the appearance of loess-like dusts in the mudflat phases (Meijer et al., 2021; Licht et al., 2014). This hints a marked influence of high latitudes dynamics, such as incipient ice-sheets at the poles (Abels et al.,

2011; Xiao et al., 2010) and variations in the Siberian High intensity (Meijer et al., 2021), on inland Asian climate at that time.

3.1.3 Oligocene climate fluctuations and inception of major modern Asian deserts

The Oligocene evolution of inland Asian climate appears both regionally and timely contrasted. In the early Oligocene, a few sites situated within the westerly moisture region tend to show increased humidity trends, recorded by $\delta^{18}O$ isotopic measurements in pedogenic carbonates (Kent-Corson et al., 2009) in the Tarim and western Qaidam basins together with $\delta^{2}H$ measurements in leaf waxes (Wu et al., 2021) and leaf fossil CLAMP analysis suggesting wet environment with weak (not monsoonal) precipitation seasonality (Song et al., 2020) from western Qaidam. On the other hand, many testimonies for drier climate are reported within the eastern Asian monsoon domain by $\delta^{18}O$ isotopic measurement in pedogenic carbonates from the eastern Qaidam basin (Y. Sun et al., 2020; Kent-Corson et al., 2009), Lanzhou basin in the Chinese Loess plateau area (B. Li et al., 2016), together with CLAMP analysis on fossil leaves advocating for an increased (and monsoon-like) precipitation seasonality in Lanzhou (Miao, 2013), and Markam basin in southeastern TP (T. Su, Spicer, et al., 2019), in agreement with records of increased monsoon-like precipitation seasonality in Eastern China introduced in the previous section. Interpretations nevertheless diverge and suggest that this aridification trend may indicate either weakened East Asian summer monsoon precipitation due to global cooling after the EOT (Wu et al., 2021), increased winter aridity due to the final Paratethys Sea retreat, global sea level fall after the EOT and/or global cooling (Miao, 2013; B. Li et al., 2016), or be due to TP uplift (T. Su, Spicer, et al., 2019).

In the Taatsin Gol region, at the southern edge of the Hangay Dome and extreme north of the modern Gobi desert, isotope measurement from pedogenic carbonates indicate aridification since the early Oligocene (Caves Rugenstein et al., 2014). Finer resolved records reveal several bursts of aridification at ∼34-33, ∼31, ∼28 and ∼23 (Baldermann et al., 2021) and the presence of loess as soon as ∼34 Ma (J. Sun & Windley, 2015). Proposed mechanisms for such aridification involve increased continentality due to land-sea distribution fluctuations at 34 Ma (J. Sun & Windley, 2015) and an early Hangay Dome uplift that would have acted as a barrier to moisture advection from Siberia to Mongolia as soon as the Oligocene (Caves Rugenstein et al., 2014). Better resolved records however highlight the good correlation in time between ice sheets expansion phases and these aridification pulses, and therefore propose that large scale climate fluctuations at that time were the main drivers of Mongolia hydrologic dynamics (Baldermann et al., 2021). Further south, in the Bayanhot basin (southern Gobi), two bursts of aridification inferred from environmental magnetic, mineralogical and geochemical study at ∼31 and ∼28 Ma seem to further confirm the influence of high latitude ice sheet fluctuation on Mongolian Oligocene climate (Wasiljeff et al., 2022).

In the mid to late Oligocene, massive eolian dust deposits are reported in three major sites: in the Chinese loess plateau in Northeastern Tibet starting at ∼29 Ma (Garzione et al., 2005; Qiang et al., 2011) (see (Meijer et al., 2021) for a full review), in the Tarim Basin (hosting today the Taklamakan desert) at ∼27-22 Ma (Zheng et al., 2015) and in the Junggar basin at ∼24 Ma (J. Sun et al., 2010). Aridification is also inferred from $\delta^{18}O$ isotopic measurements from ostracods and pedogenic carbonates from the Tarim basin at ∼25 Ma (Bougeois et al., 2018; Kent-Corson et al., 2009) and from isotopic records in stromatolites from the Junggar basin loosely dated in the early Miocene (W. Yang et al., 2019). This second step of aridification is coeval with $\delta^{18}O$ and $\delta^{13}C$ isotopic measurements from pedogenic carbonates suggesting increased orographic precipitation in the Issyk Kul and Ili basins, both situated on the western side of the Tian Shan ranges (Hellwig et al., 2018; Macaulay et al., 2016). Collectively, these observations are interpreted as the sign that the Tian Shan-Pamir uplift had reached an elevation threshold that would have started

shielding the Tarim and Junggar basins from westerlies moisture input, thus favoring their aridification (Bougeois et al., 2018; W. Yang et al., 2019).

This late Oligocene to early Miocene aridification phase seems to be recorded by several oceanic drillings, for example in Central North Pacific, with an increase in dust mass accumulation rate recorded at ∼25 Ma by (drilling site GPC3) (D. K. Rea, 1994; Pettke et al., 2002) and at ∼22 Ma (ODP site 1215) (Ziegler et al., 2007). These drillings are however situated far from the Asian coast and underwent important plate motion throughout the Cenozoic, making it difficult to disentangle variations due to inland Asia climate changes, possible global atmospheric/oceanic circulation patterns changes, and variations in the recorded signal due to plate motion. The presence of a proto winter monsoon wind circulation is also suggested by increased proportion of dusts, inferred from magnetic susceptibility measurement in the Maldives (IODP sites U1467, U1468) at ∼ 24 Ma (Betzler et al., 2016), and by an increase in water column mixing and ventilation evidenced by a reduction in $\Delta\ \delta^{13}$C, increase in bulk sediment Mn/Fe and Mn/Ti and foraminiferal Mn/Ca in the eastern Arabian Sea (Beasley et al., 2021).

3.2 Strengthening of summer and winter monsoon patterns in the Neogene

3.2.1 An East-West gradation in Miocene South Asian summer monsoon variations and the expansion of grassland

Despite a better coverage in both continental and marine records in the Neogene, substantially diverging interpretations remain regarding the evolution of the monsoons winds and precipitation seasonality, especially during the late Miocene. Precipitation proxies from the South Asian Monsoon domain allow to highlight an East-West gradation in climate evolution throughout the Miocene, recorded in the Siwaliks deposits of the Himalayan foreland basin. In northeasternmost India (Arunachal Pradesh), modern-like monsoon precipitation seasonality is inferred from plant macrofossils since the middle Miocene (13 Ma) and displays little variation in intensity when compared to early Pleistocene fossils from the same locality (Khan et al., 2014). Further west, plant macrofossils and pollen from Darjeeling, Nepal, northwestern India and Pakistan show a progressive replacement of middle Miocene evergreen forests by deciduous forests in the late Miocene, and finally a massive expansion of grassland in the latest Miocene (Hoorn et al., 2000; Bhatia et al., 2022; Bhatia, Srivastava, et al., 2021; Srivastava et al., 2018). This late Miocene floristic change is also accompanied by several shifts in δ^{13}C toward more positive values, recorded between 10.5 and 6 Ma by isotopic measurements in pedogenic carbonates and organic matter and lipid biomarkers in the Central Siwaliks (Nepal) (Quade et al., 1995; Neupane et al., 2020; Dettman et al., 2001), and in the Western Siwaliks (northwestern India and Pakistan) (Sanyal et al., 2004; Vögeli et al., 2017; Quade & Cerling, 1995). Similar trends are also recorded in nearby marine basins by isotopic measurements from bulk sediments and leaf wax, pollen and macrofossils at ∼8-7 Ma in the Arabian Sea (ODP 722 and IODP U1457) (Feakins et al., 2020; Y. Huang et al., 2007) and at ∼7-6 Ma in the Bengal fan (Polissar et al., 2021).

This marked carbon isotope excursion is observed in other localities of the globe and testify of an important ecological change, characterized by the replacement of plants using the C3 photosynthetic pathway by grasslands using the C4 photosynthetic pathway (Cerling et al., 1993; Tauxe & Feakins, 2020; Edwards et al., 2010). Recent re-calibration of these Asian continental carbon isotope records and comparison to other available records allow to show that C4 expansion occurred at distinct times: ∼10 Ma in Africa, ∼8 Ma in Pakistan, ∼7 Ma in peninsular India, ∼6 Ma in Nepal and later during the Pliocene in Australia and South America (Tauxe & Feakins, 2020). Although a late Miocene pCO_2 drawdown was initially proposed as the main driver for the C3/C4 transition, such distinct timing in ecological turnover over the globe is assumed to reflect the multiplicity of forcing factors at play in this major biome reorganization. In the Siwaliks, this East-West climate gradation likely reflects the crossing of a precipitation threshold somewhere in Nepal (Central Siwa-

liks), with northwestern India, Nepal and Pakistan experiencing drier winters and overall aridification in the late Miocene compared to the more stably humid northeastern Indian region. The C4 grasslands expansion would thus possibly result from a combination of pCO_2 decrease, reduced moisture advection from the westerlies in this region, Tibetan Plateau and Himalayas uplift and to more frequent forest fire that would have favored grasses over trees (Sanyal et al., 2004; Vögeli et al., 2017; Quade & Cerling, 1995; Srivastava et al., 2018; Tauxe & Feakins, 2020; Polissar et al., 2021; Feakins et al., 2020).

Precipitation proxies recovered from marine drillings offer contrasting information. In the central Bay of Bengal (ODP site 758), relatively undisturbed isotopic composition of clays issued from silicate weathering since the Oligocene (∼27 Ma) are interpreted as signs of a stable South Asian summer monsoon presence since that time (S. Ali et al., 2021). On the other hand, chemical weathering (CIA, K/Al ratio) and sediment accumulation rates from both the Indus Fan and the Bay of Bengal recording the physical erosion of the Himalayas and southern Tibet, suggest that SASM precipitation reached a maxima in the middle Miocene (∼10-16 Ma) before declining between ∼8-3 Ma (P. Clift et al., 2008). This decline was primarily interpreted as reflecting a weakened SASM precipitation (P. Clift et al., 2008), although other studies based on similar proxies from the Bay of Bengal argue it may rather reflect an intensification of the winter monsoon (S. Ali et al., 2021), possibly coupled to a weakening of the South Asian summer monsoon (J. Lee et al., 2020), which seem in better agreement with continental proxies, and with marine records from the South China Sea (Wan et al., 2010) (developed in the next section).

Wind proxies retrieved from the Arabian Sea and the Bengal Fan pointing to the presence of seasonal wind reversal (hence of a winter monsoon) since the middle Miocene seem to corroborate this explanation, although some aspects of the SAM wind circulation evolution remain debated. In the Arabian Sea, the appearance of *Globigerina Bulloides* in the sediments had initially been used to infer an intensification (or an onset) of the South Asian summer monsoon wind circulation at ∼8 Ma (Kroon et al., 1991), based on the assumption that stronger SASM winds would translate into stronger upwelling activity. Those records have since then been extended back in time (Bialik et al., 2020; Zhuang et al., 2017; Gupta et al., 2015) and combined with analysis of current-controlled drift sediments and geochemical tracers from the Maldives archipelago (Betzler et al., 2016). These new studies now point to a settlement of a "proto" South Asian monsoon wind circulation since the late Oligocene (∼25 Ma), and of its reinforcement in the middle Miocene (∼13-10 Ma) (Betzler et al., 2016; Zhuang et al., 2017; Bialik et al., 2020) and possibly also in the late Miocene (∼8-7 Ma) (Gupta et al., 2015). Nevertheless, increasing number of studies based on marine records from both the Arabian Sea and the Bengal Fan do not observe this latest Miocene (8-7 Ma) SASM peak (Bolton et al., 2021; Tripathi et al., 2017; Betzler et al., 2016; Y. Huang et al., 2007). Strong SAM wind circulation since at least 10 Ma is also supported by clay mineralogy, detrital isotopes, export productivity and sediments accumulation from records in the southern Bay of Bengal (IODP 1443) (Bolton et al., 2021; J. Lee et al., 2020)) and the eastern Arabian Sea (IODP 1456) (Tripathi et al., 2017)).

3.2.2 EASM in the Neogene

Summer precipitation typical of the East Asian summer monsoon is assumed to occur throughout the Neogene (22-3 Ma), as attested by sediments exported to the South China Sea, such as weathering indices (P. Clift et al., 2008), $\delta^{13}C$ measurements in black carbon (Jia et al., 2003), pollen, biomarkers, kerogen composition and clay mineralogy (W. Ding et al., 2021). On land, $\delta^{18}O$ from paleosol carbonates in the CLP (Suarez et al., 2011) and most Chinese floras, studied with Coexistence Approach, CLAMP or Bayesian method applied to pollen, point to summer precipitation comparable to modern amounts (Q. Wang et al., 2021; Yao et al., 2011; Xing et al., 2012; Hui et al., 2021; B. Wang et al., 2021; Q.-g. Sun et al., 2002). Most of those studies nevertheless suggest wetter winters due to weaker winter monsoon until the latest Miocene, with a few exceptions, such as the mid-Miocene floras

from the Zhangpu biota in southeastern China characteristic of megathermal seasonal forest which CLAMP signature showing affinities with EAM and SAM floras (B. Wang et al., 2021). The variations in EASM intensity throughout the Miocene remain controversial in both continental and marine deposits, but two intensification peaks usually emerge, tentatively linked to the Middle Miocene Climatic Optimum (∼17-14 Ma) and to the Miocene-Pliocene boundary (∼8-5 Ma).

The middle Miocene EASM peak is inferred from sediments from the South China Sea by chemical weathering proxies at 15-12 Ma (P. Clift et al., 2008), and $\delta^{13}C$ in black carbon (Jia et al., 2003), although the latter rather point to a step-wise intensification of EASM in the course of the Neogene (at ca. 20, 15, 10, 6 and 2 Ma). On land, characterization of iron oxides from the Chinese Loess Plateau suggest an EASM peak at 16-14 Ma (H. Zhao et al., 2020). The proportion of *Fupingopollenites*, an extinct palynomorph supposed to be highly dependent on summer moisture, has also been used in an extensive compilation spanning available Miocene Chinese pollen records and point to an important penetration of EASM moisture, up to the eastern Qaidam basin, during the MMCO, before retreating to the East in the rest of the Neogene (Miao, Song, et al., 2016).

A substantial increase in EASM strength is also robustly suggested by many lines of evidence in the late Miocene to Pliocene, although with notable variations in onset timing (10-4 Ma). In the South China Sea, it is inferred from $\delta^{18}O$ and Mg/Ca derived temperature records of surface and sub-surface water (IODP U1501) (C. Yang et al., 2021), clay minerals, grain size, major and trace elements analysis from terrigenous sediments (ODP 1146) (Wan et al., 2007, 2010) and by black carbon $\delta^{13}C$ (Jia et al., 2003). In China, this EASM intensification is recorded through mineralogical, chemical and magnetic analysis of sedimentary deposits in the Chinese Loess Plateau (Ao et al., 2016, 2021; H. Zhao et al., 2020), and by pollen from the Tianshui (Hui et al., 2021) and the Weihe Basin (L. Zhao et al., 2020). The forcing factors responsible for these EASM intensification peaks remain debated, but are usually attributed to global warming (Ao et al., 2021; H. Wang et al., 2019) and/or to Neogene TP uplift phases (Hui et al., 2021; X. Ren et al., 2020; H. Zhao et al., 2020). Although EASM and EAWM evolution show few correlation during most of Cenozoic, this late Miocene EASM increase is notably accompanied with EAWM increase (described in next section).

3.2.3 Miocene to Pliocene aridification pulses in response to regional uplifts

Throughout the Miocene, dust deposition continues in the Chinese Loess Plateau (Guo et al., 2002; Meijer et al., 2021), Tarim-Taklamakan (Kent-Corson et al., 2009; Zheng et al., 2015; Heermance et al., 2018) and Junggar basins (J. Sun et al., 2010). In parallel with previously mentioned indices for an increased EASM during the MMCO (∼17-14 Ma) (P. Clift et al., 2008; Jia et al., 2003; H. Zhao et al., 2020), a warmer and less arid climate interval is suggested by pollen showing relatively lower proportion of xerophytic taxa in the Junggar (J. Sun et al., 2010) and Qaidam basins (Miao et al., 2011). After the MMCO, a pronounced step-wise aridification is recorded in most of inland Asia until the Miocene-Pliocene boundary (Lu et al., 2010; Lu & Guo, 2014; Z.-H. Tang & Ding, 2013). Here again, the timing for aridification steps varies with the region and is usually tentatively explained by a combination of global cooling, ice-sheet expansion and multiple regional uplift episodes occurring at that time.

In the eastern part of inland Asia, encompassing the Chinese Loess Plateau, central China and northeastern Tibetan Plateau, this aridification is attributed to northeastern TP uplift (Miao et al., 2012), Altai mountains uplift (Caves Rugenstein et al., 2014) and/or late Miocene cooling (Lu et al., 2010; Lu & Guo, 2014; Peng et al., 2016). Such aridification is supported by overwhelming evidences, such as pollen and biomarkers documenting a step-wise transition from sub-humid to arid environment starting at ∼15 Ma (J. Liu et al., 2016;

Miao et al., 2011; Jiang & Ding, 2008; Peng et al., 2016), massive grasses expansion at ∼11-7 Ma (Suarez et al., 2011; Barbolini et al., 2020; Y. Ma et al., 2005; L. Zhao et al., 2020; H. Wang et al., 2019), widespread eolian deposition at ∼8-7 Ma (X. Ma & Jiang, 2015; Guo et al., 2002; Qiang et al., 2011; B. Li et al., 2016; Jiang et al., 2017), increased δ^{18}O of pedogenic carbonates and terrestrial mammals tooth enamel at ∼14-13 and ∼7-5 Ma (B. Li et al., 2016; Kent-Corson et al., 2009; Wu et al., 2021; W. Liu et al., 2014; Y. Sun et al., 2020; Kaakinen et al., 2006; Y. Wang & Deng, 2005), *n*-alkanes analysis from Qaidam sediments since 13 Ma (Z. Liu et al., 2014) and dominance of cold-aridiphilous mollusks proportion in the CLP from 7-5 Ma (F. Li et al., 2008).

The western part of inland Asia, comprising the Tarim and Junggar basins and several sites in eastern Kazakhstan, which all add to the body of evidence indicating mid to late Miocene aridification, as shown by increased xerophytic and grasses pollen proportions at ∼7-5 Ma (J. Sun et al., 2010; J. Sun & Zhang, 2008; Z. Zhang & Sun, 2011; Barbolini et al., 2020; J. Sun et al., 2008), massive eolian deposition in the western Tarim at ∼12-7 Ma (Heermance et al., 2018) and permanent drying of lakes in the eastern Tarim at ∼5 Ma (W. Liu et al., 2014). The pedogenic carbonates δ^{18}O record of these regions nevertheless offers diverging pattern evolution, that have been tentatively explained by their location with respect to the Tian Shan and Altai mountains (Caves Rugenstein et al., 2017). Regions today lying upwind of the Tian Shan and Altai mountains, such as the Issyk Kul (Macaulay et al., 2016), Junggar (Charreau et al., 2012) and Zaysan basins (Caves Rugenstein et al., 2017) show a decline in δ^{18}O between 10-5 Ma (varying from ∼1.5 to 4 ‰) which was interpreted as a change in precipitation seasonality following the uplift of the Altai Mountains (Caves Rugenstein et al., 2017). On the other hand, increased δ^{18}O values since ∼15 Ma and peaking at ∼7-5 Ma in the Tarim basin, situated downwind of the Tian Shan ranges display trends similar as those of the Qaidam basin (Kent-Corson et al., 2009), which are interpreted as indicating aridification at that time.

EAWM intensification peaks are also recorded offshore at ∼15-12, ∼8-5 and ∼3 Ma, in usually good coherence with continental data. In the South China Sea, it is suggested by increased black carbon concentration and accumulation (whose transportation to the Sea would be favored by stronger winter winds) (Jia et al., 2003), planktic and benthic δ^{18}O records and mixed layer temperature (A. Holbourn et al., 2021; A. E. Holbourn et al., 2018), clay mineralogy and grain size analysis (Wan et al., 2007), and by indices of decreased chemical weathering (G. Wei et al., 2006). In the Sea of Japan, clay mineral assemblage and isotopic analysis of silicate fraction covering the last 15 Ma suggests a stepwise drying of Central Asia suggested at 12, 8 and 3.5 Ma (Shen et al., 2017). In the North Pacific, an increase in Asian dusts proportion is recorded at ∼10 and ∼4 Ma (D. Rea et al., 1985; Pettke et al., 2002). Last, brutal onset of SAM wind seasonality (and therefore occurrence of winter monsoon reversed winds) is inferred at ∼12 Ma in the Maldives (Betzler et al., 2016) and in the eastern Arabian Sea (X. Yang et al., 2020).

3.3 Assessing forcings and mechanisms through climate models

3.3.1 SAM forcings assessed by modeling experiments derived from modern geography

Major forcings proposed to explain multi-million year monsoon variability are global climate variations, changes in topography and changes in land-sea distribution. Attributing a specific change to one or several of these forcings is nevertheless complicated by the fact that they may vary at the same time, produce non-linear responses with potentially antagonizing effects and because they are sometimes poorly dated or quantified. Modeling experiments, first derived from modern geographies and boundary conditions, have helped better understanding the role played by these different forcings in shaping the regional monsoons.

The Tibetan Plateau has long been seen as instrumental in driving the South Asian monsoon circulation and precipitation, its elevated heated surface acting as a "heat pump" driving the convergence of the surrounding air masses (Kutzbach et al., 1993; Zoura et al., 2019; Molnar et al., 1993). It seems now that it is rather the physical barrier created by the landform (the Himalayas or the Tibetan Plateau) that is essential to induce abundant orographic precipitation over northern India, through steering and lifting of moist air masses (Abbott et al., 2016; Boos & Kuang, 2010; Acosta & Huber, 2020). The condensation of moisture in these ascending air masses leads to important latent heat release in the high troposphere over northern India, which acts as a positive feedback sustaining summer convection and precipitation in South Asia (He, 2017). The large-scale monsoon circulation seasonal reversal resulting in the initial advection of these moist air masses over Asia in late spring and early summer, on the other hand, is essentially driven by surface ocean-continent temperature gradients and resulting pressure patterns (Acosta & Huber, 2020; Merlis et al., 2013).

Smaller orographic features were also shown to play a critical role in shaping and strengthen the South Asian monsoon. By channeling the Somali Jet and insulating it from the subtropical dry westerly flow, the Anatolian-Iranian landform were shown to greatly contribute to enhance moisture transport towards India and Eastern Asia (Acosta & Huber, 2020; He, 2017; H. Tang et al., 2013). The Eastern African highlands, positioned on the way of the ITCZ flow, are critical in shaping both African and South Asian climate (Bannon, 1979; Rodwell & Hoskins, 1995; Sepulchre et al., 2006). Recent studies have specifically demonstrated that Eastern African highlands presence contribute greatly to strengthen and concentrate the Somali Jet, but that their absence would result, quite counter-intuitively, into higher summer precipitation over SAM region, due to increased advection directly from the ocean to the continent (H.-H. Wei & Bordoni, 2016; Chakraborty et al., 2009). This last aspect hints that strong upwellings, due to strong atmospheric circulation, may not correlate with strong precipitation on land. The effect of the Pamirs, Tian Shan and northeastern TP uplifts on SAM remains unclear. When these uplift together with Mongolian landforms, H. Tang et al. (2013) simulate increased moisture advection to eastern China but decreased precipitation over India, while the opposite effect is obtained when not modifying (modern) Mongolian topography (R. Zhang et al., 2017). Apart from differences coming from the model and boundary conditions, this likely points to the complex interactions existing between the SAM and EAM regional monsoons.

3.3.2 EAM forcings assessed by modeling experiments derived from modern geography

In contrast with the modest effect it has on the SAM, the Tibetan Plateau uplift is instrumental for the EASM, as the heating of the Plateau, induces a cyclonic circulation anomaly promoting advection of moist air masses towards Eastern Asia (Z. Zhang et al., 2007; H. Tang et al., 2013; R. Zhang et al., 2017). Additionally, simulations testing the effects of increased Asian continentality (to mirror a global sea level fall or the retreat of the Paratethys Sea, for example), have shown that it results in amplified summer moisture convergence from the Indian Ocean towards Asia, due to changes in surface temperature gradients deepening the continental low pressure belt (Z. Zhang et al., 2007).

Although smaller than the HTP complex, the Pamir, Tian Shan and Mongolian landforms are adequately situated in latitude to interfere both dynamically and thermally with planetary-scale atmospheric circulation. Their uplift was shown to enhance the aridity in inland Asia (actual Gobi and Taklimakan deserts), as it reinforces the EAWM circulation patterns (X. Liu & Yin, 2002; X. Liu, Sun, et al., 2015; Baldwin & Vecchi, 2016; Sato, 2009). By creating a cold pool and deviating the westerlies towards northern Siberia, the Mongolian orography has been proposed to be responsible for the Jet Stream northward migration in summer and intensity in winter (White et al., 2017; Shi et al., 2015; Sha et al., 2020), and for most of the Siberian High location and intensity (Sha et al., 2015).

3.3.3 Modeling experiments derived from paleo boundary conditions

Modeling studies based on modern geographies are nevertheless limited in to what extent they allow to understand past changes, especially for periods where very different geographies and climate prevailed. Paleoclimate simulations, using sets of realistic (as much as possible) paleo-boundary conditions are however rarer. Indeed, they usually imply high computational cost, and require important background knowledge on past constraints (paleogeography, CO_2, solar constant, ice-sheets volume).

More specifically, paleoclimate modeling has confirmed that increasing Asian continentality during the Oligocene and the Miocene, mirroring either the Paratethys Sea retreat and/or global eustatic sea level fall, was a key leverage of increased moisture advection toward Asia in summer (Fluteau et al., 1999; Ramstein et al., 1997; Z. Zhang et al., 2014; Sarr et al., 2022). In Oligocene conditions, the uplift of the peripheral Tian Shan, Pamir and northeastern portions of the TP was also shown to promote inland Asian aridity, when compared to the sole uplift of the "core" Tibetan plateau (R. Zhang et al., 2017). In late Eocene conditions, the latitude of the Tibetan Plateau was also shown to impact significantly and non-linearly East Asian climate: with a TP uplifting in the tropics (∼11°N) inducing precipitation on the reliefs but aridification in most of China, while a TP uplifting at its modern latitude (∼26°N) would increase moisture advection to eastern China and aridification of inland Asia (R. Zhang et al., 2018).

Although paleoclimate studies offer contrasted views regarding Eocene climate, some suggesting the presence of monsoons at that time (Huber, 2003) and others not (Tardif et al., 2020; Z. Zhang et al., 2012; R. Zhang et al., 2018), this divergence is most likely due to the very different paleogeographic reconstructions that were used. Indeed, as many features of the Eocene paleogeography remain highly controversial (height of the incipient Tibetan topography, shape of Indo-Asian collision zone, height of peripheral landforms, land-sea distribution, etc.), the geographic reconstructions may diverge widely from one study to another. Paleoclimate modeling have nevertheless allowed to emphasize the prevalence of geography impact on climate, rather than pCO_2 variations or far-field ice-sheets effects when it comes to the SAM and EAM settlement and intensification over long time scales (Farnsworth et al., 2019; Thomson et al., 2021). Collectively, these information rather reinforce the need for good paleogeographic constraints, and for more sensitivity experiments in paleo context, which we aim at doing in the present contribution.

3.4 Summary: a diachronous settlement of SAM and EAM seasonal features, potential forcings and mechanisms and remaining uncertainties

The past decade have brought plenty of new analysis based on fossil material, both onshore and offshore. The history of SAM, EASM and EAWM settlement and intensification now clearly seem to have been diachronous and its evolution tightly linked to land-sea mask, topography and global climate evolution over long time scales. Some questions nevertheless remain to be answered.

First, it is unclear whether Paleogene records of highly seasonal precipitations at low latitudes (<20°N) do describe an actual monsoon, given that no wind proxies can be provided at this period, and that Eocene paleoclimate studies propose widely diverging scenarios. CLAMP (Climate Leaf Analysis Multivariate Program) paleobotanical analysis (Feng & Poulsen, 2016; Wolfe, 1993; Jacques, Su, et al., 2011) have brought interesting insight on this point. Generally, they show that, although strong precipitation seasonality was likely present since the Paleogene in broad parts of Southeastern Asia (Bhatia, Khan, et al., 2021; R. Spicer et al., 2017; Herman et al., 2017), these floras did not yet developed the characteristics of plants growing today in modern SAM or EAM regions until the middle Miocene (∼13 Ma) (R. Spicer et al., 2017; Bhatia, Srivastava, et al., 2021). Instead, Paleogene Asian floras display a signature typical of the regions today dominated by the ITCZ seasonal migrations (referred to as Indonesian-Australian monsoon, or IAM in Fig-

ure 2). The reorganization from an ITCZ dominated to a monsoonal wind circulation may have initiated in the Oligocene (∼28-23 Ma), according to fossils from northeastern India displaying a mixture of SAM and IAM leaf signatures (R. Spicer et al., 2017). These typical monsoonal signatures likely emerged from a combination of both biotic and abiotic factors, although CLAMP method is unable to disentangle the forcings responsible for these specific signatures. They however add to the body of evidence suggesting that precipitation seasonality and typical monsoonal wind circulation may have been decoupled in the past.

Second, although modeling studies have started to explore localized landforms effect in paleo context, there is plenty of room for improvement. For example, many of these landforms have been tested collectively (eg. Tian Shan and Mongolia uplifting together), and analyzed within the scope of a single time period. Significant hypotheses remain to be tested in a paleo context, such as identifying the leverage for a Siberian High pressure development, and its actual impact on inland Asian aridity. Indeed, the presence of loess-like deposits since the Eocene, that were tentatively explained by the presence of an active Siberian High at that time (Meijer et al., 2021; Licht et al., 2014), question its actual dependence to the presence of Tian Shan and/or Mongolian orogens, which are usually dated later in the Oligocene to late Miocene. In addition, the notion of threshold elevation is a key point to tackle, as strongly non-linear responses of climate circulation with respect to this parameter are expected. These considerations highlight the need for a finer understanding of the actual drivers of today's regional Asian monsoons. Given the demonstrated prevalence of geography in shaping the Asian Monsoons, an accurate representation of its evolution is therefore paramount to study their history over long time-scales.

4 Cenozoic paleogeography evolution

Simulations in this study have been performed with Eocene, Oligocene and Miocene paleogeographic configurations from previous studies (Poblete et al., 2021; Tardif et al., 2020; Sarr et al., 2022; Barbolini et al., 2020), which are coherent with geological history. The Eocene and the early Miocene paleogeographic configurations are from Poblete et al. (2021); Tardif et al. (2020) reconstruction at 40 and 20 Ma. The early Oligocene geography is based on the Eocene geography with an homogeneous sea level drop of 70 meters to account for sea level changes related to Antarctic ice-sheet building during the Eocene-Oligocene transition (Miller et al., 2020). The mid and late Miocene geographies are based on the PRISM4 (Dowsett et al., 2016) reconstruction used in PlioMIP2 (Haywood et al., 2020) with modifications to include a southward shift of the Australian continent and an emerged Sunda Shelf (see Sarr et al. (2022) for details). We in addition performed sensitivity experiments to test the impact of specific topographic features on different characteristics of the Asian monsoons.

In this section, we provide an overview of the main landmarks and persistent uncertainties regarding the paleogeography evolution during the Cenozoic in our region of interest (see Fig. 2). The paleogeographic configurations used in our simulations are introduced, for each of these key regions (Fig. 3 and Table 1).

4.1 Asia

4.1.1 Indo-Asia collision and land-sea distribution uncertainties

The initiation of the Indo-Asian collision, marking the closure of the Neotethys Ocean (J. R. Ali & Aitchison, 2008; Chatterjee et al., 2013), is dated around ∼50 Ma (C. Wang et al., 2014; D. J. J. van Hinsbergen et al., 2012; Dupont-Nivet et al., 2010; Jagoutz et al., 2015; Lippert et al., 2014; W. Huang et al., 2015), or alternately around ∼58 Ma (D. J. van Hinsbergen et al., 2019; Ingalls et al., 2016), via sedimentology and paleomagnetic evidence. The morphology of the *Greater India* portion (i.e. northern India) before collision remains unclear. Depending on the collision scenario considered (see Kapp and DeCelles

Table 1. List of reference simulations (in bold) and sensitivity experiments used in this study. Abbreviations stand for East Antarctic Ice Sheet (EAIS), Antarctic Ice Sheet (AIS) and Greenland + Antarctic Ice Sheet (G+AIS). The last column explains the relationship between the different paleogeographic configurations, and therefore define the anomalies that can be tested (e.g. the effect of a lowered TP will be studied through the "LEo2_TP - LEo2_TPlow" difference, while the effect of pCO_2 halving in the Eocene is obtained with the "LEo1_REF - LEo1_2X". Likewise, all paleogeography sensitivity experiment from the Middle to late Miocene will be compared to the "LMio_smallT" simulation.

Simulation	pCO_2	Ice sheets	Paleogeography
LEo1_REF	**1120**	-	from (Tardif et al., 2020)
LEo2_TP	1120	-	from (Poblete et al., 2021)
LEo2_TPlow	1120	-	from LEo2_TP, with TP lowered to 800 m
LEo2_TPhigh	1120	-	from LEo2_TP, with TP raised to 4500 m
LEo2_TPsouth	1120	-	from LEo2_TP, with TP shifted to the South (Poblete et al., 2021)
LEo2_BengalSea	1120	-	from LEo2_TP, with a Bengal Sea (Poblete et al., 2021)
LEo1_2X	560	-	from LEo1_REF, with pCO_2 halved to 560 ppm
EOli_REF	**560**	**AIS**	from LEo1_REF, with 70m sea level drop
EMio_REF	**560**	**EAIS**	from (Poblete et al., 2021)
EMio_TetSw	560	EAIS	from EMio_REF, with open Tethyan Seaway (120 m depth)
EMio_EAfr	560	EAIS	from EMio_REF, with modern East African landforms
MMio_REF	**560**	**AIS**	from (Sarr et al., 2022)
LMio_smallT	560	AIS	from MMio_REF, with a reduced Paratethys
LMio_noAr	560	AIS	from LMio_smallT, with immersed Arabia
LMio_noM	560	AIS	from LMio_smallT, with Mongolia lowered to 800 m
LMio_noTS	560	AIS	from LMio_smallT, with Tian Shan lowered to 800 m
LMio_noTSM	560	AIS	from LMio_smallT, with TienShan + Mongolia lowered to 800 m
LMio_noTSP	560	AIS	from LMio_smallT, with TienShan + Pamir lowered to 800 m
LMio_REF	**560**	**G+AIS**	from (Sarr et al., 2022)
LMio_1.5X	420	G+AIS	from LMio_REF with pCO_2 lowered to 420 ppm

(2019); Poblete et al. (2021) for a review), *Greater India* is represented as fully emerged (Ingalls et al., 2016; C. Wang et al., 2014), or partially flooded until the middle-late Eocene (D. J. J. van Hinsbergen et al., 2012; D. J. van Hinsbergen et al., 2019; W. Huang et al., 2015). From the Eocene onward, India's progressive migration to the North, indentation into the Asian continent and counterclockwise rotation (Molnar et al., 2010) triggered widespread orography changes in Asia, which are summarized below. The most salient of these events is of course the Tibetan Plateau and Himalayas uplift, and the spreading of deformation and uplift to peripheral terranes.

4.1.2 Himalayas-Tibetan Plateau uplift history

The early uplift history of the Tibetan Plateau is highly debated. Oxygen isotopic paleoaltimetry studies suggest that the Gangdese (Southern TP, Lhasa terrane) and Qiangtang mountains (Central TP) are already as high as ∼4000-5000 m during the early Eocene (Rowley & Currie, 2006; L. Ding et al., 2014; Xu et al., 2013; Xiong et al., 2020; C. Wang et al., 2014). The robustness of this method is however questioned by isotope-enabled climate models demonstrating that other factors than elevation affect the $\delta^{18}O$ precipitation signature, such as the air masses provenance, climate change, or water recycling (Poulsen & Jeffery, 2011; Botsyun et al., 2016). Considering these additional factors, a revised Ti-

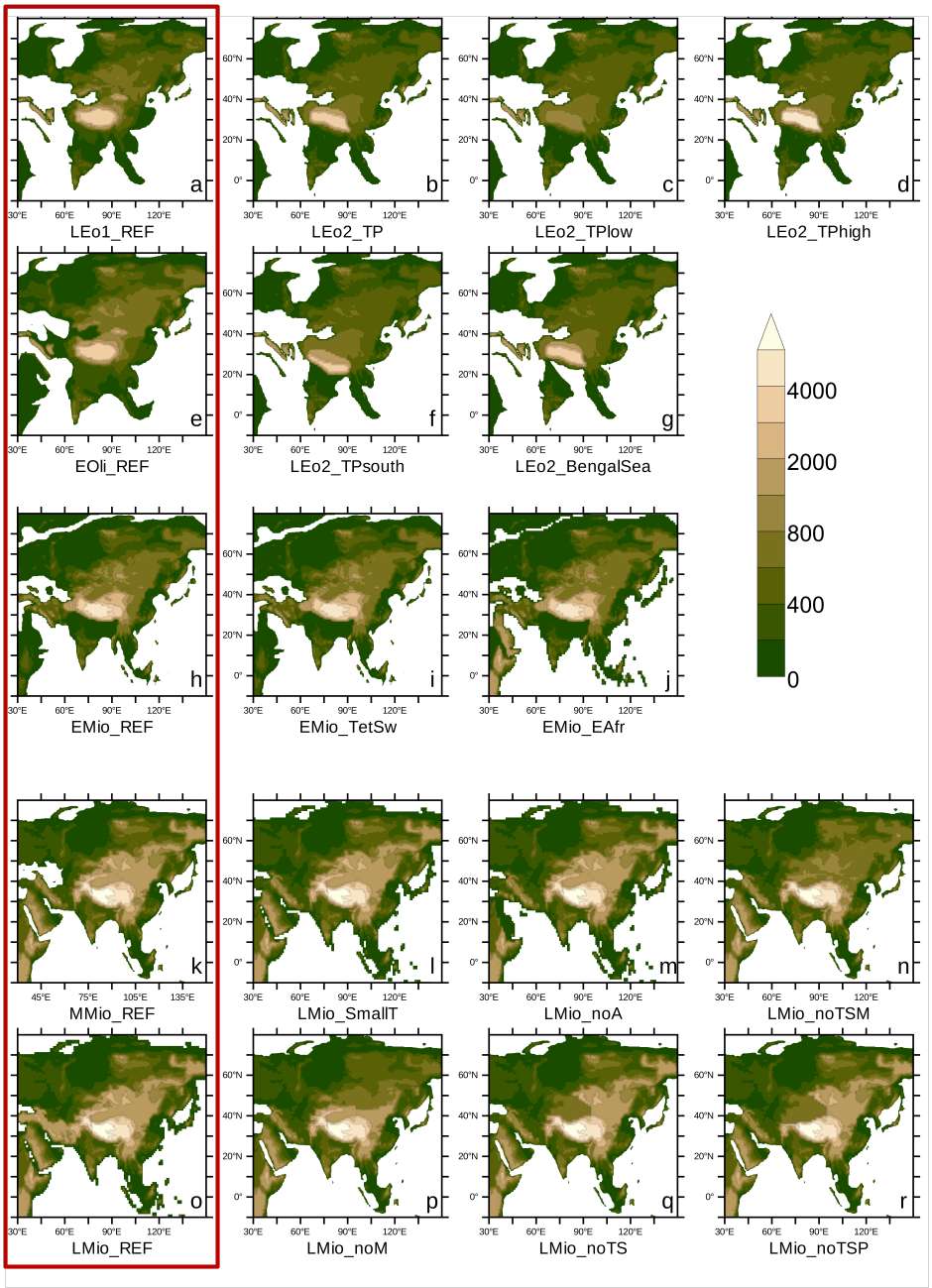

Figure 3. paleogeographic configurations used in this study. (**a,e,h,k,o**) Reference paleogeographic configurations for the late Eocene (∼40 Ma), early Oligocene (∼34 Ma), early (∼20 Ma), mid (∼12 Ma) and late Miocene (∼8 Ma) are aligned in the first column (red box). Alternative configurations used for sensitivity tests are also presented, for the late Eocene (**b,c,d,f,g**), the early Miocene (**i,j**) and the mid to late Miocene (**l,m,n,p,q,r**)

betan Plateau paleo-elevation, most likely inferior to ∼3000 m in the Oligocene, is suggested (Botsyun et al., 2019). The presence of frost-intolerant fossil flora assemblage in Central TP in the middle Eocene (T. Su et al., 2020) and late Oligocene (T. Su, Farnsworth, et al., 2019), as well as clumped isotope measures (Xiong et al., 2022), advocating for a subtropical climate in this region, seems incompatible with a TP exceeding 4000 m. Therefore, a more complex morphology for this proto-TP, with the presence of a low-elevated (∼1500 m) valley dividing the almost fully uplifted (∼3000-4000 m) Lhasa and Qiangtang terranes until the late Oligocene has been proposed (T. Su, Farnsworth, et al., 2019; Xiong et al., 2020; R. Spicer et al., 2020; Xiong et al., 2022).

In the periphery of the proto-TP, data collected from different basins offer contradictory information. In southeastern Tibet, at the extremity of the Qiangtang terrane, T. Su, Spicer, et al. (2019) use paleo-elevation calculated from the CLAMP method to suggest that the Markam Basin was already high in the late Eocene (∼3000 m) and could have reached its modern elevation (∼3900 m) by the earliest Oligocene. Alternately, paleo-elevation based on oxygen isotopic measurements of the nearby Jianchuan Basin (belonging to the Qiangtang terrane as well) could have not exceeded ∼1200 m in the late Eocene (Gourbet et al., 2017). The northern TP is proposed to remain relatively low (maximum ∼2000 m) in the Eocene before uplifting in the Oligocene or the early Miocene, based on $\delta^{18}O$ measurements from the Hoh Xil Basin (Cyr et al., 2005; C. Wang et al., 2014). An early uplift of the northeastern TP is however suggested as early as the late Eocene by increased coniferous pollen proportion in the Xining Basin (Hoorn et al., 2012), although cooling and Paratethys Sea retreat were also shown to promote coniferous trees expansion in this region (Barbolini et al., 2020).

The history of the TP build-up from the Miocene onward is less controversial. The Central TP would have reached modern elevation by the early Miocene, while the northern TP uplift is completed by the late Miocene (C. Wang et al., 2014). Stratigraphy and detrital zircon analysis indicate that the western TP (Pamir-Karakoram-Hindu Kush) may have underwent several phases of uplift between the mid Eocene to latest Miocene (Bershaw et al., 2012; L. Li et al., 2021; Blayney et al., 2016; Carrapa et al., 2015). Finally, the Himalayas start uplifting in the early Miocene (∼20 Ma) and reach their modern elevation by the mid-late Miocene (∼15 Ma) (Gébelin et al., 2013; L. Ding et al., 2017; Xu et al., 2018; C. Wang et al., 2014; Webb et al., 2017).

4.1.3 Inland Asia and Myanmar mountain building

Asian terranes located in the vicinity of the HTP complex are impacted by the Indo-Asian collision. In Myanmar, the Sino and Indo-Burman Ranges have distinct uplift histories. Indo-Burma ranges build-up in a three-step process in the late Eocene, at the Oligo-Miocene boundary and Pliocene respectively (Najman et al., 2020; Morley, 2018; Maurin & Rangin, 2009; Westerweel et al., 2020; Licht et al., 2018), as a result of the progressive indentation of the Burma block into the Eastern Himalayan collision zone. The Sino-Burman Ranges inherited old landforms from previous collisions between Indochina and Sibumasu terranes (Metcalfe, 2013) and experienced major uplift in the mid-late Miocene (∼13-9 Ma) (Cook & Royden, 2008; Clark et al., 2005), as a result of the Tibetan crustal flow eastward propagation.

North of the Tibetan Plateau, the collision propagated through reactivated pre-existing tectonic structures and triggered the uplift of the inland Asia orogenic belt: the Tian Shan and the Mongolian (Altai, Hangay and Sayan) landforms (Jolivet et al., 2010). The southwestern and Central Tian Shan uplift initiation is very loosely constrained, either in the middle to late Miocene (∼15 Ma, (Käßner et al., 2016)), late Oligocene to early Miocene (∼25 Ma, (Bande et al., 2017; Macaulay et al., 2016, 2014)), or in the Eocene-Oligocene (D. Liu et al., 2017; Tapponnier & Molnar, 1979). The northeastern Tian Shan, together with the Sayan and Altai regions (in western Mongolia), likely remained quiescent until the

late Miocene (Bullen et al., 2003; Caves Rugenstein et al., 2017). After a global pulse of uplift at the latest Miocene (∼8 Ma) for the whole Tian Shan, Sayan and Altai mountains (W. Yuan et al., 2006; Caves Rugenstein et al., 2017; Charreau et al., 2005), regional landforms would have reached their full elevation after a last Pliocene uplift phase (∼5-3 Ma, (Bullen et al., 2003; Caves Rugenstein et al., 2014; De Grave et al., 2007, 2009; Jolivet et al., 2007; Vassallo et al., 2007)). The Hangay Dome uplift (in central Mongolia) began in the mid-Oligocene (Caves Rugenstein et al., 2014; Cunningham, 2001), but the date of completion of the uplift remains debated, either in the mid-Miocene (∼13 Ma, (Smith et al., 2016)), or the Pliocene (∼3 Ma, (Yarmolyuk et al., 2008)).

4.1.4 Evolution of Asia in our reference paleogeographic configurations and sensitivity experiments performed

Our late Eocene reference paleogeography (**LEo1_REF**, ∼40 Ma, Fig. 3 a), previously introduced in (Tardif et al., 2020), displays a fully emerged *Greater India* and a TP elevation set to ∼3000 m. Considering the persistent controversy surrounding the extension of India and the TP morphology at that time, other configurations are tested to better understand the sensitivity of our results to these features. **LEo2_TP** (Fig. 3 b) is an alternative late Eocene paleogeography, with a slightly different Tibetan Plateau shape (obtained with the "double collision model" in Poblete et al. (2021)), from which we derived sensitivity tests with a lowered Tibetan Plateau (∼800 m, **LEo2_TPlow**, Fig. 3 c) and a high Tibetan Plateau (∼4500, **LEo2_TPhigh**, Fig. 3 d). Two additional tests are performed, with a Tibetan Plateau translated more to the South (**LEo2_TPsouth**, Fig. 3 f), obtained with the collision model from Jagoutz et al. (2015) and the presence of a remaining Bengal Sea (**LEo2_sea**, Fig. 3g), obtained with the collision model from D. J. J. van Hinsbergen et al. (2012); D. J. van Hinsbergen et al. (2019).

The early Oligocene simulation (**EOli_REF**, ∼33 Ma, previously introduced in Barbolini et al. (2020)), is designed to represent the Asian climatic state right after the Eocene-Oligocene Transition (Fig. 3 e). We use the same late Eocene paleogeography from LEo1_REF, in which the sea level is lowered by 70 m to account for an ice sheet over Antarctica with a modern extent (it is an end-member scenario). This leads to important changes in terms of land-sea distribution, principally in the Paratethys Sea region, detailed in section 4.2.3.

The early Miocene paleogeography (**EMio_REF**, ∼20 Ma, Fig. 3 h) (previously introduced in Sarr et al. (2022) and Burls et al. (2021), from Poblete et al. (2021)) displays an Indian subcontinent translated 5° further north compared to the Eocene, and an uplifted Central TP close to its present elevation (∼5000 m), while western and northeastern TP portions are lower (∼2000-3000 m). In the middle (**MMio_REF**, ∼12 Ma, Fig. 3 k) and late Miocene (**LMio_REF**, ∼8 Ma, Fig. 3 o) paleogeographic configurations, the Himalayas and Tibetan Plateau have reached their present day configuration, along with the peripheral landforms in Myanmar and inland Asia (Fig. 3). Sensitivity tests are performed on inland Asian landforms, lowering to ∼800 m the elevation of Mongolia (**LMio_noM**, Fig. 3 p), the Tian Shan (**LMio_noTS**, Fig. 3 q), both Mongolia and Tian Shan (**LMio_noTSM**, Fig. 3 n), and finally, the Tian Shan and Pamir (**LMio_noTSP**, Fig. 3 r).

4.2 The Peri-Tethys region evolution under the complex interplay of tectonics and global sea level changes

Throughout the Cenozoic, global sea level fluctuations in an active tectonic convergence context have lead to a profound paleogeographic reorganization and a general increase in continentality of the regions encompassing the Mediterranean Sea, Middle East and inland Asia. We resume here the main paleogeography changes (in terms of sea connections between Indian, Atlantic and Arctic Oceans).

4.2.1 Retreat of the Paratethys Sea and closure of the Neotethys Ocean

During the Paleocene-Eocene, Eurasia is largely flooded by the proto-Paratethys, an epicontinental sea connected to the Arctic Ocean *via* the Turgai Strait and to the Neotethys Ocean (Meulenkamp & Sissingh, 2003; Golonka, 2009). Paleoenvironmental analysis suggest a maximal extension of the proto-Paratethys Sea reaching the Tajik and Tarim Basins, in inland Asia, at the Paleocene-Eocene transition (∼56 Ma), followed by a long-term westward retreat, punctuated by marine transgressions of decreasing magnitude (Kaya et al., 2019; Bosboom et al., 2014b, 2017; Carrapa et al., 2015). In Central Asia, the shrinkage of the proto-Paratethys Sea during the Eocene is attributed to far-field effect of the Indo-Asia collision and to the early indentation of the Pamir and TP, leading to the progressive basins infilling with sediments (Kaya et al., 2019; Carrapa et al., 2015). The build-up of the Antarctic ice-sheet initiated in the late Eocene, resulted in a sea-level drop that culminated at the EOT (∼33.5 Ma, sea-level fall estimated at ∼70 m by Miller et al. (2020)), which drastically reduced the extent of the Paratethys and favored its isolation (Kaya et al., 2019; Bosboom et al., 2014b, 2017). Water exchanges between the Paratethys and global oceans are progressively restricted, as attested by δ^{18}O and δ^{13}C of foraminifera shells diverging increasingly from global oceanic signals at that time (Ozsvárt et al., 2016). The Paratethys Sea is fully isolated from the Mediterranean Sea at ∼12 Ma, with the final uplift of the Dinarides belt (Harzhauser & Piller, 2007). A connection with the Mediterranean Sea is restored between 6.9–6.1 Ma when the Aegean region subsides during the latest Miocene (Krijgsman et al., 2020).

The Tethyan Seaway (or Mesopotamian Seaway) which connected Indian and Atlantic Oceans remained fully open before the Miocene (Straume et al., 2020). ϵNd data suggest that it became strongly restricted around ∼22 Ma (Bialik et al., 2019), with intermittent periods of closure, as attested by evidence of mammal exchanges between Eurasia and Africa through the Gomphotherium landbridge (Rögl, 1999; Harzhauser & Piller, 2007). The Tethyan Seaway permanently closed at ∼14 Ma (Bialik et al., 2019), due to combined effect of Arabian-Eurasian plates collision and glacio-eustatic sea level fall associated with the cooling following the Mid-Miocene Climatic Optimum (MMCO).

4.2.2 Middle-East: Eastern Anatolian-Iranian Plateau and Zagros Mountains

The Middle-East experienced multiple changes in land-sea distribution and topography, forced by the collision of the Arabian plate with Eurasia, which drove the uplift of the Zagros mountains and of the Iranian Plateau. The exact timing of the Arabia-Eurasia collision in eastern Anatolia remains highly debated with estimated date ranging from the Eocene-Oligocene (Karaoğlan et al., 2016; Darin et al., 2018; McQuarrie & Hinsbergen, 2013; Pirouz et al., 2017), the early Miocene (Okay et al., 2010; Gülyüz et al., 2020), to the late Miocene (H. Su & Zhou, 2020; Z. Zhang et al., 2017). Most studies however propose an early Miocene age (∼20 Ma) for the hard collision related to the arrival of thick Arabian crust along the Bitilis suture zone (Okay et al., 2010; Cavazza et al., 2018; Gülyüz et al., 2020). After the collision, the Zagros orogen built up during three successive pulses occurring within the last ∼20 Ma (Agard et al., 2011; Mouthereau, 2011).

The Alborz mountains uplift (northwest of the Zagros) is dated during the middle Miocene (∼17.5-13 Ma), according to sediments stable isotopic signatures (Ballato et al., 2010, 2015) and may have continued until the latest Miocene (Mouthereau et al., 2012). A Miocene age for the commencement of the eastern Anatolian Plateau growth has been estimated based on the youngest marine unit of the eastern Anatolian Plateau (∼17 Ma) (Gülyüz et al., 2020) and apatite fission-track data (18-13 Ma) (Okay et al., 2010; Karaoğlan et al., 2016). Stratigraphic evidence suggest a rise due to crustal shortening and thickening occurring between 15 and 12 Ma (Mouthereau et al., 2012). Numerical simulations suggest a buildup of the Plateau within ∼15-20 Ma after the continental collision, likely sustained

by slab break-off, mantle flow disruption and associated changes in dynamic topography, followed by isostatic adjustment (François et al., 2014). With this mechanism, the modern elevation (∼1500 m.a.s.l) is only reached during the late Miocene (∼7-10 Ma).

4.2.3 Evolution of the Peri-Tethys region in our reference paleogeographic configurations and sensitivity experiments performed

Our paleogeographic reference configurations are consistent with the geological history of the Paratethys Sea demise and with uplift phases in the region. In our late Eocene geography (**LEo1_REF**, Fig. 3 a) the proto-Paratethys Sea fills the Tarim Basin ; it is still connected to the Neotethys and Indian Oceans, but not to the Arctic, as the Turgai Strait is already closed. In the Oligocene reconstruction (**EOli_REF**, Fig. 3 e), the 70 m sea level drop (Miller et al., 2020)) leads to the emergence of continental portions in Arabia and North-Africa, and to the drying of the Tarim Basin and lowlands north of the Turgai Strait, which all conspire to increase greatly Asian continentality. The former shallow connection between the Paratethys and the Tethys ceases in the Pamir-Zagros region at that time. In the early Miocene geography (**EMio_REF**, Fig. 3 h), an emerged land-bridge interrupts the Tethyan seaway that previously connected the Mediterranean Sea and the Indian Ocean, but shallow sea persists at the location of the present-day Arabian Peninsula. Given the uncertainty surrounding the precise closure time of the seaway, an alternative early Miocene configuration is also tested, with a 120 m deep Tethyan seaway (**EMio_TetSw**, Fig. 3 i). In the middle Miocene reference simulation (**MMio_REF**, Fig. 3 k), the Iranian Plateau and Zagros mountains are halfway uplifted (∼1000 m) compared to present-day and the Paratethys extends up to 60°E. By the late Miocene (**LMio_REF**, Fig. 3 o), the Paratethys is strongly reduced and the Iranian landforms have reached their modern elevation. An intermediate reconstruction is proposed, testing the impact of the Paratethys retreat only, in the mid-late Miocene (**LMio_smallT**, Fig. 3 l). Note that LMio_smallT is the mid-late Miodene paleogeography to which all others late and middle Miocene simulations can be compared to, to single out the effect of regional changes.

4.3 East Africa and Arabian Peninsula evolution

While much attention has been paid to the Eastern African topography evolution in the Neogene due to its implication on early hominins development, its history fits in a broader paleogeographic context rooted in the late Eocene to early Oligocene times (see Couvreur et al. (2021); Guillocheau et al. (2018) for a synthesis). Landforms in East Africa (Kenyan and Ethiopian plateaux) developed during the late Cenozoic, triggered by a combination of tectonics, basaltic flooding, and large wave-length deformation related to the African superswell activity (Moucha & Forte, 2011; Faccenna et al., 2019; Roberts et al., 2012). Uplift in the Ethiopian region would have began during the Eocene, with doming event sustained by dynamic topography (Roberts et al., 2012; Faccenna et al., 2019) that then propagates to Kenya during the middle Miocene. In the early Oligocene, basaltic flooding in Ethiopia would have contributed to the formation of these large-scale elevated features (Sembroni et al., 2016). Rifting initiated during the middle Miocene, with main uplift of rift shoulders (Wichura et al., 2015). Overall, past elevations in the course of the Cenozoic are poorly constrained in East Africa, but modern elevations were most likely reached by the late Miocene to early Pliocene (Couvreur et al., 2021).

4.3.1 Arabian Peninsula

The Arabian Peninsula records successive marine and freshwater environments from the early Oligocene to the late Miocene, as attested by paleo-ichthtyofaunas (Otero & Gayet, 2001). Before the Neogene, the Arabian plate is assumed to be flat and low elevated (Daradich et al., 2003), making it particularly sensitive to sea-level changes. It is therefore largely submerged during the Eocene, and its southwestern part becomes par-

tially emerged after the sea-level fall at EOT (Barrier et al., 2018). During the Miocene, the Arabian plate is tilted when transiting over the East-Africa mantle plume (Vicente de Gouveia et al., 2018), leading to the uplift of the Red sea margin, and the flooding of its northeastern corner, due to mantle convective drawdown (Daradich et al., 2003; Moucha & Forte, 2011). This mechanism favored temporary transgression phases in the subdued northeastern region in early Miocene times (Barrier et al., 2018), until its full emergence in the late Miocene, possibly favored by global sea-level fall after the MMCT (Golonka, 2009; Harzhauser & Piller, 2007; Miller et al., 2020).

4.3.2 Evolution of East Africa and Arabia in our reference paleogeographic configurations and sensitivity experiments

Our reference paleogeographic configurations (Fig. 3 a,e,h,k,o) display a low East Africa during the Eocene-Oligocene, which rises to ∼750-1,000 m in the early Miocene and a modern-like elevation in the mid and late Miocene reconstructions. Given the large uncertainties on east African topography precise elevation, we perform a sensitivity experiment on an early Miocene paleogeography, with fully uplifted east African landforms (**EMio_EAfr**, Fig. 3 j). Additionally, a mid-late Miocene configuration displaying an almost fully flooded Arabian Peninsula is tested (**LMio_noAr**, Fig. 3 m), to account for its high sensitivity to sea level fluctuations at that period.

5 Materials and Methods

5.1 IPSL-CM5A2 model

We performed the simulations with the IPSL-CM5A2 Earth System Model (Sepulchre et al., 2020), an updated version of the IPSL-CM5A model (Dufresne et al., 2013) suitable for deep-time paleoclimate simulations. It is composed of the atmospheric model LMDz5A (Hourdin et al., 2013), the land surface and vegetation model ORCHIDEE (Krinner et al., 2005) and the oceanic model NEMO (v3.6) (Madec, 2016) that also includes the LIM2 model (Fichefet & Maqueda, 1997) for sea-ice. OASIS coupler ensures synchronization between the different model components (Valcke et al., 2006). Atmospheric component has a nominal horizontal resolution of 96x95 grid points (3.75° in longitude by 1.9° in latitude) with 39 irregularly distributed vertical levels from the surface to 40 km high. The land surface ORCHIDEE model is coupled with LMDZ5a and redirects runoff water toward the ocean. The vegetation cover is represented through 11 Plant Functional Types (PFTs), including one describing bare soil. NEMO uses a tripolar grid, with two poles in the Northern hemisphere to avoid singularity (Madec & Imbard, 1996). It has a resolution of 2° by 2° refined at 0.5° in the equatorial region, with 31 vertical levels, whose thickness span from 10 meters near the surface to 500 meters in the deep ocean. Full description of IPSL-CM5A2 can be found in Sepulchre et al. (2020); Dufresne et al. (2013).

IPSL-CM5A2 has been previously used for paleoclimatic simulations of the Miocene (Burls et al., 2021; Sarr et al., 2022) and the Eocene (Toumoulin et al., 2020; Tardif et al., 2020; Barbolini et al., 2020; Tardif et al., 2021; Toumoulin et al., 2022). The ability of the model to simulate the modern Asian climate was previously assessed (Sepulchre et al., 2020; Tardif et al., 2020) and a comparison with observations is provided (SI, Fig. 15). While general atmospheric circulation patterns are well reproduced, IPSL-CM5A2 overall underestimates precipitation amounts and delays inland monsoonal precipitation onset by about a month, a feature shared with IPSL-CM5A version (Sepulchre et al., 2020; Valdes et al., 2017).

5.2 Experiments design

The boundary conditions are summarized in Table 1. Experiments at Late Eocene are considered ice-free, as pCO_2 is above the threshold for permanent Antarctic glaciation

(Ladant et al., 2014; DeConto & Pollard, 2003). Unipolar glaciation, with Antarctic ice-sheet only, is used for the Oligocene and early Miocene and both Greenland and Antarctic ice-sheets are accounted for in the late Miocene (Bierman et al., 2016) configurations. CO_2 concentration varies from 1,120 ppm for the late Eocene to 560 ppm in the late Miocene (Table 1) Foster et al. (2017); Rae et al. (2021), while other greenhouse gases are kept at preindustrial values. Given the persistent uncertainties regarding precise pCO_2 concentration during the Cenozoic, we performed two additional sensitivity tests on this parameter, in the late Eocene (**LEo1_2X**, 560 ppm), and in the late Miocene (**LMio_1.5X**, 420 ppm). The solar constant was adjusted according to Gough (1981) and set to 1360.19 $W.m^{-2}$ for late Eocene and early Oligocene simulations, to 1362.92 $W.m^{-2}$ for early Miocene simulations and to 1364.30 $W.m^{-2}$ for late and middle Miocene simulations. Although orbital variations are known to impact monsoonal circulation (Zhisheng et al., 2015; P. Wang et al., 2005; Tardif et al., 2021), we prescribed a modern-like configuration to focus on the impact of paleogeography on the monsoon system. Considering the lack of congruent global vegetation reconstruction over the Cenozoic, the same PFT map was used throughout the experiments, prescribing latitudinal bands of idealized vegetation cover based on modern distribution, as done in previous studies (Tardif et al., 2020; Laugié et al., 2020). The reference experiments have been run for 3000 years and deep ocean layers reached quasi-equilibrium after ∼2000 years of integration. Sensitivity experiments were restarted from there reference experiments an run for 300 to 500 years until reaching stable sea surface temperatures. Model outputs are averaged over the last 50 years.

5.3 Monsoon metrics

The evolution of Asian monsoons back in time is assessed through specific markers that are characteristic of the present-day phenomenon. We favored SAM and EAM features offering means of comparison with paleoclimate records, which typically involve precipitation amounts, seasonality and wind direction and strength. Several features of the monsoons, however, are not recorded by proxies, or in a very indirect way. This is for example the case of the pressure patterns, and of all mid-to-high tropospheric features associated with the modern monsoons. In that aspect, numerical simulations are a valuable tool to grasp the full signature of eventual paleo-monsoons.

For both SAM and EAM, we evaluated the evolution of precipitation seasonality using the Monsoon Precipitation Index (MPI) (B. Wang & Ding, 2008), expressed as follow:

$$\mathrm{MPI} = \frac{\text{Seasonal range of precipitation}}{\text{Mean annual precipitation}}$$

where the seasonal range of precipitation is the difference between May to September (MJJAS) precipitation minus November to March (NDJFM) precipitation. Regional occurrence of a monsoon-like seasonality is considered providing a seasonal range superior to 300 mm and a majority of precipitation falling during the extended summer season (MPI > 0.5). This criteria has the benefit of not being exclusive (with or without monsoon), as it proposes a discrete metric for seasonality amplitude (from 0 to 1). It also imposes the wet season to be in summer, as in the present-day monsoon region, as opposed to other existing precipitation metrics (such as the ratio of the 3 wettest month over the 3 driest month precipitation, commonly used in paleobotanic studies), which enables us to test the presence of modern-like climate patterns.

The wind patterns, described through their shape and strength, are the second fundamental characteristic observed. The latitudinal migration of the Somali Jet is tracked over the Arabian sea (Fluteau et al., 1999). The wind shear between low and high troposphere over India, that describes the vigor of the SASM zonal circulation and its inclusion in the Walker circulation, is calculated through the Webster-Yang Index (U_{850}-U_{200}, calculated in an area from 0°:20°N to 40°E:110°E) (Webster et al., 1998). The positive thermal anomaly

observed at 200-300 hPa over northern India in summer has additionally been used as a marker of the deep convection characterizing the modern SASM (Boos & Kuang, 2010; Acosta & Huber, 2020). This feature is due to the important latent heat release provoked by the condensation of moisture in convecting air masses and in air masses ascending on the southern flank of the Himalayas, which heat the high troposphere (see Fig. 14 c). Fewer criteria exist to formally describe the EAM. In addition to the precipitation seasonality described through the Monsoon Precipitation Index, we tracked the EASM via the description of the latitudinal displacement of the Jet Stream with respect to Tibetan and inland Asia landforms, and the surface wind patterns that constitute the Meiyu-Bayu front at present-day. The EAWM is tracked principally through the evolution of temperature and pressure gradients, leading to the Siberian High formation in winter, and of its associated wind patterns. Here we used the EAWM index defined by L. Wang and Chen (2014) that accounts for both the North-South (Siberia-Maritime continent) and West-East (Siberia-North Pacific) pressure gradients and is expressed as follow:

$$I_{EAWM} = (2xSLP_S\text{-}SLP_{NP}\text{-}SLP_{MC})/2$$

where SLP_S, SLP_{NP} and SLP_{MC} is the area-averaged Sea Level Pressure (SLP) over Siberia (40°:60°N, 70°:120°E), North Pacific (30°:50°N, 140°E:170°W) and the Maritime continent (20°S:10°N, 110°:160°E), respectively.

6 Results

We present the results obtained for the five reference simulations as well as for the different sensitivity numerical experiments, first for the South Asian Monsoon, then for the East Asian Monsoon domain. Main outcomes in terms of seasonal winds and precipitations are qualitatively summed up in Table 6.

6.1 South Asian summer monsoon controlled by the orography surrounding the Indian Ocean

6.1.1 Spatial and seasonal precipitation patterns evolution

In the late Eocene a wide arid region (< 500 mm/yr) spreads from northern India to north of the proto-Tibet (Fig. 4 a). High mean annual precipitation amounts (> 3000 mm/yr) are simulated over equatorial regions, in southern India and southeastern Asia. There is no monsoon-like seasonality according to the MPI index in India, because the rainy season in this region occurs in winter (as previously described in Tardif et al. (2020)). The precipitation pattern evolves from the early Oligocene onward, with the progressive translation of the arid region to Arabia and Northern Africa (Fig. 4 e,i,m,q). This in turn allows the penetration of rainfall in summer in South-Eastern Asia, and the onset of a monsoon-like seasonality in this region, as well as a reinforcement of monsoon-like seasonality in Eastern Asia.

In the course of the Miocene, as India drifts northward, its southern tip receives less precipitation (∼1500 mm/yr in the late Miocene, Fig. 4 q), and the intensity and extent of highly seasonal precipitation increases greatly over southern and eastern Asia (red dotted regions in Fig. 4 e,i,m,q). Orographic precipitation over the southern flank of the Himalayas initiate by the mid Miocene simulation (∼900 mm/yr, Fig. 4 m), and further increase in the late Miocene (∼1200 - 1500 mm/yr, Fig. 4 q). These changes in precipitation patterns in both space and time are triggered by a profound reorganization of surface pressure patterns and winds throughout the Cenozoic.

Overview of the effect simulated in each region. Abbreviations stand for Transition Area (TA), cardinal directions (E, W, S, N), Basins mentioned in Fig. 1 (eg. Tadjik I

	SAM				EAM					Inland Asia	
	Precipitation			Winds	Precipitation			Winds		Precipitation	
	Winter	Summer	Seasonality	Summer	Winter	Summer	Seasonality	Summer	Winter	Winter	Summer
No TP (LEo)	~	++			+	- -	-	~	+ (W)	~	~
High TP uplif (LEo)	~	+	~		++	+	-			-	~
TP South (LEo)	-	+			~	+	+			~	~
Bengal Sea (LEo)	+	++	-		+	+	~			+	+
CO2 decrease (EOT)	- -	++	+ (TA)	+	+	~	~	~	+	+	+
CO2 and sea level fall (EOT)	- - -	+++	+ (TA, North. India)	++	- -	++	+	+ (E)	++ (W/ NW)	- -	+
East Africa uplift (EMio)	+	++	- (India) + (TA, Himalaya)	+++ (Somali Jet)	+	+	-	+ (SW)		+	-
Paratethys retreat (LMio)	~	++	+	++	+	+	~	+(SW)		- -	~
Arabian peninsula emergence (LMio)	+	+	~	+ (Somali Jet)	-	+	+	~	+ (NW)	-	-
Iranian uplift (LMio)	- -	++	+++	+++ (Somali Jet)	-	+	+			+	++
Mongolia uplift (LMio)	~	~	+		- - -	~	+++		+++ (NW)	+ (orog.)	++(orog) - - (Gobi, Takl., TS, Tjk)
TienShan uplift (LMio)	+	~	-		-	~	+	+ (S)		+(orog.) - - (Gobi Takl.)	+(orog.)
TienShan+Mongolia uplift (LMio)	+	~	+		- - -	~	+ + +		+++ (NW)	+(orog.) -(Gobi)	+(orog.) -(Takl. Tjk.)
TienShan+Pamir uplift (LMio)	+	+	- -	+ (Somali Jet)	~	~	~	+ (SW)		+(orog.) -(Gobi, Takl.)	++(orog.) -(Tjk)

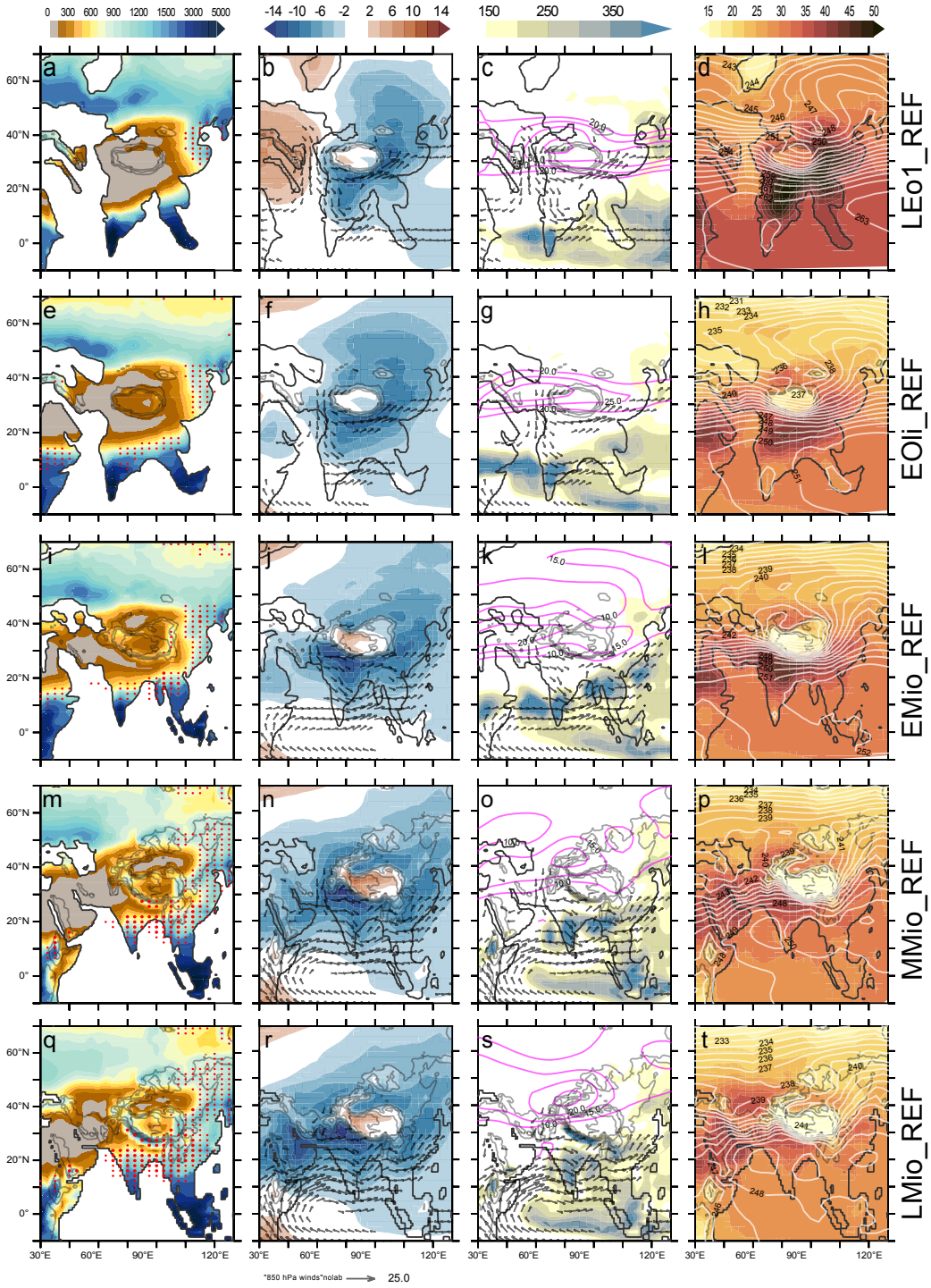

Figure 4. Evolution of the summer monsoon diagnostics since the Eocene. **First column:** Mean Annual Precipitation (shading, mm/yr) overlain with regions where the Monsoon Precipitation Index is over 0.5 (thin red dots) and 0.75 (thick red dots); **Second column:** June-August (JJA) normalized Sea Level Pressure (SLP) anomaly defined as the difference between summer SLP and mean annual SLP (shading, hPa) and 850 hPa winds over 4 m/s (vectors); **Third column:** August Jet Stream speed (magenta contour, maximal zonal wind velocity in the mid to high troposphere, in m/s), August monthly precipitation amounts (shading, mm/month) and 850 hPa winds over 4 m/s (vectors) ; **Fourth column:** JJA mean temperature at 2m (shading, Celsius) and 300 hPa atmospheric temperature (white contour, Kelvin). On all captions, topography is overlain in gray contour each 1000 m.

6.1.2 Summer pressure and wind patterns reorganization

The summer (June to August, JJA) sea level pressure (SLP) patterns in Eurasia in the late Eocene experiment (Fig. 4 b) contrast strongly with the modern ones (Fig. 14 d). While a low-pressure center driven by extreme summer temperature forms over southeastern Asia (up to 50°C over *Greater India*, Fig. 4 d), the Paratethys Sea and Neotethys Ocean are the locus of a wide high pressure cell (Fig. 4 b). This induces low tropospheric anticyclonic wind patterns, that counteract potential moisture advection from the Indian Ocean towards South Asian regions. From the early Oligocene onward, the Paratethys Sea and Neotethys shrinkage increase the Eurasian continentality and emerging landforms, such as Anatolia and Arabia, become the locus of high summer temperature (35-45°C, Fig. 4 l,p,t). This leads to the progressive widening of the South Asian low-pressure belt, while the Neotethyan anticyclone gradually regresses westward (Fig. 4 f,j,n,r). This low pressure cell reaches its modern-like extent in the mid Miocene simulation (Fig. 4 n), but only attains its current values (∼-14 hPa over Arabia and northern India) by the late Miocene (Fig. 4 r).

Mirroring this progressive strengthening and widening of the summer low-pressure belt over South Asia and Arabia, humidity-loaded air masses are gradually advected from the Indian Ocean towards the continent over the Cenozoic. A weak cross equatorial flow (<4 m/s against ∼25 m/s today), confined to low latitudes (<10°N, Fig. 5 a, simulations LEo1_REF and EOli_REF) is simulated over the Arabian Sea in the late Eocene and early Oligocene experiments (Fig. 4 b,f). A proto-Somali Jet, mostly zonal and confined to low latitudes (<11°N) is simulated in the early Miocene simulation (Fig. 5 b, simulation EMio_REF). From the mid Miocene onward, and following the reinforcement of the Asian low-pressure belt, the now fully-formed Somali Jet increases in strength and migrates further north over the Arabian Sea (∼18-24°N) (Fig. 4 n,r and Fig. 5 b, simulations MMio_REF and LMio_REF).

The simulated tropospheric circulation above southern Asia deeply evolves since the Late Eocene, as exemplified by the calculation of the Webster-Yang Index. This index doubles between the late Eocene and the early Oligocene (from ∼5 to 11 m/s, Fig. 5 c, reference simulations LEo1_REF and EOli_REF), and keeps increasing through the Miocene (from ∼16 to 21 m/s, Fig. 5 d, simulations EMio_REF, MMio_REF and LMio_REF). Finally, while heating of the high troposphere (∼300 hPa) due to deep convection is observed in most experiments (Fig. 4 d,h,l,p,t), its settlement over Northern India is only reached by the mid Miocene experiment, following the increase in summer convective precipitation in this region driven by orographic lifting.

6.1.3 Limited effect of pCO_2 drawdown and Tibetan Plateau changes on South Asian summer monsoon evolution

The non-linearity in the response of the Somali Jet through time calls for a more thorough analysis of the different forcing at stakes between each of these simulations. In this section, we take advantage of our different alternative paleogeography reconstructions and $p\mathrm{CO}_2$ to attribute the simulated changes to their respective underlying drivers. Overall, the SASM presents a low sensitivity to $p\mathrm{CO}_2$ changes, when compared to paleogeographic forcings. This is true for the late Eocene experiments, where a change from 1120 ppm to 560 ppm only induces minimal variations in the WYI (Webster-Yang Index) strength, summer northward ITCZ migration (difference between experiments LEo1_2X and LEo1_REF in Fig. 5 a,c), or monsoon-like seasonality extension (Fig. 7 f). This is also the case for the late Miocene experiments, with a switch from 560 ppm to 420 ppm (difference between experiments LMio_1.5X and LMio_REF in Fig. 5 b,d).

The paleogeography of *Greater India* and Tibetan regions have been recurrently proposed as a driver of monsoon onset or intensification (R. Zhang et al., 2012; Yu et al., 2018; Molnar et al., 1993). While alternative TP configuration lead to slightly different results (detailed below), their impact on the SASM large-scale wind circulation remains limited in

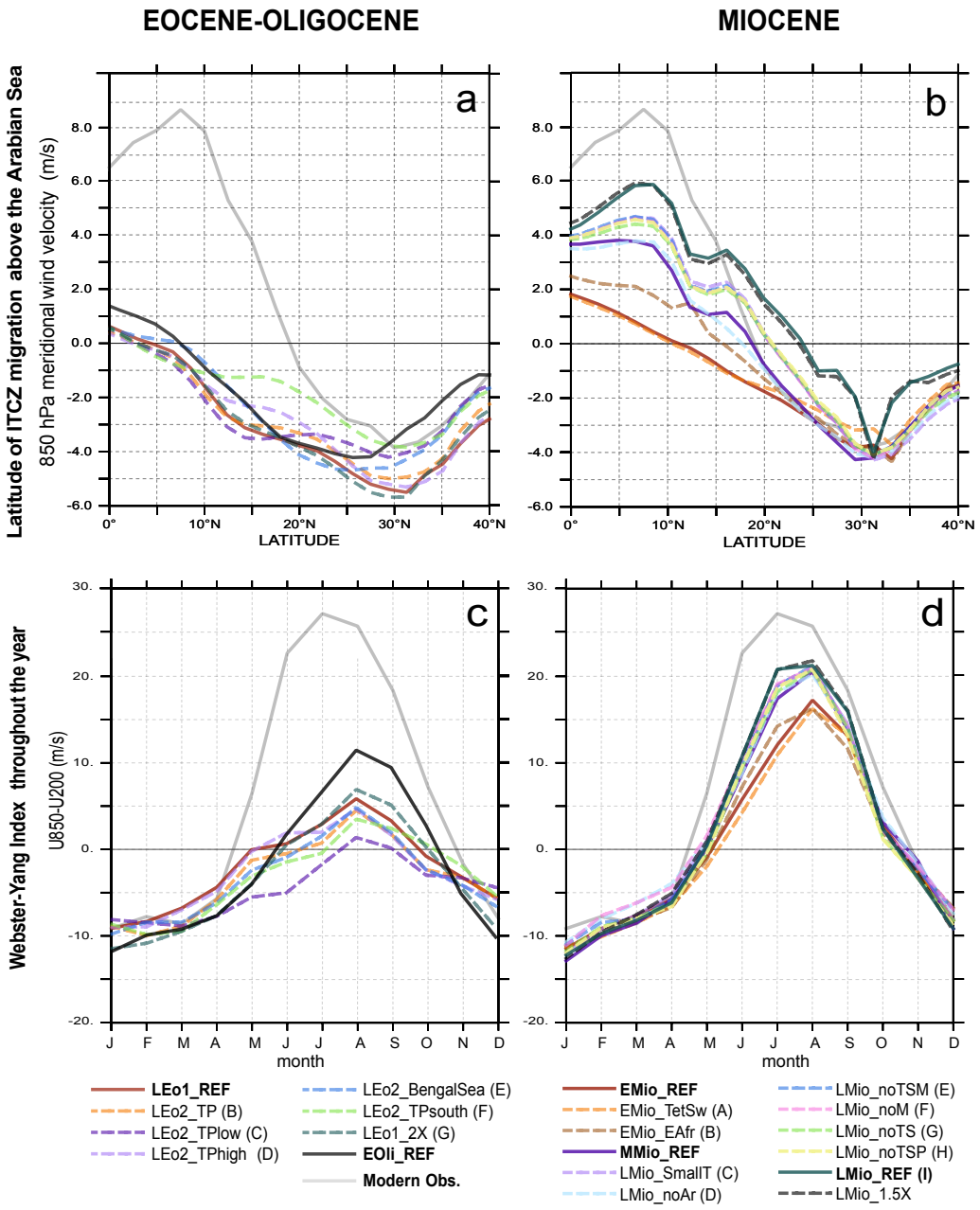

Figure 5. Estimation of the South Asian monsoon strength evolution in all the simulations via: (**a,b**) the calculation of the summer (JJA) cross-equatorial flow latitude over the Arabian Sea, after Fluteau et al. (1999) and (**c,d**) the calculation of the Webster-Yang Index (850 hPa minus 200 hPa zonal wind velocity, in the region 0:20 °N ; 40:110 °E, after Webster and Yang (1992)). For better readability, the experiments are split into Eocene-Oligocene (a,c) and Miocene (b,d) simulations. Reference simulations are highlighted in bold characters and full lines, while sensitivity tests are in dotted lines.

our simulations (Fig. 5 a,c and Fig. 6). In the late Eocene, increasing TP elevation strengthens the zonal wind shear over India (3000 m, WYI = ∼6 m/s, for experiment LEo2_TP, Fig. 5 c), when compared to Eocene experiment with low topography in the region (800 m, WYI = 1 m/s, LEo2_TPlow). Additionally, the magnitude of the WYI gradually increases with the TP latitude, with values spanning from 3 m/s when its southern edge is at ∼20°N (LEo2_TPsouth), 4 m/s (southern edge at ∼25°N in LEo2_TP), to finally 6 m/s (southern edge at ∼30°N, experiment LEo1_REF). The sea inlet that flooded the northern *Greater India* during the late Eocene, as sometimes suggested in the literature (D. J. J. van Hinsbergen et al., 2012; D. J. van Hinsbergen et al., 2019), limits the northward migration of the ITCZ in summer (from ∼7 to 3°N between experiments LEo2_BengalSea and LEo2_TP, Fig. 5 c). It also produce a decrease in year-round precipitation, especially in South and inland Asia (Fig. 6 m,n,o).

6.1.4 Continentality increase and East African and Iranian uplifts as major drivers of the South Asian summer monsoon

The changes induced by the Tibetan plateau uplift or by its latitudinal location on the South Asian climate are however out-competed by far by the effects of other paleogeography changes, namely a global sea-level fall, reflecting the Antarctica glaciation at the EOT and the uplift of peripheral terranes (Fig. 5). Indeed, the increase in continentality driven by the sea level fall, together with the pCO_2 halving, induces a colder and drier winter (Fig. 7 g) as well as hotter and wetter summer (Fig. 7 h), which results into a monsoon-like seasonality signal stretching over Southeastern Asia (Fig. 7 i). It also translates into a doubling of the WYI (from 6 to 11 m/s between experiments EOli_REF and LEo1_REF, Fig. 5 c) and a strong reorganization of summer Jet Stream behavior (see dedicated section below).

Likewise, increasing continentality during the Miocene appears to be the key leverage for inducing a more pronounced migration of the ITCZ over the Arabian Sea (from 18 to 21°N in more continental case, Fig. 5 b), as well as a slight increase of the WYI (Fig. 5 d). This is achieved either with the emergence of the Arabian platform (Fig. 8 g,h,i), or with the narrowing of the Neotethys Ocean and the shrinkage of the Paratethys Sea (Fig. 8 d,e,f). In both cases, the amplification of the summer low pressure belt results into increased moisture advection from the Arabian Sea, and therefore increased summer precipitation in SAM and EAM domains. The overall precipitation seasonality increase is however not homogeneous, because of contrasted effects on the winter season precipitation. Our results point that the Arabian platform emergence, by amplifying the winter Siberian high pressure would dry Eastern Asia and southeastern Tibet, which would increase precipitation seasonality in parts of SAM but mostly in EAM domain (Fig. 8 d,f). The retreat of the Paratethys Sea, on the other hand, would mostly increase precipitation seasonality in the South Asian monsoon domain (Fig. 8 i). Moreover, a clear dichotomy emerges between Central Asia, that becomes drier after the Paratethys Sea retreat, and all surrounding regions that become wetter (Fig. 8 i).

Additionally, the successive buildup of both East African (difference between experiments EMio_EAfr-EMio_REF) and Iran-Zagros landforms (difference between experiments LMio_REF-LMio_smallT) is critical for the amplification of the ITCZ migration and strengthening of SAM. Each uplift triggers a ∼4-5° northward migration of the ITCZ over the Arabian Sea in summer, as well as a slight increase in July WYI (Fig. 5 b,d). The uplift of East African landforms under Early Miocene conditions reinforces the Somali Jet and brings moisture to Iran-Zagros and SAM domain in summer (Fig. 9 e), which results in intensification of monsoon-like seasonality on the Himalayan foothills and in Southeastern Asia (mainly Myanmar, Fig. 9 f). Iran-Zagros landforms final uplift under late Miocene conditions promotes winter aridity and summer precipitation in SAM domain through a strong strengthening of the Somali Jet, resulting in a reinforced monsoon-like seasonality (Fig. 9 j,k,l). By preventing the advection of westerly mid-latitudes winds to lower latitudes, it channels this humidity towards inland Asia in summer, thus reducing the aridity

of the region. On the other hand, and although being sometimes put forward as a plausible event contributing to modification of monsoon strength during the Miocene (Bialik et al., 2019, 2020; Rögl, 1997; J. Sun et al., 2021), the mechanical effect of the Tethyan seaway closure, without strong modification of land extension in the Arabian Peninsula region, remains limited in our experiments (+1 m/s for the WYI between experiments EMio_REF and EMio_TetSw in Fig. 5 d).

6.2 The Eastern Asian monsoon under the crossed influence of Asian orography, continentality and pCO_2

6.2.1 EASM: precipitation patterns and summer Jet Stream position evolution

As opposed to the South Asian region, monsoon-like precipitation seasonality is simulated in Eastern Asia in all reference experiments, although it remains initially confined to Northeastern China in the Eocene (Fig. 4 a). As this region of monsoon-like precipitation regime expands to southeastern and inland China throughout the Cenozoic and reaches modern-like extension in the mid Miocene experiment, the Paleogene broad zonal arid band retreats from China (Fig. 4 m). Today, precipitation in eastern China are triggered by the penetration of the Meiyu-Bayu front as it follows the migration of the Jet Stream north of the Tibetan Plateau during summer (Kong et al., 2017). In our simulations, the summer Jet Stream (approximated through the location of maximum zonal wind velocity in the troposphere in August), transits above the proto-Tibetan Plateau and Eastern China in a strong zonal flux in the Eocene and Oligocene experiments (up to 30-35 m/s centered at ∼30°N Fig. 4 c,g). It then weakens (10-20 m/s) and progressively migrates north of the Plateau in the Miocene experiments (Fig. 4 k,o,s). The Jet also looses its very zonal configuration and undulates towards Japan. This relocation of the Jet Stream is accompanied by increased precipitation in eastern China, southeastern Siberia and Japan, reaching 200-300 mm in August (Fig. 4 k,o,s), and locally accounting for up to 25% of the annual precipitation in this sole month. These results suggest that the Jet Stream seasonal displacement indeed amplifies the EASM rainy season, although seasonal precipitation have been observed in this region in Late Eocene experiments.

6.2.2 Summer Jet Stream migration and associated EASM precipitation driven by pCO_2 decrease at the EOT and the Northern TP, Tian Shan, Pamir and Mongolian uplift in the Miocene

To identify the drivers responsible for the Jet Stream seasonal migration about the Tibetan Plateau, we here again take advantage of the available sensitivity experiments. All 1120 ppm (or 4X) late Eocene simulations display a behavior of the Jet opposite to its modern counterpart, with a northward migration in winter, and a southward migration in summer, below or over the proto-Central TP (Fig. 10 a). This tendency remains relatively undisturbed with alternative TP configurations (Fig. 10 a and Fig. 6 e,h,k,n). The pCO_2 halving in the Eocene-Oligocene reverses this tendency (LEo1_2X and EOli_REF, compared to LEo1_REF). It induces a migration northward of the Tibetan landform in late summer to early fall (Fig. 10 a and Fig. 7 e,h), and an important decrease in winter zonal speed (∼50m/s against ∼70 m/s in other Eocene simulations, Fig. 10 a and Fig. SI 21 a to h). This migration is however restricted to the TP region, and the Jet Stream remains at low latitude over eastern Asia (∼35°N, Fig. 10 b and Fig. SI 19), with few summer precipitation (100-150 mm/month).

All subsequent Miocene simulations display an important latitudinal migration of the Jet along the year, both in the TP region (Fig. 10 c,e), and over eastern Asia (Fig. 10 d,f). The northward migration of the Jet is comparable between early Oligocene and early Miocene experiments (up to ∼38-40°N in September), despite a higher Central Tibet (from 3000 to 4000 m) and a wider Tibetan landform, due to the incipient uplift of Northeastern

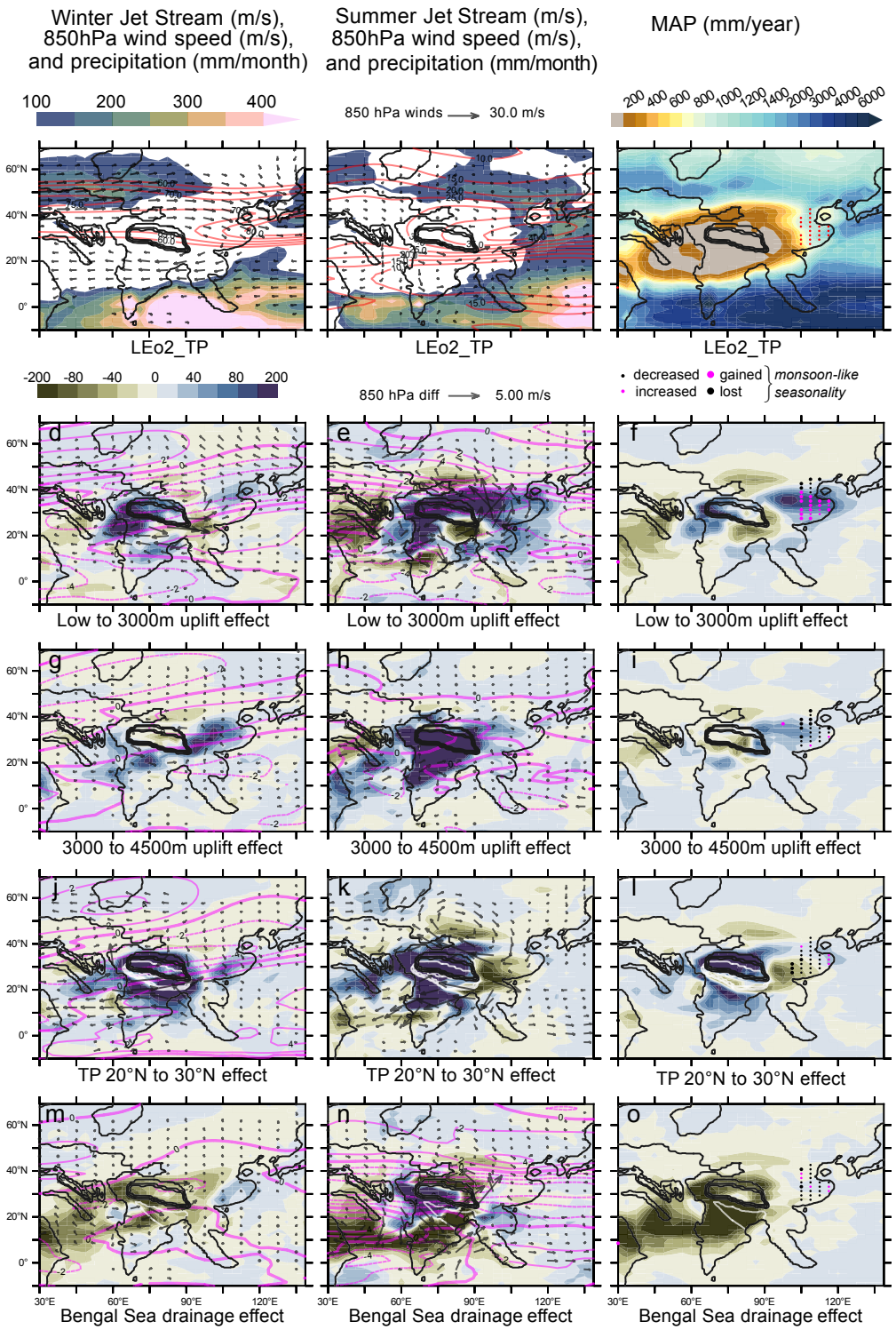

Figure 6. Sensitivity to the Tibetan configurations on Eocene climate: (**a,d,g,j,m**) winter precipitation (shading), 850 hPa winds (vectors), jet stream speed (contour) ; (**b,e,h,k,n**) on summer precipitation (shading), 850 hPa winds (vectors), jet stream speed (contour); (**c,f,i,l,o**) mean annual precipitation (shading) and monsoon-like seasonality according to the MPI index (red dots). Sensitivity tests are compared to the simulation LEo2_TP (**a,b,c**) and anomalies (**d to o**) are expressed as "test minus LEo2_TP", except for the "lowered TP effect" which is "LEo2_TP minus LEo2_TPflat"). Precipitation anomalies (shading) are expressed in % and normalized by the averaged precipitation of both simulations (therefore, a change from or to zero mm/year accounts for +/- 200%). In (**f,i,l,o**): four types of seasonality changes induced by uplift are displayed (e.g. regions showing a decrease of monsoon-like seasonality after lowering the TP are in small black dots) ; white and black topographic contours indicate the LEo2_TP and test topography.

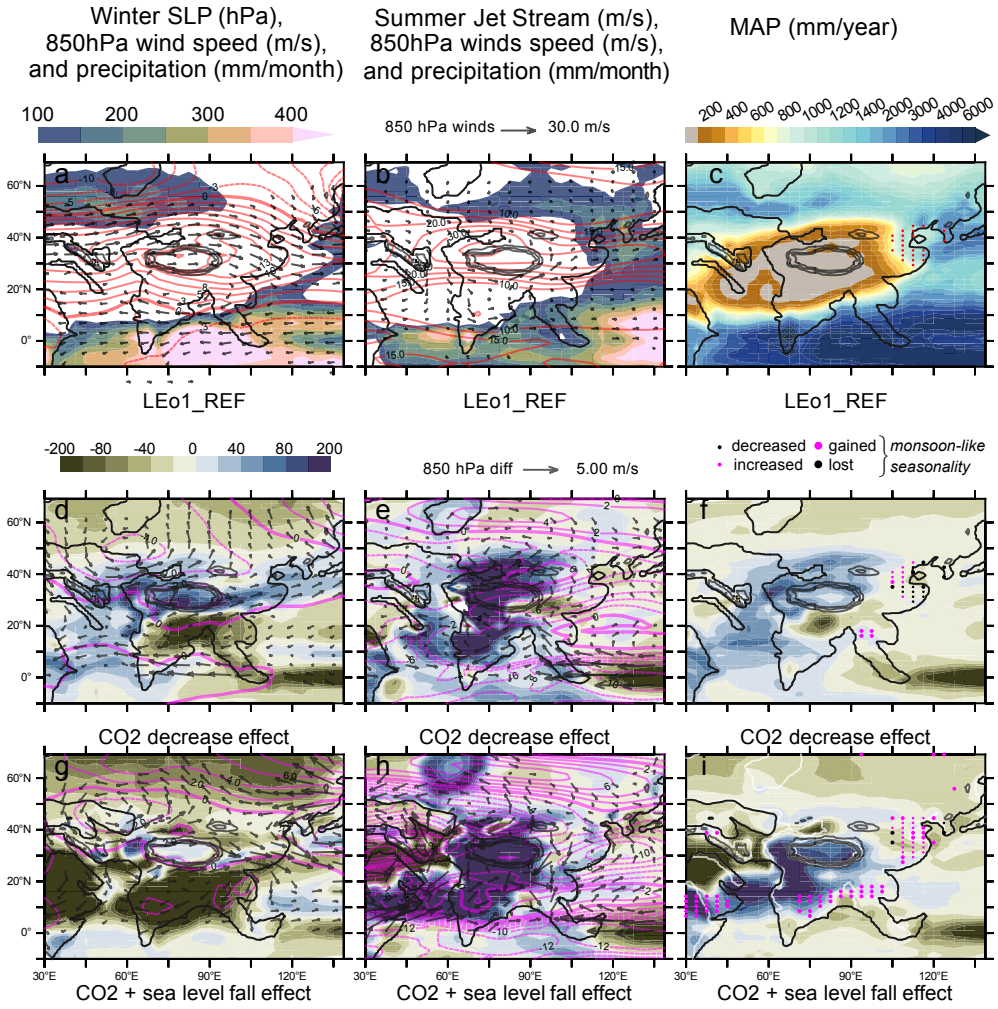

Figure 7. Influence of the pCO_2 decrease and sea level drop at the EOT on: (**a,d,g**) winter precipitation (shading), 850 hPa winds (vectors), Sea Level Pressure (contour) ; (**b,e,h**) on summer precipitation (shading), 850 hPa wind (vectors), jet stream speed (contour); (**c,f,i**) mean annual precipitation (shading) and monsoon-like seasonality according to the MPI index (red dots). Sensitivity tests are compared to the simulation LEo1_REF (**a,b,c**) and anomalies (**d to i**) are expressed in order to highlight the impact of the test (i.e. test-LEo1_REF). Precipitation anomalies (shading) are expressed in % and normalized by the averaged precipitation of both simulations (therefore, a change from or to zero mm/year accounts for +/- 200%). In (**f,i**): four types of seasonality changes induced by uplift are displayed (e.g. regions switching from no monsoon to monsoon-like seasonality after the sea level fall and pCO_2 decrease in thick magenta dots) ; white topographic contours indicate the LEo1_REF contour.

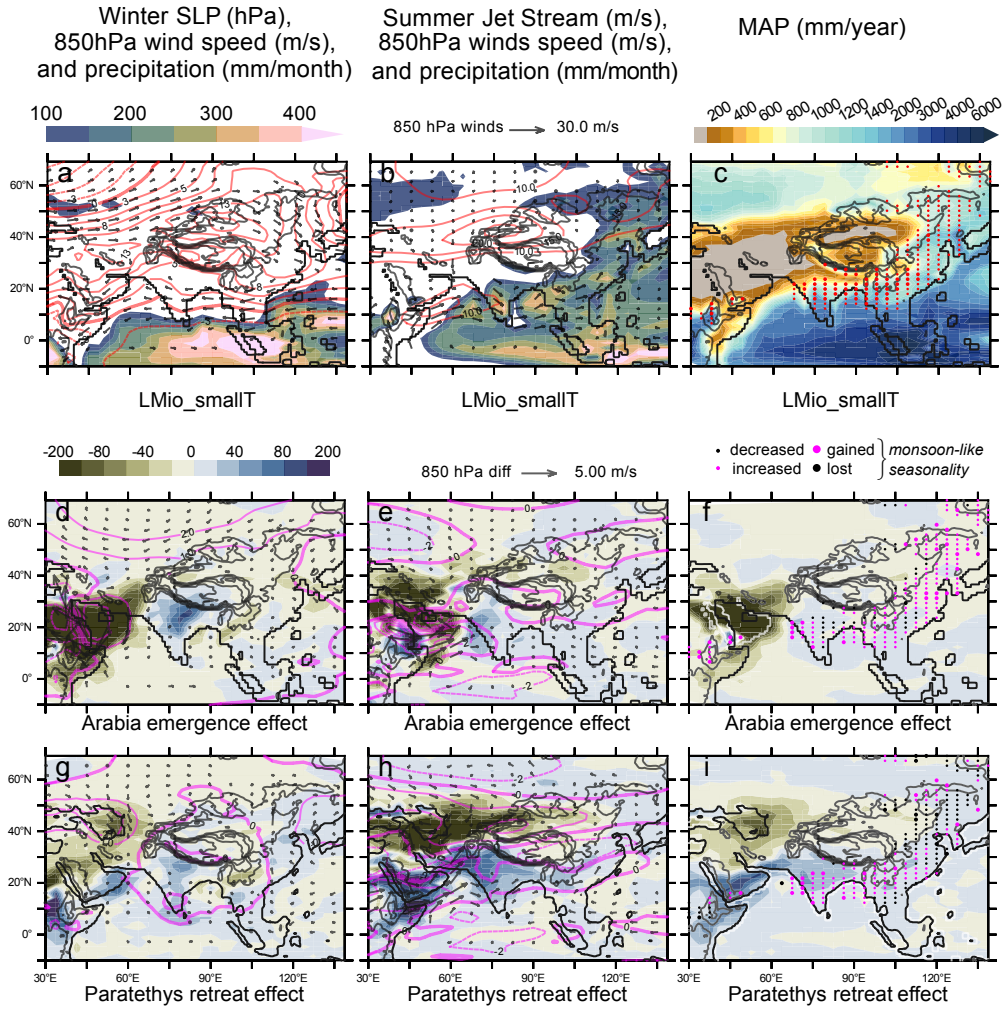

Figure 8. Influence of continentality increase in a Mid-late Miocene context on: (**a,d,g**) winter precipitation (shading), 850 hPa winds (vectors), Sea Level Pressure (contour) ; (**b,e,h**) on summer precipitation (shading), 850 hPa winds (vectors), jet stream speed (contour); (**c,f,i**) and on mean annual precipitation (shading) and monsoon-like seasonality according to the MPI index (red dots). Sensitivity tests are compared to the simulation LMio_smallT (**a,b,c**) and anomalies (**d to i**) are expressed in order to highlight the impact of the continentality increase (i.e. LMio_smallT-test). Precipitation anomalies (shading) are expressed in % and normalized by the averaged precipitation of both simulations (therefore, a change from or to zero mm/year accounts for +/- 200%). In (**f,i**): four types of seasonality changes induced by continentality are displayed (e.g. regions switching from no monsoon to monsoon-like seasonality after continentality increase in thick magenta dots) ; white topographic contours indicate the test simulation.

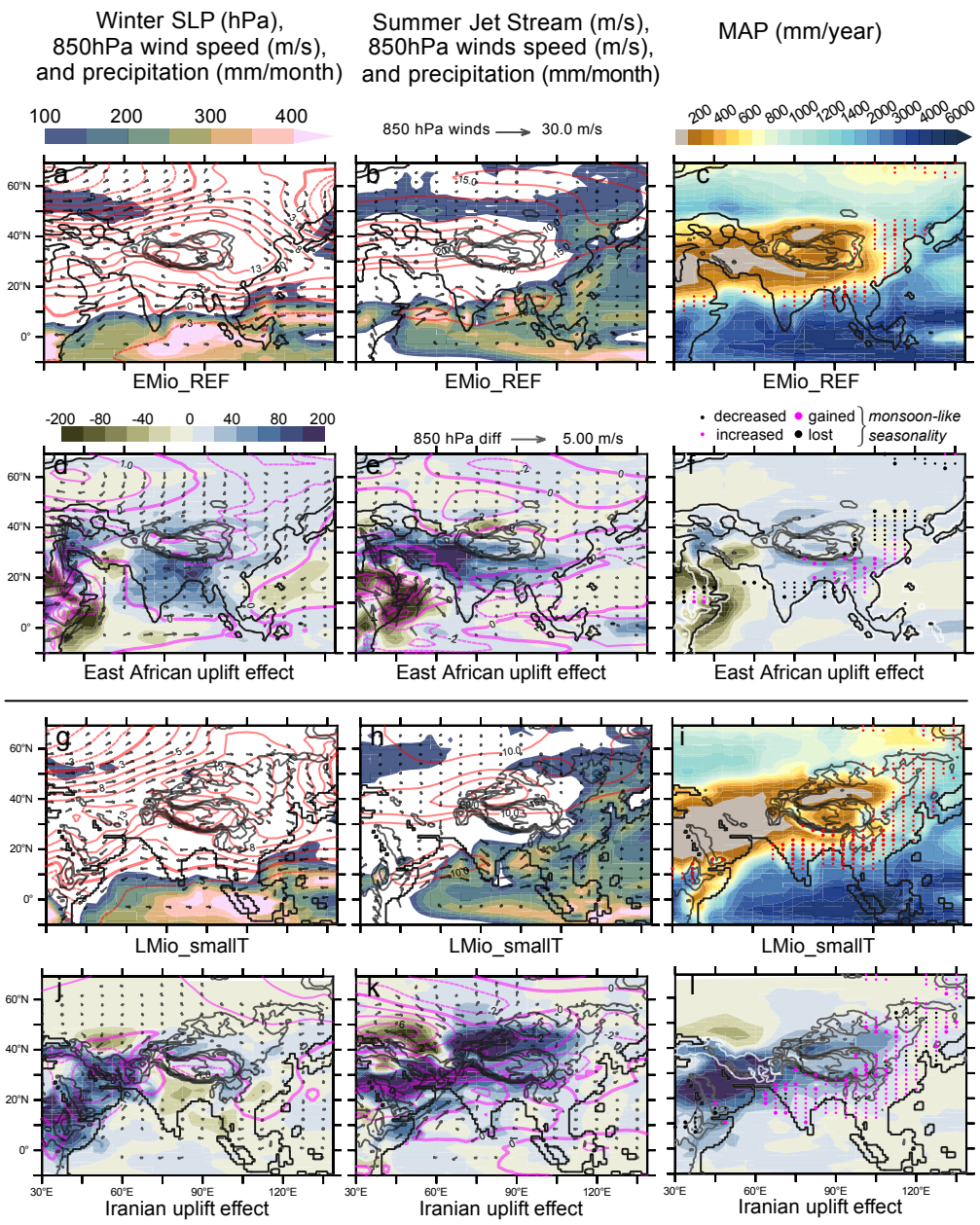

Figure 9. Influence of the East African uplift in the Early Miocene (a to f) and of Iran-Zagros uplift in the late Miocene (g to l) on: (**a,d,g,j**) winter precipitation (shading), 850 hPa winds (vectors), Sea Level Pressure (contour) ; (**b,e,h,k**) on summer precipitation (shading), 850 hPa winds (vectors), jet stream speed (contour); (**c,f,i,l**) and mean annual precipitation (shading) and monsoon-like seasonality according to the MPI index (red dots). East African (Iran-Zagros) uplift is compared to the simulation EMio_REF (LMio_SmallT) (**a,b,c** and **g,h,i**) and anomalies (**d,e,f** and **j,k,l**) are expressed in order to highlight the impact of upliftt (i.e. EMio_EAfr-EMio_REF and LMio_REF-LMio_smallT respectively). Precipitation anomalies (shading) are expressed in % and normalized by the averaged precipitation of both simulations (therefore, a change from or to zero mm/year accounts for +/- 200%). In (**f,i**): four types of seasonality changes induced by continentality are displayed (e.g. regions switching from no monsoon to monsoon-like seasonality after continentality increase in thick magenta dots) ; white topographic contours indicate the uplifted area.

and Northwestern TP portions in the early Miocene simulation (the Tian Shan is ∼1000 m and the NE Tibet ∼2000 m high). We therefore suggest that the Jet Stream latitudinal migration is primarily triggered by pCO_2 drawdown, and resulting tropospheric temperature gradients, and that a significant threshold is crossed at the Greenhouse-Icehouse transition (EOT, ∼34 Ma). In contrast, the subsequent variations in the Jet Stream latitudinal migration in the course of the Miocene, appear to be mainly driven by topography changes.

The opening of the Tethyan seaway in the early Miocene (comparing EMio_REF and EMio_TetSw), the Iran-Zagros landform uplift (comparing LMio_SmallT and LMio_REF), or a pCO_2 decrease (comparing LMio_REF and LMio_1.5X) in the late Miocene do not appear to trigger important variations in the Jet Stream migration (Fig. 10 c to f). Other experiments, on the other hand, induce notable variations in response to localized uplift of specific landforms, especially in the mid-late Miocene. Sensitivity experiments removing either Mongolia, Tian Shan, or a combination of both, or Tian Shan and Pamir show that these landforms all contribute to amplify the northward migration of the Jet in summer, both in the TP region and in Eastern Asia (from 39-41°N in LMio_noTS, LMio_noTSP, LMio_noTSM and LMio_noM to 43°N in MMio_REF and LMio_REF, Fig. 10 e and Fig. 11 h,k,n). This is especially marked in the experiment removing specifically the Tian Shan orogen, which results in the Jet staying above the TP, without passing its northern edge (Fig. 11 h,k,n). We therefore propose that the final uplifts of the Tian Shan, and in a lesser way of the Pamir (from ∼1000 m in the early Miocene to ∼3000 m in the mid and late Miocene experiments) and Mongolian mountains (from ∼500 m in the early Miocene to ∼1500 m in the mid and late Miocene experiments) are critical to deviate the Jet northward in summer (Fig. 11 e,h,k,n and Fig. SI 19 o to r). This relocation of the Jet Stream in summer induces orographic precipitation on the uplifted landforms, aridification of the regions standing to the west (-20 to -60% of summer precipitation in eastern Kazakhstan and Uzbekistan) and increased precipitation in Eastern Mongolia (+20 to 60%). This translates into increased monsoon-like seasonality in Northeastern Asia (magenta dots in Fig. 11 f,i,l,o).

6.2.3 East Asian winter monsoon: the Siberian High genesis

Modern EAWM is characterized by cold and dry climate, together with northwesterly low tropospheric winds above 20°N and northeasterly winds below 20°N. This peculiar atmospheric circulation is driven by the strong pressure gradients settling between the Siberian High anticyclone, the Aleutian Low and the Maritime Continent Low (L. Wang & Chen, 2014; T. Ma & Chen, 2021). Our results suggest strong changes in surface temperature gradients throughout the experiments, that induce an important remodeling of associated pressure and wind patterns (Fig. 12 and Fig. 13). In our Eocene experiment, a high-pressure band centered around 30°N is simulated, but it remains mainly zonal, following large-scale Hadley winter descending branch driven by latitudinal surface temperature gradients (Fig. 12 b). Indeed, the temperature difference between Tibetan region (∼10°C) (located below the high pressure cell) and neighboring North Pacific Ocean (∼30°C) remains relatively low (∼20°C, Fig. 12 a), when compared to modern temperature difference at the same season (∼40°C, Fig. 14). As a result, no significant pressure difference is simulated between the Asian continent and the North Pacific in the Eocene and the calculated EAWM index is low (<5, Fig. 13), reflecting only the North-South pressure gradient between Asia and the Maritime Continent.

The extent of the Asian high pressure zone increases gradually in the early Oligocene and early Miocene experiments (Fig. 12 d,f), but its modern-like Siberian High shape is only simulated in the mid and late Miocene experiments, when its center relocates over Siberia (∼40-60°N, Fig. 12 h,j). Additionally, the North Pacific low relocates 10° to the south from the early Oligocene simulation onward and steadily decreases until the late Miocene (from over ∼14 to 10 hPa anomaly). All these changes conspire to increase progressively both North-South and East-West pressure gradients, and therefore the global EAWM index, which reaches maximal values in the mid and late Miocene experiments (∼15, Fig.

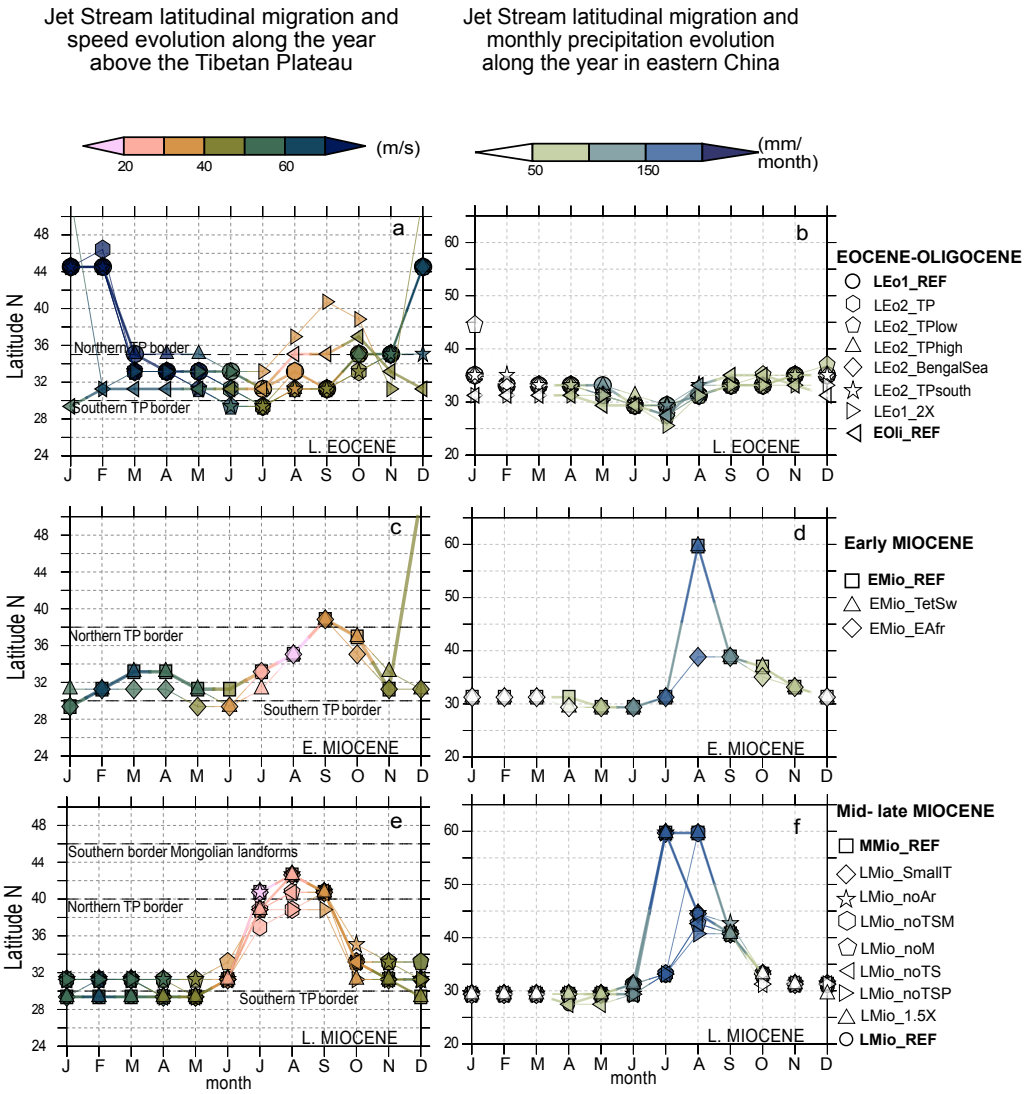

Figure 10. Jet Stream behavior along the year over the Tibetan Plateau and eastern China for all sensitivity experiments, divided into (**up**) Late Eocene, (**mid**) early Miocene and (**bottom**) mid to late Miocene. (**left**) Jet Stream latitudinal migration and speed (shading) evolution along the year in the Tibetan region (averaged over 80:90°E). Mean latitudes of the northern and southern bounds of the Himalaya-Tibet and Mongolian landforms are indicated. (**right**) Jet Stream latitudinal position and precipitation (shading) amounts along the year in East Asia (averaged over 100:120°E).

13). Following this reorganization in pressure patterns simulated during the Cenozoic, low tropospheric winds transiting over China display a progressive change in orientation. While their zonal component remains important in the Paleogene and early Miocene experiments (Fig. 12 b,d), the development of the Siberian High triggers a marked increase in their meridional component in the mid and late Miocene experiments (Fig. 12 h,j).

This profound atmospheric circulation reorganization is driven by temperature gradient changes, and mainly due to progressive cooling of the Tibetan, Mongolian and Siberian regions, as illustrated by the ∼22° shift southward of the 0°C isotherm between the late Eocene and the late Miocene simulations (Fig. 12 a,i). Several factors may be responsible

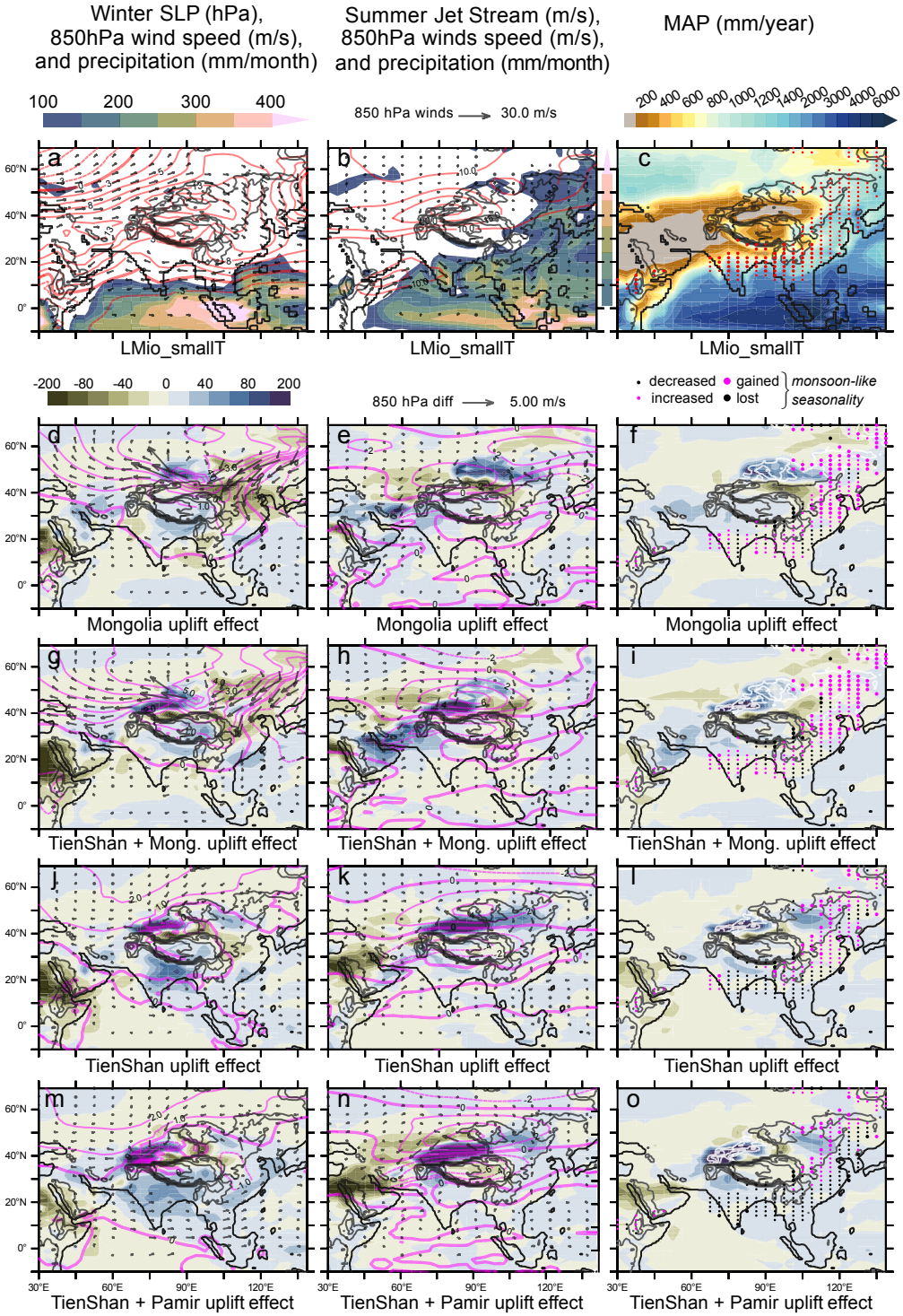

Figure 11. Influence of Mongolia, Tian Shan and Pamir regional uplifts on (**a,d,g,j,m**) winter precipitation (shading), 850 hPa winds (vectors), Sea Level Pressure (contour) ; (**b,e,h,k,n**) on summer precipitation (shading), 850 hPa wind (vectors), jet stream speed (contour); (**c,f,i,l,o**) mean annual precipitation (shading) and monsoon-like seasonality according to the MPI index (red dots). Sensitivity tests are compared to the simulation LMio_smallT (**a,b,c**) and anomalies (**d to o**) are expressed in order to highlight the impact of the uplift (i.e. LMio_smallT-test). Precipitation anomalies (shading) are expressed in % and normalized by the averaged precipitation of both simulations (therefore, a change from or to zero mm/year accounts for +/- 200%). In (**f,i,l,o**): four types of seasonality changes induced by uplift are displayed (e.g. regions switching from no monsoon to monsoon-like seasonality after uplift in thick magenta dots) ; white topographic contours indicate the landforms that were added.

for this important winter cooling, such as the pCO_2 drawdown, local topography changes or increased continentality.

6.2.4 Siberian High inception driven mainly by Mongolia uplift in the Miocene and its impact on precipitation seasonality

The Eocene sensitivity experiments display a stable zonal high pressure pattern at mid latitudes (Fig. SI 18 a to g), with weak response to changing Tibetan orography or pCO_2 values (Fig. 13). Likewise, our Miocene sensitivity experiments allow to highlight that the winter pressure patterns in Asia (comprising the Siberian High, the North Pacific Low and the Maritime Continent Low) are not impacted by African or Iran-Zagros landforms uplifts, the Arabian platform configuration, the Paratethys extent, or a pCO_2 drop from 560 to 420 ppm (Fig. 13 and Fig. SI 18 i to n and s,t).

On the other hand, sensitivity experiments reveal the impact of the Mongolian landform uplift in the mid-late Miocene (either Mongolia alone, or both Tian Shan and Mongolia). Indeed, their settlement induces a strengthening of both the Siberian High (up to ∼6 hPa, Fig. 11 d,g) and the North Pacific low, resulting in a reinforcement of the East-West and North-South pressure gradients, and ultimately of the EAWM index (from ∼8 to ∼15, Fig. 13). Mongolian (and/or Tian Shan and/or Pamir) uplift also results in increased precipitation localized over the landforms (Fig. 11 d to o), despite the overall dryness of inland Asia region (SI Fig. 16). As Mongolian uplift deviates the winter westerlies flux northward, Eastern China is swept by colder and drier winds coming from Siberia, which translates into a marked decrease in winter precipitation (up to 80% decrease, Fig. 11 d). The uplift of Tian Shan landforms, alone or together with the Pamir, has a lower impact on the global winter pressure patterns (Fig. 13), but nonetheless provokes an almost complete drying on its eastern flanks (modern Gobi and Taklimakan deserts), as it acts as an orographic barrier to westerly moisture flux (Fig. 11 g,j,m).

These changes on winter wind circulation and precipitation amounts, combined to those observed in summer and described above, produce contrasted responses in terms of monsoon-like precipitation seasonality. As the Mongolian uplift generates a mixed response on summer precipitation in eastern China (Fig. 11 e,h), but dries consistently the region in winter (Fig. 11 d,g), it induces important spreading of new regions displaying monsoon-like precipitation seasonality in eastern China (thick magenta dots in Fig. 11 f,i). At the opposite, Tian Shan and Pamir uplift, let alone the important year-round increase in orographic precipitation, triggers overall increased winter precipitation amounts in Southeastern Asia (Fig. 11 j,m), which leads to widespread reduction of precipitation seasonality in the SAM domain (Fig. 11 l,o).

7 Discussion

A long-standing debate opposes the effect of continentality against orography regarding the Asian climate evolution (Prell & Kutzbach, 1992; Kutzbach et al., 1993; Ramstein et al., 1997; Fluteau et al., 1999; Z. Zhang et al., 2007; Roe et al., 2016; Zoura et al., 2019; R. Zhang et al., 2021). Our results hint that these two features most likely impacted different climatic characteristics of the Asian Monsoons and all concurred to the settlement of current Asian climate (see Table 6 for a sum-up of the main effects of each forcing on monsoonal features). In the following sections we put our main findings in perspective with available paleoclimatic indicators and previous modeling work.

7.1 A possible inception of monsoons in the Paleogene: which dependence to pCO_2, Tibetan paleogeography and continentality ?

Our late Eocene set of simulations follows a previous study, in which we introduced the results from LEo1_REF, displaying no monsoon circulation, and discussed a possible dry

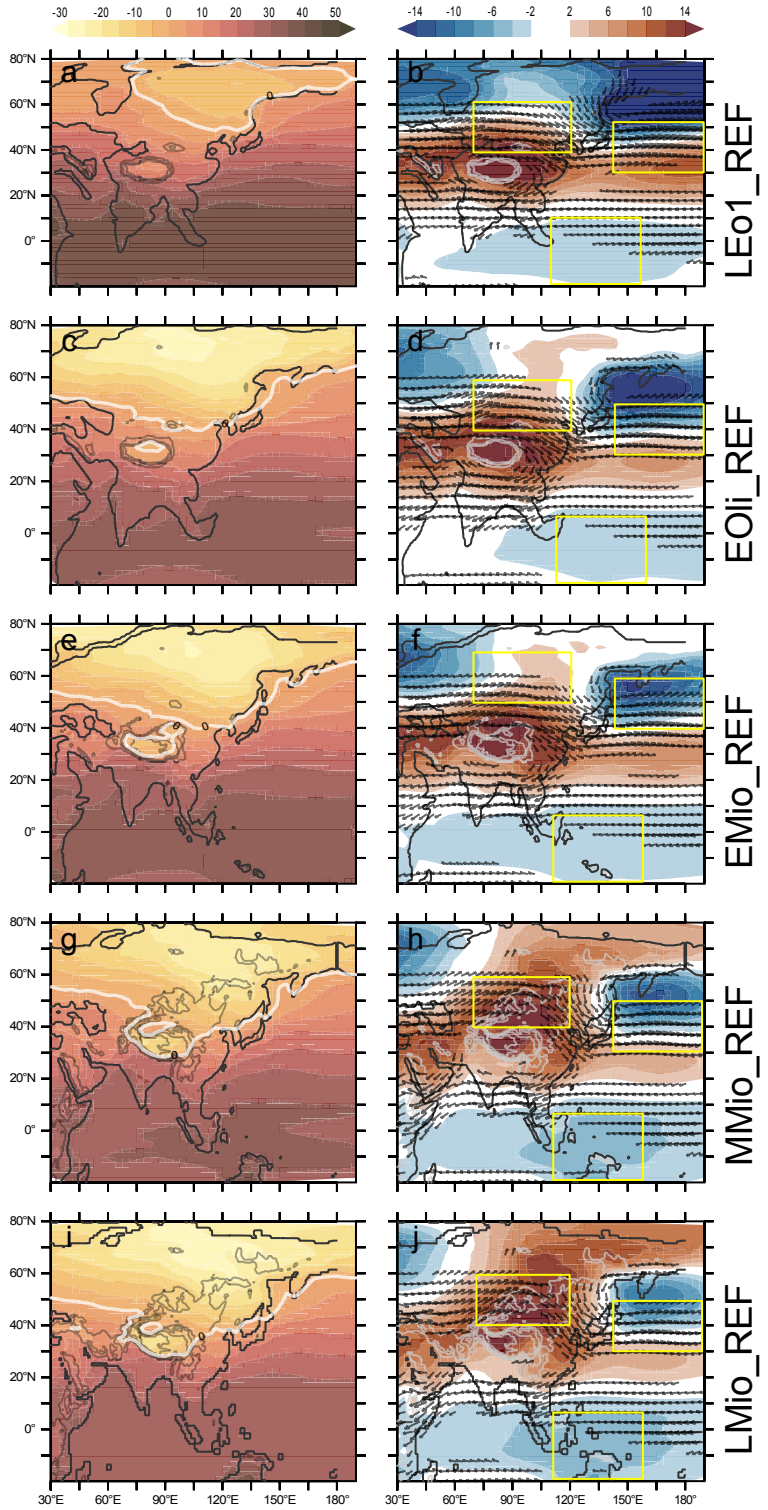

Figure 12. Evolution of the winter monsoon diagnostics throughout the Cenozoic. **Left column:** December-February (DJF) mean 2m temperature (shading, Celsius), overlain with a white contour line marking the 0°C isotherm ; **Right column:** DJF normalized Sea Level Pressure anomaly (shading, hPa) and 850 hPa winds above 4 m/s (vectors). In all captions, topography is overlain in gray contour each 1000 m. Yellow boxes indicate the regions over which are calculated the sea level pressure gradients from the East Asian Winter Monsoon Index, presented in section 5.3

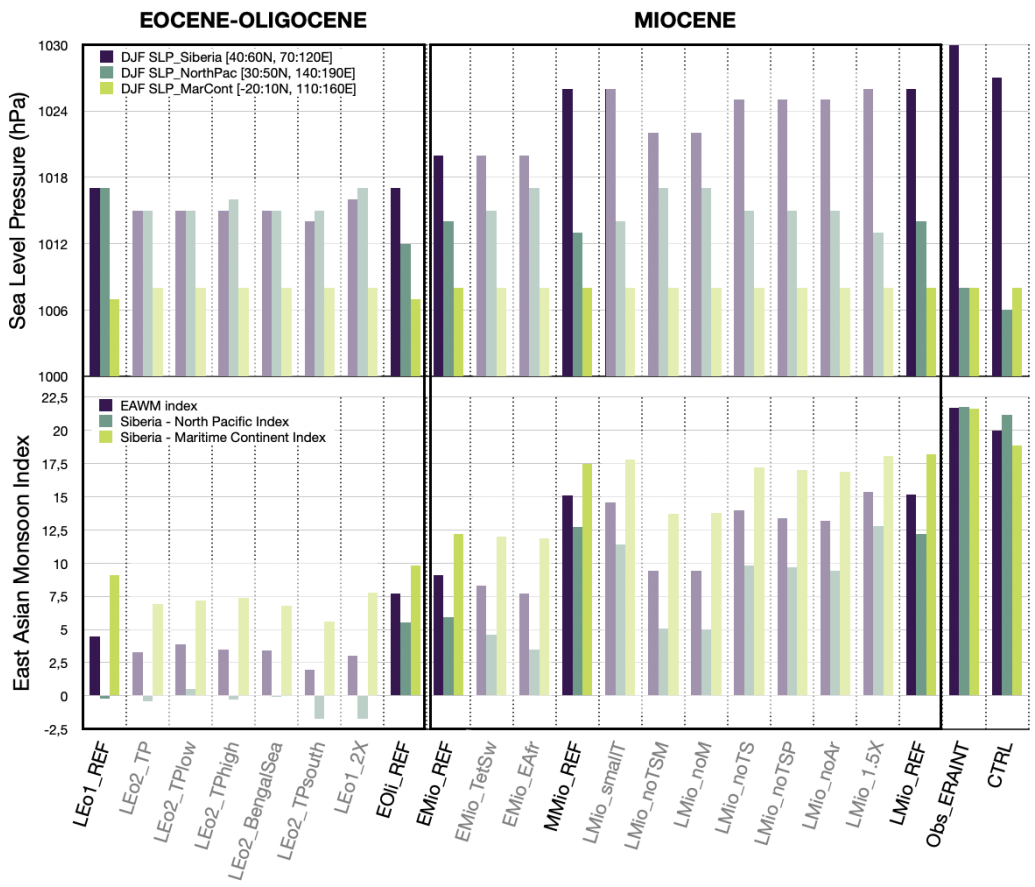

Figure 13. Upper panel: Winter (DJF) Sea Level Pressure (hPa) evolution over Siberia, North Pacific and the Maritime Continent ; **lower panel:** Evolution of the East Asian Winter Monsoon index (purple) and of the East-West and North-South regional indexes throughout the different reference and sensitivity experiments, after (L. Wang & Chen, 2014).

bias in our simulations, when comparing our results to several proxy localities indicating significantly wetter environments (Tardif et al., 2020). Indeed, while markers of arid to sub-arid climate are widespread for the late Eocene for example in Northeastern TP (J. X. Li et al., 2018; Meijer et al., 2019), Tajikistan (Carrapa et al., 2015) or on the Tarim Basin shores (Bougeois et al., 2018), our Eocene experiment fails to render the wetter climate inferred from fossil paleoflora and paleofauna in Northern India (Saxena & Trivedi, 2009) and Tibet (T. Su et al., 2020; Sorrel et al., 2017). Asian overall aridity in this reference Eocene simulation was interpreted as resulting from the hot surface temperatures simulated in the region, together with strong mid-tropospheric subsidence that inhibits deep convection and condensation, especially over Northern India (Tardif et al., 2020). Nevertheless, much wetter and closer to monsoon-like summer climate patterns were simulated in both EAM and SAM domains for the late Eocene with the same model and paleogeography, but with orbital configurations inducing summer solar maxima (Tardif et al., 2021). This potential orbitally-paced wet/dry climate dichotomy is, at least qualitatively, in agreement with stratigraphic and paleobotanic evidence from Eastern China (C. Huang & Hinnov, 2019; Tong et al., 2002). Another hypothesis for this mismatch was an eventual sensitivity of the simulated climate to Asian paleogeography which, as introduced before, is still highly debated for this period.

7.1.1 Late Eocene climate sensitivity to alternative paleogeographic configurations: persistent mismatch with paleoclimate indicators in SAM domain

In this study, we explored the Asian climate sensitivity to different late Eocene Tibetan configurations, which aimed at reflecting the main theories regarding the paleogeography at that time. We also evaluated the effect of decreased pCO_2 values (1120 to 560 ppm). Our results reveal that the arid pattern previously described shows low sensitivity to the Tibetan Plateau configuration or to a reduced pCO_2, and is only disturbed by the presence of a Bengal Sea (LEo2_BengalSea), which lowers the surface temperatures and slightly enhances precipitation in this region (Fig. SI 16 f). This tendency is however opposite to similar modeling studies comparing an early and a late Eocene paleogeography, and which suggest increased precipitation after the drainage of this Bengal Sea (X. Li et al., 2017, 2018). Comparing these different simulations is nevertheless hampered by the significant difference between other boundary conditions that were used. Collectively, these results rather points to the high sensitivity of late Eocene climate to surface temperature gradients, at least with the IPSL-CM5A2 model, which is further emphasized by the changes induced by the sea level fall tested in our Oligocene simulation and presented in the next section.

The EAM region displays higher sensitivity to the paleogeography changes that were tested. We simulate that an uplift in the Tibetan region (compared to a low ∼800 m TP in LEo2_TPLow) would result into an onset or increase in EAM monsoon-like precipitation seasonality due to increased summer precipitation (up to 50, Fig. 6e, Fig. SI 16 b,c,d), in agreement with previous modeling works (R. Zhang et al., 2018, 2017, 2021; Z. Zhang et al., 2007; X. Liu & Yin, 2002; X. Li et al., 2017; Farnsworth et al., 2019; Thomson et al., 2021). Likewise, the decreased EAM intensity and increased inland Asian aridity due to the northern migration of the TP (its southern edge translating from ∼20 to 30°N) is coherent with previous study testing the impact of the latitudinal position of the incipient TP (R. Zhang et al., 2017).

7.1.2 Imprint of the Eocene-Oligocene transition on summer monsoon and inland Asia aridification

Paleoclimatic indicators from inland Asia suggest increased precipitation seasonality in EAM and SAM domains, wetter conditions localized in the Tarim and western Qaidam basins and overall aridification everywhere else in inland Asia (described in section 3.1.3). This aridification was attributed either to global cooling a the EOT (J. Sun et al., 2015;

X. Li et al., 2017), to the Paratethys Sea retreat (Barbolini et al., 2020; Z. Zhang et al., 2007), or both (J. Sun & Windley, 2015). Our sensitivity experiment testing the effect of cooling alone (LEo1_2X) seems to better render wetter conditions in the Tarim-Qaidam region and global drying in the Yunnan region (Fig. 7 f). Taking into account the EOT global sea level drop in addition to global cooling (EOli_REF) on the other hand, better simulates the monsoon-like precipitation seasonality suggested by paleofloras in both EAM (Vornlocher et al., 2021; R. Spicer et al., 2017; J. Ren et al., 2021; J. Huang et al., 2022; Herman et al., 2017; Ling et al., 2021) and SAM domains (R. Spicer et al., 2017; Srivastava et al., 2012), as well as precipitation amounts in Kazakhstan (Averyanova et al., 2021). Although the comparison to existing modeling studies is limited by the many additional parameters that may variate from our experiments (ice sheets, pCO_2, etc.), those which explicitly tested the effect of the Paratethys Sea retreat (R. Zhang et al., 2021; Z. Zhang et al., 2007), tend to simulate similar SAM and EAM precipitation seasonality increase. Our Oligocene experiment however still underestimates precipitation over Tibet (Deng et al., 2021; Song et al., 2020) and does not simulate the drying trend indicated by proxies in the Tajik and Junggar basins as well as in the Gobi region after the EOT (J. Sun & Windley, 2015; Baldermann et al., 2021; J. Sun et al., 2015, 2020), although simulated Oligocene mean annual precipitation remain very low in these regions. We suggest this mismatch may be due to the shape of the proto-Tibetan orogen or paleoshorelines used in LEo1_REF and EOli_REF, as all of these locations stand very close to the boundary between regions that became indeed drier (Fig. 7). To further explore the impact of land-sea distribution change, the Miocene experiments offer additionnal input.

7.1.3 Continentality increase as a potential driver of Paleogene wintertime climate variability

The precocious observation of loess deposits in northeastern Tibet at 40 Ma was interpreted as resulting from the periodical inception (or reinforcement) of the Siberian High in winter due to enhanced continentality after the Paratethys Sea retreat (Meijer et al., 2021). Other loess deposits are reported during the Oligocene in the Chinese Loess Plateau and Mongolia, apparently coeval with periods of cooling and ice-sheets expansion (J. Sun & Windley, 2015; Wasiljeff et al., 2022). These discoveries question the presence of a Siberian High in the Paleogene, of its role in dust transport and accumulation, and of its forcing factors. Indeed, most modeling studies so far focused on the link between regional uplift and enhanced Siberian High and winter monsoon circulation rather than on the influence of continentality or global climate cooling. Our results suggest that both increased continentality and regional uplift have concurred to the progressive inception of modern Siberian High, while pCO_2 fall had apparently little impact on its intensity (Fig. 13).

Oligocene global sea level fall increases winter sea level pressure by ∼2 to 4 hPa over Siberia (Fig. 7 g) and induces the southward expansion of the North Pacific Aleutian low, which altogether increase the pressure gradient between those two regions. Similar trend is obtained, although in a lower magnitude, with our simulation testing the effect of the Arabian platform emergence, while the final retreat of the Paratethys Sea tested in Miocene configuration does not trigger changes (Fig. 13). A modern-like Siberian High with typical EAWM wind patterns is however not simulated until our middle and late Miocene simulations, when the current Tian Shan and Mongolian landforms are set to their present elevations. Collectively, these results suggest that continentality increase may have induced changes in wintertime pressure gradients and atmospheric circulation mostly before the uplift of Tian Shan and Mongolian landforms, but would have had a decreasing importance afterwards.

We also acknowledge that the Mongolian and Tian Shan uplifting history was likely more complex than depicted here, with signs of early uplift in the Hangay region as soon as the Oligocene. Performing additional experiments allowing to test the role of an uplifted Hangay dome in an Oligocene configuration should allow us to evaluate the potential

presence of a Siberian High at that time. This may help interpreting precocious loess-like deposits observed at that time in the Chinese Loess Plateau and Mongolia (J. Sun & Windley, 2015; Wasiljeff et al., 2022). The presence loess-like deposits in the Xining Basin at ∼40 Ma however, seems too old to be attributed to the development of the modern Siberian High, if its full development is conditional to uplift of the Mongolian and Tian Shan landforms. This discrepancy suggest that additional mechanisms for dust transport over long distances should be explored for this period, although testing this hypothesis would require further investigation, likely with daily to hourly wind speed outputs (Aoki et al., 2005).

7.2 Peripheral landforms critical role in monsoon seasonal feature settlement in the Miocene

7.2.1 Tian Shan, Pamir and Mongolia: small mountains, strong effect

The role played by Mongolian landform uplift in the inception of the Siberian High is one of the most salient outcomes of these experiments. Previous modeling works based on modern geography that have tested the effect of Mongolia uplift (Sha et al., 2015; Shi et al., 2015; Yu et al., 2018) reproduce the same tendencies we have presented, namely a strong increase of the winter sea level pressure over Siberia and typical deflation of the westerly flow towards northern latitudes resulting in a pronounced drying of Eastern Asia and EAWM amplification (Fig. 11 d). Other studies simulate increased EASM precipitation and wind circulation, although they incorporate Tian Shan uplift together with Mongolia (Yu et al., 2018; R. Zhang et al., 2012; H. Tang et al., 2013; Zhisheng et al., 2001), which remains coherent with our findings testing the uplift of both features (Fig. 11 h). Paleoclimate simulations using more realistic paleogeographic reconstructions (Eocene or Oligocene) tend to confirm such tendencies, although the effect of Mongolian landforms was not explicitly tested. Generally, we can observe that when a modern-like Mongolia was prescribed, the simulated winds and precipitation were close to modern-like EAWM (Licht et al., 2014; X. Li et al., 2017), while it is not the case with a reduced Mongolia elevation (Huber & Goldner, 2012).

The effect of the Tian Shan ranges uplift on Asian climate is less conspicuous and seems also more sensitive to the degree of uplift of other surrounding landforms (such as the Pamir-Karakoram, the Hindu Kush or Iran-Zagros), likely owing to its lower latitude. While a rigorous comparison between our results and previous studies is hampered by too many diverging boundary conditions, all tend to point that the Tian Shan uplift would have i) increased yearly orographic precipitation on the ranges, ii) decreased it in the Tarim Basin located in their rain shadow and in inland Asia mid latitudes and iii) reinforced the EAM through increased summer precipitation (Fig. 11 m,n,o) (Baldwin & Vecchi, 2016; H. Tang et al., 2013; Yu et al., 2018; R. Zhang et al., 2017). The key role played by the Tian Shan ranges, together with the Pamirs and Mongolian landforms in triggering the Jet Stream northward migration in summer (Fig. 19e,f and Fig. 9e,h,k,n), as suggested by previous modeling works derived from modern geography (Sha et al., 2020; Shi et al., 2015), likely contributes to increase the EAM. Nevertheless, substantial differences are noted with other modeling studies, especially regarding the effect on SAM domain: where we simulate a weakening of SAM seasonality due to increased winter precipitation, opposite trend is simulated in studies where the Iran-Zagros and Hindu Kush are fully uplifted and prevent the westerly flux to bring moisture to India (Baldwin & Vecchi, 2016; H. Tang et al., 2013; Yu et al., 2018; R. Zhang et al., 2017; X. Wang et al., 2020).

7.2.2 East Africa and Zagros-Anatolia: the Far West uplifts and SAM evolution

Our set of simulation highlight in addition that paleogeographic evolution in the Middle Eastern and East African regions have been important for the Neogene evolution of the SASM as they strongly contributed to the settlement of modern-like atmospheric circulation

as discussed by Sarr et al. (2022). The presence of intermediate to high elevation topography in East Africa in the early Miocene is for example crucial for the "early" bending of the Somali Jet, before the closure of the West Tethys seaway and settlement of Iran-Zagros topography with modern-like elevation (Fig. 9).

Increasing elevation in the East African region is also responsible, in our simulations for increasing SAWM precipitation (Fig. 9), which contrast with previous studies that simulate reduced SASM precipitation instead (H.-H. Wei & Bordoni, 2016; Chakraborty et al., 2009) as topography would block the advection of moisture from equatorial Africa towards India. We hypothesize that such difference may come from these studies using present-day paleogeography, and/or unchanged fixed SSTs for all the experiments, thereby neglecting the potential effect of the East Africa uplift on Indian Ocean SSTs and SST gradients. These studies however critically highlight that a reinforced Somali Jet may not be systematically correlated with increased SAM precipitation, although this genetic relationship is commonly found in the literature. Alongside, increasing land exposure in the Arabian platform region in the middle Miocene, the uplift of the Iran-Zagros topography strongly reinforces the Somali Jet speed and northward migration, together with the summer precipitation amounts (Fig. 5, Fig. 9), as previously suggested by (R. Zhang et al., 2017; Acosta & Huber, 2020; H. Tang et al., 2013).

Given their respective impact in the SAM, knowledge of the evolution of those western topographies, although seldom taken into account, is critical to interpret paleoenvironmental indicators. This is especially true for inland Asia and northwestern India regions, because of their key location with respect to the westerlies flux. Westerlies may indeed be deviated either to the North or the South depending on the Zagros-Iran and Tian Shan respective elevation. Indication of increased SAM precipitation during the Miocene (X. Yang et al., 2020) could for example be, at least partly due to Zagros-Iran uplift, as geological evidences indicate that the high topography settled at that time (Austermann et al., 2017; François et al., 2014).

7.3 Miocene continentality increase as an amplifier of SAM, EAM and inland aridity

The northward motion of the ITCZ over the Arabian Sea and the stronger SASM precipitation in response to continentality increase in the Miocene is a feature clearly simulated in our experiments, and which is obtained with either the Paratethys Sea retreat or the Arabian peninsula emergence (Fig. 8 e,h). The role of the Paratethys Sea retreat as a vector of amplified summer low sea level pressure zone and resulting moisture advection via strengthened Somali Jet is well established by modeling experiments (Ramstein et al., 1997; Fluteau et al., 1999; R. Zhang et al., 2021; Z. Zhang et al., 2007). The Paratethys Sea retreat also drastically dries the "westerly corridor" (centered around 40°N, Fig. 8 h) which overall results in increased inland Asian aridity and moderately increases EAM seasonality, north and south of this latitudinal band (Fig. 8 i). These patterns are mostly coherent with those obtained by previous modeling studies (R. Zhang et al., 2021; Z. Zhang et al., 2007), although here again, important differences in the paleogeography and type of model that were used prevent a rigorous comparison.

On the other hand, the effect of increased land exposure in the Arabian peninsula region on Asian climate was, to our knowledge, significantly less explored by modeling studies and is never mentioned as a potential forcing by field work. In most modeling studies, the region usually evolves together with the global paleogeography, without being specifically tested. We putatively attribute this to the lack of constraints and data in this region. Given the shallowness and extension of the Arabian peninsula (∼3 million square meters, roughly comparable to India area), it is very likely that the episodes of partial or complete flooding that it witnessed from the Oligocene to the late Miocene (Barrier et al., 2018; Otero & Gayet, 2001) may have had great consequences on atmospheric circulation

patterns. Our results show that increased peninsula exposure reinforces the Somali Jet in summer and enhances summer precipitation in SAM and EAM domains (Fig. 8 e). Additionally, it drives the onset of upwelling in the Arabian Sea (see Sarr et al. (2022), with the same set of simulations), which are traditionally used as proxies indicating the establishment of a monsoon regime in South Asia. These findings imply that a proto-Somali Jet and intense summer precipitation settled before the emergence the Arabian peninsula in the middle Miocene, and therefore before the recording of upwelling in the Arabian Sea. In any cases, the onset of upwellings in the Arabian Sea was likely decorrelated from potential Miocene uplifts events in the Himalaya-Tibet region (Sarr et al., 2022).

7.4 Persistent uncertainties and directions for further works

Our study demonstrates the key role played by land-sea distribution and by all topographic features surrounding the Indian Ocean in shaping the modern SAM, EAM and inland Asia aridity. Nevertheless, additional work is required from both modeling and the field research to help refine our understanding of the complex mechanisms at play throughout the Cenozoic in Asia.

7.4.1 Opposite effect and thresholds crossings: the need for improved relative and absolute timing and elevation constraints on uplift events

Overall, our results highlight the strong crossed influence of the various sub-geographical units on resulting monsoons and therefore the conceptual limitations of performing tests based on modern geographies or assuming homogeneous Asian orography uplift in the course of time to evaluate past monsoon evolution. In that aspect, it is not surprising that most of such studies simulate somehow modern-like summer and winter monsoons when keeping uplifted African, Mongolian and Iranian landforms, as well as an emerged Arabia (Roe et al., 2016; Zoura et al., 2019; Acosta & Huber, 2020).

The need to better constrain the evolution in time, elevation and shape of the various Asian, East African and Anatolian landforms, appears paramount, in order to refine our understanding of Cenozoic paleoclimate evolution. Our results also suggest that some paleogeographic events may have had contrary influences on either SAM or EAM, although we might picture them as roughly coeval. This is for example the case of the Tien-Shan and Pamir uplifts that weaken SAM seasonality, while Mongolian and Iran-Zagros uplifts, together with continentality strengthen it. Here, we chose to perform our mid-late Miocene sensitivity tests based on a halfway uplifted Iran-Zagros orogen (LMio_SmallT), but it is likely that we may obtain different results if testing the uplift on Mongolia (for example) in a paleogeography with an already fully uplifted Iran-Zagros topography. Refining the relative chronology of these various paleogeographic events is therefore critical to better interpret the variations in monsoon intensity recorded by the proxies. Additionally, paleoelevation thresholds are likely to be critical for constraining the Asian climate evolution, due to interactions of the topography with either low level (e.g. the summer monsoon winds) or mid troposheric (e.g. the Jet Stream) air masses (X. Liu & Yin, 2002; X. Wang et al., 2020; Zhisheng et al., 2001; Prell & Kutzbach, 1992).

7.4.2 Land-sea distribution and gateway closure

A more precise view of land-sea distribution and regional seaways evolution is also paramount. Indeed, they influence the surface temperature gradients, and therefore condition sea level pressure patterns, low tropospheric circulation as well as oceanic surface circulation. Although our results point to a minimal effect of the mechanical closure of the Tethyan Seaway on regional results, other features need to be tested. For example, a better understanding of the Indonesian Gateway and Indonesian throughflow evolution would be of great interest, as they control part of Indo-Pacific Warm Pool SSTs distribution (Cane & Molnar, 2001). While the final step of the gateway constriction likely occurs during

the Pliocene (Auer et al., 2019), its paleobathymetric and geometric configuration remains however largely undocumented between 17-3.5 Ma, due to difficulties in reconstructing the complex configuration of the region (Kuhnt et al., 2004). Although no major tectonic deformation is supposed to have occurred during this period, the shallow depth of the gateway likely made it sensitive to middle Miocene sea level fluctuations (Sosdian & Lear, 2020), with possible impact the Eastern Indian and Western Pacific oceans surface temperatures and therefore on SST gradients.

8 Conclusions

In this study, we took advantage of the rich discoveries that have allowed to extend the fossil record to the Paleogene in Asia, as well as the consolidation of the understanding of the physical concepts underpinning the monsoons brought by modeling studies. Overall, we simulate an intensification of all considered monsoon metrics throughout the Cenozoic, in response to specific forcings. We find that, in agreement with paleoclimate indicators, modern-like monsoons, in terms of atmospheric circulation, seasonality and precipitation amounts, likely exist since at least the mid-late Miocene. We however show that high seasonality in precipitation may have existed since the Paleogene in both SAM and EAM domains, before the settlement of modern atmospheric circulation patterns. In agreement with previous studies, our results highlight the rather limited effect of pCO_2 when compared to paleogeographic changes, with the notable exception of the effect of the pCO_2 drawdown at the EOT on the Jet Stream latitudinal migration over the year in the Tibetan region.

First, although the exact shape and extent of coastal shallow environments remain poorly constrained, our results strongly hint that any variations in the land-sea distribution, whether due to tectonic activity, or sea level fluctuations, would have strongly impacted the Asian climate. Many episodes of increased continentality are documented in the course of the Cenozoic, including the regional regressions of the Paratethys epicontinental Sea, periodical exposure of the Arabian platform due to sea level fluctuations, and global sea level fall at the Eocene Oligocene Transition. All of these events likely favored the enhancement of summer moisture penetration into Asia, by promoting the extension of the wide subtropical low pressure belt and thus amplifying the seasonal latitudinal migration of the ITCZ on land.

Second, while the HTP complex was recurrently put forward as the leading mechanism in Asian climate evolution, our results rather points toward a shared responsibility between all landforms surrounding the modern Indian Ocean. We also stress the fact that all paleogeographic features do not bear the same importance on SASM, EASM or EAWM respectively. The Tibetan Plateau uplift likely favored the onset of monsoon-like precipitation seasonality in eastern Asia in the Eocene, by promoting the advection of moist air masses in summer, and by partially shielding the region from westerly moisture input in winter. The Miocene Eastern African and Iran-Zagros uplift were critical to intensify and redirect the Somali Jet towards the Indian subcontinent, and thus develop the modern-like South Asian monsoon summer circulation and amplify moisture advection to Asia in summer. Additionally, Iranian-Anatolian uplift, by blocking moisture advection from the westerlies to lower latitudes likely contributed enhance winter aridity in most of Southeastern Asia. The Himalaya-Tibet complex then conditions the SASM precipitation distribution over the South Asian region, triggers heavy orographic precipitation and upper atmosphere heating over northern India.

We show that the uplift of the Tian Shan and the Mongolian mountains was key for the settlement of the winter Siberian high pressure cell, and resulting aridification of inland and eastern Asia in winter. The summer Jet Stream migration northward of the Tibetan Plateau was likely amplified in the mid-late Miocene, as the Pamir and Tian Shan landforms approached their modern elevation and contributed to its channeling toward higher latitudes. This relocation of the Jet Stream amplifies the penetration of moist air masses over eastern

China, thus contributing to increase the EAM precipitation seasonality. Overall, our results, in agreement with available paleoclimate indicators and most previous modeling studies, show the fundamentally polygenetic history of monsoonal evolution, suggesting that the very concept of a "monsoon onset" is inappropriate. We also stress the need for more accurate constrains regarding paleoshorelines evolutions, relative timing of uplift and landforms paleoelevations in order to propose better global climate evolution scenarios.

Acronyms

ITCZ Inter Tropical Convergence Zone
SASM South Asian Summer Monsoon
EASM East Asian Summer Monsoon
EAWM East Asian Winter Monsoon
HTP Himalaya-Tibetan Plateau
IGLLJ Indo-Gangetic Low Level Jet
MMCO Mid Miocene Climatic Optimum
EOT Eocene Oligocene Transition

Acknowledgments

The scientific colour maps (https://www.fabiocrameri.ch/colourmaps/) (Crameri, 2021) used in most of the Figures prevent visual distortion of the data and exclusion of readers with colourvision deficiencies (Crameri et al., 2020). D.T., G.L.H., F.F., A.T., Y.D., P.S., J-B.L. and A-C.S. were granted access to the HPC resources of TGCC under the allocations 2018-A0050107601, 2018-A0030102212, 2019-A0070107601, 2019-A0050102212 and 2020-A0090107601 made by GENCI. Y.D. acknowledges support from ANR AMOR (ANR-16-CE31-0020). Most of the Figures were done using NOAA pyferret within Jupyter notebooks, thanks to the ferretmagic add-on developed at LSCE by Patrick Brockmann. Ferret is a product of NOAA's Pacific Marine Environmental Laboratory. Information is available at http://ferret.pmel.noaa.gov/Ferret (last access: 1 Jan 2022; NOAA's Pacific Marine Environmental Laboratory, 2020), distributed under the Open Source Definition. The Jupyter notebook is an open-source web application. The paleogeographic configurations from F.P. were produced using the paleoenvironment online application (https://map.paleoenvironment.eu/). Other reconstructions were obtained with NetCDF editor online tools developed by the Paleoclimate modelling group at CEREGE laboratory (https://paleoclim-cnrs.github.io/documentation-processing/IPSL_Boundary_Conditions/).

References

Abbott, A. N., Haley, B. A., Tripati, A. K., & Frank, M. (2016, April). Constraints on ocean circulation at the Paleocene–Eocene Thermal Maximum from neodymium isotopes. *Climate of the Past*, *12*(4), 837–847. Retrieved 2017-10-09, from http://www.clim-past.net/12/837/2016/ doi: 10.5194/cp-12-837-2016

Abels, H. A., Dupont-Nivet, G., Xiao, G., Bosboom, R., & Krijgsman, W. (2011, January). Step-wise change of Asian interior climate preceding the Eocene–Oligocene Transition (EOT). *Palaeogeography, Palaeoclimatology, Palaeoecology*, *299*(3-4), 399–412. Retrieved 2017-10-09, from http://linkinghub.elsevier.com/retrieve/pii/S0031018210007042 doi: 10.1016/j.palaeo.2010.11.028

Acosta, R. P., & Huber, M. (2017). The neglected Indo-Gangetic Plains low-level jet and its importance for moisture transport and precipitation during the peak summer monsoon. *Geophysical Research Letters*, *44*(16), 8601–8610. Retrieved 2021-03-08, from https://agupubs.onlinelibrary.wiley.com/doi/abs/10.1002/2017GL074440 (_eprint: https://agupubs.onlinelibrary.wiley.com/doi/pdf/10.1002/2017GL074440) doi: https://doi.org/10.1002/2017GL074440

Acosta, R. P., & Huber, M. (2020, February). Competing Topographic Mechanisms for the Summer Indo-Asian Monsoon. *Geophysical Research Letters*, *47*(3). Retrieved 2020-06-19, from https://onlinelibrary.wiley.com/doi/abs/10.1029/2019GL085112 doi: 10.1029/2019GL085112

Agard, P., Omrani, J., Jolivet, L., Whitechurch, H., Vrielynck, B., Spakman, W., ... Wortel, R. (2011, November). Zagros orogeny: a subduction-dominated process. *Geological Magazine*, *148*(5-6), 692–725. Retrieved 2017-10-09, from http://www.journals.cambridge.org/abstract_S001675681100046X doi: 10.1017/S001675681100046X

Ali, J. R., & Aitchison, J. C. (2008, June). Gondwana to Asia: Plate tectonics, paleogeography and the biological connectivity of the Indian sub-continent from the Middle Jurassic through latest Eocene (166–35 Ma). *Earth-Science Reviews*, *88*(3-4), 145–166. Retrieved 2020-10-14, from https://linkinghub.elsevier.com/retrieve/pii/S0012825208000196 doi: 10.1016/j.earscirev.2008.01.007

Ali, S., Hathorne, E. C., & Frank, M. (2021). Persistent Provenance of South Asian Monsoon-Induced Silicate Weathering Over the Past 27 Million Years. *Paleoceanography and Paleoclimatology*, *36*(3), e2020PA003909. Retrieved 2022-05-02, from https://onlinelibrary.wiley.com/doi/abs/10.1029/2020PA003909 (_eprint: https://onlinelibrary.wiley.com/doi/pdf/10.1029/2020PA003909) doi: 10.1029/2020PA003909

Ao, H., Roberts, A. P., Dekkers, M. J., Liu, X., Rohling, E. J., Shi, Z., ... Zhao, X. (2016, June). Late Miocene–Pliocene Asian monsoon intensification linked to Antarctic ice-sheet growth. *Earth and Planetary Science Letters*, *444*, 75–87. Retrieved 2022-05-03, from https://linkinghub.elsevier.com/retrieve/pii/S0012821X16301157 doi: 10.1016/j.epsl.2016.03.028

Ao, H., Rohling, E. J., Zhang, R., Roberts, A. P., Holbourn, A. E., Ladant, J.-B., ... An, Z. (2021, November). Global warming-induced Asian hydrological climate transition across the Miocene–Pliocene boundary. *Nature Communications*, *12*(1), 6935. Retrieved 2022-05-03, from http://www.nature.com/articles/s41467-021-27054-5 (Number: 1 Publisher: Nature Publishing Group) doi: 10.1038/s41467-021-27054-5

Aoki, I., Kurosaki, Y., Osada, R., Sato, T., & Kimura, F. (2005). Dust storms generated by mesoscale cold fronts in the Tarim Basin, Northwest China. *Geophysical Research Letters*, *32*(6). Retrieved 2022-02-21, from http://onlinelibrary.wiley.com/doi/abs/10.1029/2004GL021776 (_eprint: https://agupubs.onlinelibrary.wiley.com/doi/pdf/10.1029/2004GL021776) doi: 10.1029/2004GL021776

Auer, G., Vleeschouwer, D. D., Smith, R. A., Bogus, K., Groeneveld, J., Grunert, P., ... Henderiks, J. (2019). Timing and Pacing of Indonesian Throughflow Restriction and Its Connection to Late Pliocene Climate Shifts. *Paleoceanography and Paleoclimatology*, *34*(4), 635–657. Retrieved 2021-09-02, from http://

agupubs.onlinelibrary.wiley.com/doi/abs/10.1029/2018PA003512 (_eprint: https://onlinelibrary.wiley.com/doi/pdf/10.1029/2018PA003512) doi: 10.1029/2018PA003512

Austermann, J., Mitrovica, J. X., Huybers, P., & Rovere, A. (2017, July). Detection of a dynamic topography signal in last interglacial sea-level records. *Science Advances*, *3*(7), e1700457. Retrieved 2021-04-07, from https://advances.sciencemag.org/content/3/7/e1700457 (Publisher: American Association for the Advancement of Science Section: Research Article) doi: 10.1126/sciadv.1700457

Averyanova, A., Tarasevich, V., Popova, S., Utescher, T., Li, S.-F., Mosbrugger, V., & Xing, Y. (2021, February). Rupelian Kazakhstan floras in the context of early Oligocene climate and vegetation in Central Asia. *Terra Nova*, *33*. doi: 10.1111/ter.12523

Baldermann, A., Wasser, O., Abdullayev, E., Bernasconi, S., Löhr, S., Wemmer, K., ... Richoz, S. (2021, September). Palaeo-environmental evolution of Central Asia during the Cenozoic: new insights from the continental sedimentary archive of the Valley of Lakes (Mongolia). *Climate of the Past*, *17*(5), 1955–1972. Retrieved 2022-03-09, from https://cp.copernicus.org/articles/17/1955/2021/ doi: 10.5194/cp-17-1955-2021

Baldwin, J., & Vecchi, G. (2016, August). Influence of the Tian Shan on Arid Extratropical Asia. *Journal of Climate*, *29*(16), 5741–5762. Retrieved 2021-09-23, from https://journals.ametsoc.org/view/journals/clim/29/16/jcli-d-15-0490.1.xml (Publisher: American Meteorological Society Section: Journal of Climate) doi: 10.1175/JCLI-D-15-0490.1

Ballato, P., Landgraf, A., Schildgen, T. F., Stockli, D. F., Fox, M., Ghassemi, M. R., ... Strecker, M. R. (2015, September). The growth of a mountain belt forced by base-level fall: Tectonics and surface processes during the evolution of the Alborz Mountains, N Iran. *Earth and Planetary Science Letters*, *425*, 204–218. Retrieved 2021-03-10, from https://www.sciencedirect.com/science/article/pii/S0012821X15003490 doi: 10.1016/j.epsl.2015.05.051

Ballato, P., Mulch, A., Landgraf, A., Strecker, M. R., Dalconi, M. C., Friedrich, A., & Tabatabaei, S. H. (2010, November). Middle to late Miocene Middle Eastern climate from stable oxygen and carbon isotope data, southern Alborz mountains, N Iran. *Earth and Planetary Science Letters*, *300*(1), 125–138. Retrieved 2021-04-07, from https://www.sciencedirect.com/science/article/pii/S0012821X10006308 doi: 10.1016/j.epsl.2010.09.043

Bande, A., Sobel, E. R., Mikolaichuk, A., Schmidt, A., & Stockli, D. F. (2017). Exhumation history of the western Kyrgyz Tien Shan: Implications for intramontane basin formation. *Tectonics*, *36*(1), 163–180. Retrieved 2021-03-26, from http://agupubs.onlinelibrary.wiley.com/doi/abs/10.1002/2016TC004284 (_eprint: https://onlinelibrary.wiley.com/doi/pdf/10.1002/2016TC004284) doi: https://doi.org/10.1002/2016TC004284

Bannon, P. R. (1979, November). On the Dynamics of the East African Jet. I: Simulation of Mean Conditions for July. *Journal of the Atmospheric Sciences*, *36*(11), 2139–2152. Retrieved 2019-07-05, from http://journals.ametsoc.org/doi/abs/10.1175/1520-0469%281979%29036%3C2139%3AOTDOTE%3E2.0.CO%3B2 doi: 10.1175/1520-0469(1979)036⟨2139:OTDOTE⟩2.0.CO;2

Barbolini, N., Woutersen, A., Dupont-Nivet, G., Silvestro, D., Tardif, D., Coster, P. M. C., ... Hoorn, C. (2020). Cenozoic evolution of the steppe-desert biome in Central Asia. *Science Advances*, *6*(41), eabb8227. Retrieved 2022-05-03, from https://www.science.org/doi/10.1126/sciadv.abb8227 (Publisher: American Association for the Advancement of Science) doi: 10.1126/sciadv.abb8227

Barrier, , Vrielynck, B., & Brunet-Lourdin, M.-F. (2018). *Paleotectonic Reconstruction of the Central Tethyan Realm: Tectonono-Sedimentary-Palinspastic Maps from Late Permian to Pliocene: Atlas of 20 Maps.*

Beasley, C., Kender, S., Giosan, L., Bolton, C. T., Anand, P., Leng, M. J., ... Littler, K. (2021). Evidence of a South Asian Proto-Monsoon Dur-

ing the Oligocene-Miocene Transition. *Paleoceanography and Paleoclimatology*, *36*(9), e2021PA004278. Retrieved 2022-05-03, from https://onlinelibrary.wiley.com/doi/abs/10.1029/2021PA004278 (_eprint: https://onlinelibrary.wiley.com/doi/pdf/10.1029/2021PA004278) doi: 10.1029/2021PA004278

Bershaw, J., Garzione, C. N., Schoenbohm, L., Gehrels, G., & Tao, L. (2012, January). Cenozoic evolution of the Pamir plateau based on stratigraphy, zircon provenance, and stable isotopes of foreland basin sediments at Oytag (Wuyitake) in the Tarim Basin (west China). *Journal of Asian Earth Sciences*, *44*, 136–148. Retrieved 2017-10-09, from http://linkinghub.elsevier.com/retrieve/pii/S1367912011001878 doi: 10.1016/j.jseaes.2011.04.020

Betzler, C., Eberli, G. P., Kroon, D., Wright, J. D., Swart, P. K., Nath, B. N., ... Young, J. R. (2016, July). The abrupt onset of the modern South Asian Monsoon winds. *Scientific Reports*, *6*(1), 29838. Retrieved 2022-05-03, from http://www.nature.com/articles/srep29838 (Number: 1 Publisher: Nature Publishing Group) doi: 10.1038/srep29838

Betzler, C., Eberli, G. P., Lüdmann, T., Reolid, J., Kroon, D., Reijmer, J. J. G., ... Yao, Z. (2018, January). Refinement of Miocene sea level and monsoon events from the sedimentary archive of the Maldives (Indian Ocean). *Progress in Earth and Planetary Science*, *5*(1), 5. Retrieved 2021-03-17, from https://doi.org/10.1186/s40645-018-0165-x doi: 10.1186/s40645-018-0165-x

Bhatia, H., Khan, M. A., Srivastava, G., Hazra, T., Spicer, R., Hazra, M., ... Roy, K. (2021, May). Late Cretaceous–Paleogene Indian monsoon climate vis-à-vis movement of the Indian plate, and the birth of the South Asian Monsoon. *Gondwana Research*, *93*, 89–100. Retrieved 2022-05-03, from https://linkinghub.elsevier.com/retrieve/pii/S1342937X21000289 doi: 10.1016/j.gr.2021.01.010

Bhatia, H., Srivastava, G., Adhikari, P., Tao, S., Utescher, T., Paudayal, K. N., & Mehrotra, R. C. (2022, April). Asian monsoon and vegetation shift: evidence from the Siwalik succession of India. *Geological Magazine*, 1–18. Retrieved 2022-05-02, from http://www.cambridge.org/core/journals/geological-magazine/article/asian-monsoon-and-vegetation-shift-evidence-from-the-siwalik-succession-of-india/C11DD05BB2C70B0BA4ED7930A80219D2 (Publisher: Cambridge University Press) doi: 10.1017/S0016756822000243

Bhatia, H., Srivastava, G., Spicer, R., Farnsworth, A., Spicer, T., Mehrotra, R., ... Valdes, P. (2021, January). Leaf physiognomy records the Miocene intensification of the South Asia Monsoon. *Global and Planetary Change*, *196*, 103365. Retrieved 2022-05-03, from https://linkinghub.elsevier.com/retrieve/pii/S0921818120302563 doi: 10.1016/j.gloplacha.2020.103365

Bialik, O. M., Auer, G., Ogawa, N. O., Kroon, D., Waldmann, N. D., & Ohkouchi, N. (2020). Monsoons, Upwelling, and the Deoxygenation of the Northwestern Indian Ocean in Response to Middle to Late Miocene Global Climatic Shifts. *Paleoceanography and Paleoclimatology*, *35*(2), e2019PA003762. Retrieved 2021-03-17, from http://agupubs.onlinelibrary.wiley.com/doi/abs/10.1029/2019PA003762 (_eprint: https://onlinelibrary.wiley.com/doi/pdf/10.1029/2019PA003762) doi: https://doi.org/10.1029/2019PA003762

Bialik, O. M., Frank, M., Betzler, C., Zammit, R., & Waldmann, N. D. (2019, June). Two-step closure of the Miocene Indian Ocean Gateway to the Mediterranean. *Scientific Reports*, *9*(1), 8842. Retrieved 2021-03-09, from https://www.nature.com/articles/s41598-019-45308-7 (Number: 1 Publisher: Nature Publishing Group) doi: 10.1038/s41598-019-45308-7

Bierman, P. R., Shakun, J. D., Corbett, L. B., Zimmerman, S. R., & Rood, D. H. (2016, December). A persistent and dynamic East Greenland Ice Sheet over the past 7.5 million years. *Nature*, *540*(7632), 256–260. Retrieved 2021-06-21, from http://www.nature.com/articles/nature20147 (Bandiera_abtest: a Cg_type: Nature Research Journals Number: 7632 Primary_atype: Research Publisher: Nature

Publishing Group Subject_term: Cryospheric science;Nuclear chemistry;Palaeoclimate Subject_term_id: cryospheric-science;nuclear-chemistry;palaeoclimate) doi: 10.1038/nature20147

Blayney, T., Najman, Y., Dupont-Nivet, G., Carter, A., Millar, I., Garzanti, E., ... Vezzoli, G. (2016, October). Indentation of the Pamirs with respect to the northern margin of Tibet: Constraints from the Tarim basin sedimentary record: INDENTATION OF THE PAMIRS. *Tectonics*, *35*(10), 2345–2369. Retrieved 2017-10-09, from http://doi.wiley.com/10.1002/2016TC004222 doi: 10.1002/2016TC004222

Bolton, C. T., Gray, E., Kuhnt, W., Holbourn, A. E., Lübbers, J., Grant, K., ... Andersen, N. (2021, June). *Secular and orbital-scale variability of equatorial Indian Ocean summer monsoon winds during the late Miocene* (preprint). Ocean Dynamics/Marine Archives/Milankovitch. Retrieved 2021-09-07, from https://cp.copernicus.org/preprints/cp-2021-77/ doi: 10.5194/cp-2021-77

Bolton, C. T., Gray, E., Kuhnt, W., Holbourn, A. E., Lübbers, J., Grant, K., ... Andersen, N. (2022, April). Secular and orbital-scale variability of equatorial Indian Ocean summer monsoon winds during the late Miocene. *Climate of the Past*, *18*(4), 713–738. Retrieved 2022-06-02, from https://cp.copernicus.org/articles/18/713/2022/ doi: 10.5194/cp-18-713-2022

Boos, W. R., & Kuang, Z. (2010, January). Dominant control of the South Asian monsoon by orographic insulation versus plateau heating. *Nature*, *463*(7278), 218–222. Retrieved 2017-10-09, from http://www.nature.com/doifinder/10.1038/nature08707 doi: 10.1038/nature08707

Bosboom, R., Dupont-Nivet, G., Grothe, A., Brinkhuis, H., Villa, G., Mandic, O., ... Krijgsman, W. (2014a, October). Linking Tarim Basin sea retreat (west China) and Asian aridification in the late Eocene. *Basin Research*, *26*(5), 621–640. Retrieved 2017-10-09, from http://doi.wiley.com/10.1111/bre.12054 doi: 10.1111/bre.12054

Bosboom, R., Dupont-Nivet, G., Grothe, A., Brinkhuis, H., Villa, G., Mandic, O., ... Guo, Z. (2014b, June). Timing, cause and impact of the late Eocene stepwise sea retreat from the Tarim Basin (west China). *Palaeogeography, Palaeoclimatology, Palaeoecology*, *403*, 101–118. Retrieved 2017-10-09, from http://linkinghub.elsevier.com/retrieve/pii/S0031018214001709 doi: 10.1016/j.palaeo.2014.03.035

Bosboom, R., Mandic, O., Dupont-Nivet, G., Proust, J.-N., Ormukov, C., & Aminov, J. (2017). Late Eocene palaeogeography of the proto-Paratethys Sea in Central Asia (NW China, southern Kyrgyzstan and SW Tajikistan). *Geological Society, London, Special Publications*, *427*(1), 565–588. Retrieved 2019-11-22, from http://sp.lyellcollection.org/lookup/doi/10.1144/SP427.11 doi: 10.1144/SP427.11

Botsyun, S., Sepulchre, P., Donnadieu, Y., Risi, C., Licht, A., & Caves Rugenstein, J. K. (2019, March). Revised paleoaltimetry data show low Tibetan Plateau elevation during the Eocene. *Science*, *363*(6430), eaaq1436. Retrieved 2019-07-23, from http://www.sciencemag.org/lookup/doi/10.1126/science.aaq1436 doi: 10.1126/science.aaq1436

Botsyun, S., Sepulchre, P., Risi, C., & Donnadieu, Y. (2016, June). Impacts of Tibetan Plateau uplift on atmospheric dynamics and associated precipitation ^{18}O. *Climate of the Past*, *12*(6), 1401–1420. Retrieved 2017-10-09, from http://www.clim-past.net/12/1401/2016/ doi: 10.5194/cp-12-1401-2016

Boucot, A. J., Xu, C., Scotese, C. R., & Morley, R. J. (2013). *Phanerozoic Paleoclimate: An Atlas of Lithologic Indicators of Climate*. Tulsa, Oklahoma, U.S.A.: SEPM (Society for Sedimentary Geology). Retrieved 2019-11-04, from https://pubs.geoscienceworld.org/books/book/1966/ doi: 10.2110/sepmcsp.11

Bougeois, L., Dupont-Nivet, G., de Rafélis, M., Tindall, J. C., Proust, J.-N., Reichart, G.-J., ... Ormukov, C. (2018, March). Asian monsoons and aridification response to Paleogene sea retreat and Neogene westerly shielding indicated by seasonality in Paratethys oysters. *Earth and Planetary Science Letters*, *485*, 99–110. Retrieved 2018-04-03, from http://linkinghub.elsevier.com/retrieve/pii/S0012821X17307483 doi: 10.1016/j.epsl.2017.12.036

Bullen, M., Burbank, D., & Garver, J. (2003, March). Building the Northern Tien Shan: Integrated Thermal, Structural, and Topographic Constraints. *The Journal of Geology*, *111*(2), 149–165. Retrieved 2021-03-26, from https://www.journals.uchicago.edu/doi/10.1086/345840 doi: 10.1086/345840

Burls, N. J., Bradshaw, C. D., Boer, A. M. D., Herold, N., Huber, M., Pound, M., ... Zhang, Z. (2021). Simulating Miocene Warmth: Insights From an Opportunistic Multi-Model Ensemble (MioMIP1). *Paleoceanography and Paleoclimatology*, *36*(5), e2020PA004054. Retrieved 2021-06-21, from http://agupubs.onlinelibrary.wiley.com/doi/abs/10.1029/2020PA004054 (_eprint: https://onlinelibrary.wiley.com/doi/pdf/10.1029/2020PA004054) doi: 10.1029/2020PA004054

Cane, M. A., & Molnar, P. (2001, May). Closing of the Indonesian seaway as a precursor to east African aridification around 3–4 million years ago. *Nature*, *411*(6834), 157–162. Retrieved 2021-09-09, from http://www.nature.com/articles/35075500 (Bandiera_abtest: a Cg_type: Nature Research Journals Number: 6834 Primary_atype: Research Publisher: Nature Publishing Group) doi: 10.1038/35075500

Carrapa, B., DeCelles, P. G., Wang, X., Clementz, M. T., Mancin, N., Stoica, M., ... Chen, F. (2015, August). Tectono-climatic implications of Eocene Paratethys regression in the Tajik basin of central Asia. *Earth and Planetary Science Letters*, *424*, 168–178. Retrieved 2022-03-21, from https://www.sciencedirect.com/science/article/pii/S0012821X15003325 doi: 10.1016/j.epsl.2015.05.034

Cavazza, W., Cattò, S., Zattin, M., Okay, A. I., & Reiners, P. (2018, August). Thermochronology of the Miocene Arabia-Eurasia collision zone of southeastern Turkey. *Geosphere*, *14*(5), 2277–2293. Retrieved 2022-03-04, from https://doi.org/10.1130/GES01637.1 doi: 10.1130/GES01637.1

Caves Rugenstein, J., Bayshashov, B., Zhamangara, A., Ritch, A., Ibarra, D., Mix, H., ... Chamberlain, C. (2017, February). Late Miocene Uplift of the Tian Shan and Altai and Reorganization of Central Asia Climate. *GSA Today*, *27*. doi: 10.1130/GSATG305A.1

Caves Rugenstein, J., Sjostrom, D., Mix, H., Winnick, M., & Chamberlain, C. (2014, September). Aridification of Central Asia and Uplift of the Altai and Hangay Mountains, Mongolia: Stable Isotope Evidence. *American Journal of Science*, *314*, 1171–1201. doi: 10.2475/08.2014.01]

Cerling, T. E., Wang, Y., & Quade, J. (1993). Expansion of C4 ecosystems as an indicator of global ecological change in the late Miocene. *Nature*, *361*(6410), 344–345.

Chakraborty, A., Nanjundiah, R. S., & Srinivasan, J. (2009). Impact of African orography and the Indian summer monsoon on the low-level Somali jet. *International Journal of Climatology*, *29*(7), 983–992. Retrieved 2022-06-28, from http://onlinelibrary.wiley.com/doi/abs/10.1002/joc.1720 (_eprint: https://rmets.onlinelibrary.wiley.com/doi/pdf/10.1002/joc.1720) doi: 10.1002/joc.1720

Charreau, J., Chen, Y., Gilder, S., Dominguez, S., Avouac, J.-P., Sen, S., ... Wang, W.-M. (2005, January). Magnetostratigraphy and rock magnetism of the Neogene Kuitun He section (northwest China): implications for Late Cenozoic uplift of the Tianshan mountains. *Earth and Planetary Science Letters*, *230*(1), 177–192. Retrieved 2021-03-29, from https://www.sciencedirect.com/science/article/pii/S0012821X04006739 doi: 10.1016/j.epsl.2004.11.002

Charreau, J., Kent-Corson, M. L., Barrier, L., Augier, R., Ritts, B. D., Chen, Y., ... Guilmette, C. (2012, August). A high-resolution stable isotopic record from the Junggar Basin (NW China): Implications for the paleotopographic evolution of the Tianshan Mountains. *Earth and Planetary Science Letters*, *341-344*, 158–169. Retrieved 2022-06-17, from https://linkinghub.elsevier.com/retrieve/pii/S0012821X12002622 doi: 10.1016/j.epsl.2012.05.033

Chatterjee, S., Goswami, A., & Scotese, C. R. (2013, January). The longest voyage: Tectonic, magmatic, and paleoclimatic evolution of the Indian plate during

its northward flight from Gondwana to Asia. *Gondwana Research*, *23*(1), 238–267. Retrieved 2020-10-14, from https://linkinghub.elsevier.com/retrieve/pii/S1342937X12002390 doi: 10.1016/j.gr.2012.07.001

Chen, J., Huang, W., Feng, S., Zhang, Q., Kuang, X., Chen, J., & Chen, F. (2021). The modulation of westerlies-monsoon interaction on climate over the monsoon boundary zone in East Asia. *International Journal of Climatology*, *41*(S1), E3049–E3064. Retrieved 2022-05-16, from http://onlinelibrary.wiley.com/doi/abs/10.1002/joc.6903 (_eprint: https://rmets.onlinelibrary.wiley.com/doi/pdf/10.1002/joc.6903) doi: 10.1002/joc.6903

Clark, M., House, M., Royden, L., Whipple, K., Burchfiel, B., Zhang, X., & Tang, W. (2005, June). Late Cenozoic uplift of southeastern Tibet. *Geology*, *33*(6), 525–528. Retrieved 2022-03-03, from https://doi.org/10.1130/G21265.1 doi: 10.1130/G21265.1

Clift, P., Hodges, K., Heslop, Hannigan, R., Hoang, L., & Calves, G. (2008, November). Correlation of Himalayan exhumation rates and Asia monsoon intensity. *Nature Geoscience*, *1*, doi:10.1038/ngeo351. doi: 10.1038/ngeo351

Clift, P. D. (2020, June). Asian monsoon dynamics and sediment transport in SE Asia. *Journal of Asian Earth Sciences*, *195*, 104352. Retrieved 2022-05-02, from https://linkinghub.elsevier.com/retrieve/pii/S1367912020301334 doi: 10.1016/j.jseaes.2020.104352

Cohen, J., Saito, K., & Entekhabi, D. (2001, January). The role of the Siberian high in northern hemisphere climate variability. *Geophysical Research Letters*, *28*(2), 299–302. Retrieved 2020-06-20, from http://doi.wiley.com/10.1029/2000GL011927 doi: 10.1029/2000GL011927

Cook, K. L., & Royden, L. H. (2008). The role of crustal strength variations in shaping orogenic plateaus, with application to Tibet. *Journal of Geophysical Research: Solid Earth*, *113*(B8). Retrieved 2021-03-29, from http://agupubs.onlinelibrary.wiley.com/doi/abs/10.1029/2007JB005457 (_eprint: https://onlinelibrary.wiley.com/doi/pdf/10.1029/2007JB005457) doi: https://doi.org/10.1029/2007JB005457

Couvreur, T. L. P., Dauby, G., Blach-Overgaard, A., Deblauwe, V., Dessein, S., Droissart, V., ... Sepulchre, P. (2021). Tectonics, climate and the diversification of the tropical African terrestrial flora and fauna. *Biological Reviews*, *96*(1), 16–51. Retrieved 2021-03-09, from https://onlinelibrary.wiley.com/doi/abs/10.1111/brv.12644 (_eprint: https://onlinelibrary.wiley.com/doi/pdf/10.1111/brv.12644) doi: https://doi.org/10.1111/brv.12644

Crameri, F. (2021, February). *Scientific colour maps.* Zenodo. Retrieved 2021-04-15, from https://zenodo.org/record/4491293 (Language: eng) doi: 10.5281/zenodo.4491293

Crameri, F., Shephard, G. E., & Heron, P. J. (2020, October). The misuse of colour in science communication. *Nature Communications*, *11*(1), 5444. Retrieved 2021-04-15, from http://www.nature.com/articles/s41467-020-19160-7 (Number: 1 Publisher: Nature Publishing Group) doi: 10.1038/s41467-020-19160-7

Cunningham, W. D. (2001, February). Cenozoic normal faulting and regional doming in the southern Hangay region, Central Mongolia: implications for the origin of the Baikal rift province. *Tectonophysics*, *331*(4), 389–411. Retrieved 2021-03-26, from https://www.sciencedirect.com/science/article/pii/S0040195100002286 doi: 10.1016/S0040-1951(00)00228-6

Cyr, A., Currie, B., & Rowley, D. (2005, September). Geochemical Evaluation of Fenghuoshan Group Lacustrine Carbonates, North-Central Tibet: Implications for the Paleoaltimetry of the Eocene Tibetan Plateau. *The Journal of Geology*, *113*(5), 517–533. Retrieved 2021-03-29, from https://www.journals.uchicago.edu/doi/10.1086/431907 doi: 10.1086/431907

Daradich, A., Mitrovica, J. X., Pysklywec, R. N., Willett, S. D., & Forte, A. M. (2003). Mantle flow, dynamic topography, and rift-flank uplift of Arabia. *Geology*, *31*(10), 901–904.

Darin, M. H., Umhoefer, P. J., & Thomson, S. N. (2018). Rapid Late Eocene Exhumation of the Sivas Basin (Central Anatolia) Driven by Initial Arabia-Eurasia Collision. *Tectonics*, *37*(10), 3805–3833. Retrieved 2022-03-04, from http://onlinelibrary.wiley.com/doi/abs/10.1029/2017TC004954 (_eprint: https://agupubs.onlinelibrary.wiley.com/doi/pdf/10.1029/2017TC004954) doi: 10.1029/2017TC004954

DeConto, R. M., & Pollard, D. (2003, September). A coupled climate–ice sheet modeling approach to the Early Cenozoic history of the Antarctic ice sheet. *Palaeogeography, Palaeoclimatology, Palaeoecology*, *198*(1-2), 39–52. Retrieved 2018-01-08, from http://linkinghub.elsevier.com/retrieve/pii/S0031018203003936 doi: 10.1016/S0031-0182(03)00393-6

De Grave, J., Buslov, M. M., & Van den haute, P. (2007, February). Distant effects of India–Eurasia convergence and Mesozoic intracontinental deformation in Central Asia: Constraints from apatite fission-track thermochronology. *Journal of Asian Earth Sciences*, *29*(2), 188–204. Retrieved 2021-03-26, from https://www.sciencedirect.com/science/article/pii/S136791200600071X doi: 10.1016/j.jseaes.2006.03.001

De Grave, J., Buslov, M. M., Van Den Haute, P., Metcalf, J., Dehandschutter, B., & McWilliams, M. O. (2009). Multi-method chronometry of the Teletskoye graben and its basement, Siberian Altai Mountains: new insights on its thermo-tectonic evolution. *Geological Society, London, Special Publications*, *324*(1), 237–259. Retrieved 2021-04-20, from http://sp.lyellcollection.org/lookup/doi/10.1144/SP324.17 doi: 10.1144/SP324.17

Deng, T., Wu, F., Wang, S., Su, T., & Zhou, Z. (2021, April). Major turnover of biotas across the Oligocene/Miocene boundary on the Tibetan Plateau. *Palaeogeography, Palaeoclimatology, Palaeoecology*, *567*, 110241. Retrieved 2022-03-22, from https://www.sciencedirect.com/science/article/pii/S0031018221000262 doi: 10.1016/j.palaeo.2021.110241

Dettman, D. L., Kohn, M. J., Quade, J., Ryerson, F., Ojha, T. P., & Hamidullah, S. (2001, January). Seasonal stable isotope evidence for a strong Asian monsoon throughout the past 10.7 m.y. *Geology*, *29*(1), 31–34. Retrieved 2022-05-30, from https://doi.org/10.1130/0091-7613(2001)029<0031:SSIEFA>2.0.CO;2 doi: 10.1130/0091-7613(2001)029⟨0031:SSIEFA⟩2.0.CO;2

Ding, L., Spicer, R., Yang, J., Xu, Q., Cai, F., Li, S., ... Mehrotra, R. (2017, March). Quantifying the rise of the Himalaya orogen and implications for the South Asian monsoon. *Geology*, *45*(3), 215–218. Retrieved 2017-10-09, from https://pubs.geoscienceworld.org/geology/article/45/3/215-218/195254 doi: 10.1130/G38583.1

Ding, L., Xu, Q., Yue, Y., Wang, H., Cai, F., & Li, S. (2014, April). The Andean-type Gangdese Mountains: Paleoelevation record from the Paleocene–Eocene Linzhou Basin. *Earth and Planetary Science Letters*, *392*, 250–264. Retrieved 2017-10-09, from http://linkinghub.elsevier.com/retrieve/pii/S0012821X14000612 doi: 10.1016/j.epsl.2014.01.045

Ding, W., Hou, D., Gan, J., Wu, P., Zhang, M., & George, S. C. (2021, April). Palaeovegetation variation in response to the late Oligocene-early Miocene East Asian summer monsoon in the Ying-Qiong Basin, South China Sea. *Palaeogeography, Palaeoclimatology, Palaeoecology*, *567*, 110205. Retrieved 2022-05-03, from https://linkinghub.elsevier.com/retrieve/pii/S0031018220306532 doi: 10.1016/j.palaeo.2020.110205

Ding, Z., Huang, G., Liu, F., Wu, R., & Wang, P. (2021, June). Responses of global monsoon and seasonal cycle of precipitation to precession and obliquity forcing. *Climate Dynamics*, *56*. doi: 10.1007/s00382-021-05663-6

Dowsett, H., Dolan, A., Rowley, D., Moucha, R., Forte, A. M., Mitrovica, J. X., ... Haywood, A. (2016, July). The PRISM4 (mid-Piacenzian) paleoenvironmental reconstruction. *Climate of the Past*, *12*(7), 1519–1538. Retrieved 2022-04-15, from https://cp.copernicus.org/articles/12/1519/2016/ doi: 10.5194/cp-12-1519-2016

Dufresne, J.-L., Foujols, M.-A., Denvil, S., Caubel, A., Marti, O., Aumont, O., ... Vuichard, N. (2013, May). Climate change projections using the IPSL-CM5 Earth System Model: from CMIP3 to CMIP5. *Climate Dynamics*, *40*(9-10), 2123–2165. Retrieved 2019-11-22, from http://link.springer.com/10.1007/s00382-012-1636-1 doi: 10.1007/s00382-012-1636-1

Dupont-Nivet, G., Lippert, P. C., Van Hinsbergen, D. J., Meijers, M. J., & Kapp, P. (2010, September). Palaeolatitude and age of the Indo-Asia collision: palaeomagnetic constraints: Palaeolatitude and age of the Indo-Asia collision. *Geophysical Journal International*, *182*(3), 1189–1198. Retrieved 2019-10-21, from https://academic.oup.com/gji/article-lookup/doi/10.1111/j.1365-246X.2010.04697.x doi: 10.1111/j.1365-246X.2010.04697.x

Edwards, E. J., Osborne, C. P., Strömberg, C. A. E., Smith, S. A., C4 GRASSES CONSORTIUM, Bond, W. J., ... Tipple, B. (2010, April). The Origins of C4 Grasslands: Integrating Evolutionary and Ecosystem Science. *Science*, *328*(5978), 587–591. Retrieved 2022-06-08, from http://www.science.org/doi/full/10.1126/science.1177216 (Publisher: American Association for the Advancement of Science) doi: 10.1126/science.1177216

Faccenna, C., Glišović, P., Forte, A., Becker, T. W., Garzanti, E., Sembroni, A., & Gvirtzman, Z. (2019, December). Role of dynamic topography in sustaining the Nile River over 30 million years. *Nature Geoscience*, *12*(12), 1012–1017. Retrieved 2021-03-10, from http://www.nature.com/articles/s41561-019-0472-x (Number: 12 Publisher: Nature Publishing Group) doi: 10.1038/s41561-019-0472-x

Fang, X., Yan, M., Zhang, W., Nie, J., Han, W., Wu, F., ... Yang, Y. (2021, November). Paleogeography control of Indian monsoon intensification and expansion at 41 Ma. *Science Bulletin*, *66*(22), 2320–2328. Retrieved 2022-05-02, from https://linkinghub.elsevier.com/retrieve/pii/S2095927321005041 doi: 10.1016/j.scib.2021.07.023

Farnsworth, A., Lunt, D. J., Robinson, S. A., Valdes, P. J., Roberts, W. H. G., Clift, P. D., ... Pancost, R. D. (2019, October). Past East Asian monsoon evolution controlled by paleogeography, not CO_2. *Science Advances*, *5*(10), eaax1697. Retrieved 2019-11-04, from http://advances.sciencemag.org/lookup/doi/10.1126/sciadv.aax1697 doi: 10.1126/sciadv.aax1697

Feakins, S. J., Liddy, H. M., Tauxe, L., Galy, V., Feng, X., Tierney, J. E., ... Warny, S. (2020). Miocene C4 Grassland Expansion as Recorded by the Indus Fan. *Paleoceanography and Paleoclimatology*, *35*(6), e2020PA003856. Retrieved 2022-06-07, from http://onlinelibrary.wiley.com/doi/abs/10.1029/2020PA003856 (_eprint: https://agupubs.onlinelibrary.wiley.com/doi/pdf/10.1029/2020PA003856) doi: 10.1029/2020PA003856

Feng, R., & Poulsen, C. J. (2016, February). Refinement of Eocene lapse rates, fossil-leaf altimetry, and North American Cordilleran surface elevation estimates. *Earth and Planetary Science Letters*, *436*, 130–141. Retrieved 2020-03-23, from https://linkinghub.elsevier.com/retrieve/pii/S0012821X15007852 doi: 10.1016/j.epsl.2015.12.022

Fichefet, T., & Maqueda, M. A. M. (1997). Sensitivity of a global sea ice model to the treatment of ice thermodynamics and dynamics. *Journal of Geophysical Research: Oceans*, *102*(C6), 12609–12646.

Findlater, J. (1969, April). A major low-level air current near the Indian Ocean during the northern summer. *Quarterly Journal of the Royal Meteorological Society*, *95*(404), 362–380. Retrieved 2021-09-02, from https://onlinelibrary.wiley.com/doi/10.1002/qj.49709540409 doi: 10.1002/qj.49709540409

Fluteau, F., Ramstein, G., & Besse, J. (1999, May). Simulating the evolution of the Asian and African monsoons during the past 30 Myr using an atmospheric general circulation model. *Journal of Geophysical Research: Atmospheres*, *104*(D10), 11995–12018. Retrieved 2019-05-10, from http://doi.wiley.com/10.1029/1999JD900048 doi: 10.1029/1999JD900048

Foster, G. L., Royer, D. L., & Lunt, D. J. (2017, April). Future climate forcing potentially without precedent in the last 420 million years. *Nature Communications*, *8*(1). Retrieved 2020-05-28, from http://www.nature.com/articles/ncomms14845 doi: 10.1038/ncomms14845

François, T., Burov, E., Agard, P., & Meyer, B. (2014). Buildup of a dynamically supported orogenic plateau: Numerical modeling of the Zagros/Central Iran case study. *Geochemistry, Geophysics, Geosystems*, *15*(6), 2632–2654. Retrieved 2021-03-09, from https://agupubs.onlinelibrary.wiley.com/doi/abs/10.1002/2013GC005223 (_eprint: https://agupubs.onlinelibrary.wiley.com/doi/pdf/10.1002/2013GC005223) doi: https://doi.org/10.1002/2013GC005223

Garzione, C. N., Ikari, M. J., & Basu, A. R. (2005, September). Source of Oligocene to Pliocene sedimentary rocks in the Linxia basin in northeastern Tibet from Nd isotopes: Implications for tectonic forcing of climate. *GSA Bulletin*, *117*(9-10), 1156–1166. Retrieved 2021-09-07, from https://doi.org/10.1130/B25743.1 doi: 10.1130/B25743.1

Golonka, J. (2009). Phanerozoic paleoenvironment and paleolithofacies maps : Cenozoic. *Geologia / Akademia Górniczo-Hutnicza im. Stanisława Staszica w Krakowie*, *T. 35, z. 4*, 507–587. Retrieved 2021-04-06, from http://yadda.icm.edu.pl/yadda/element/bwmeta1.element.baztech-article-AGHM-0011-0001

Gough, D. O. (1981). Solar Interior Structure and Luminosity Variations. In V. Domingo (Ed.), *Physics of Solar Variations* (pp. 21–34). Dordrecht: Springer Netherlands. Retrieved 2019-10-03, from http://link.springer.com/10.1007/978-94-010-9633-1_4 doi: 10.1007/978-94-010-9633-1_4

Gourbet, L., Leloup, P. H., Paquette, J.-L., Sorrel, P., Maheo, G., Wang, G., ... Shen, T. (2017, March). Reappraisal of the Jianchuan Cenozoic basin stratigraphy and its implications on the SE Tibetan plateau evolution. *Tectonophysics*, *700-701*, 162–179. Retrieved 2021-03-29, from https://www.sciencedirect.com/science/article/pii/S0040195117300537 doi: 10.1016/j.tecto.2017.02.007

Guillocheau, F., Simon, B., Baby, G., Bessin, P., Robin, C., & Dauteuil, O. (2018, January). Planation surfaces as a record of mantle dynamics: The case example of Africa. *Gondwana Research*, *53*, 82–98. Retrieved 2021-04-07, from https://www.sciencedirect.com/science/article/pii/S1342937X17302496 doi: 10.1016/j.gr.2017.05.015

Guo, Z. T., Ruddiman, W. F., Hao, Q. Z., Wu, H. B., Qiao, Y. S., Zhu, R. X., ... Liu, T. S. (2002, March). Onset of Asian desertification by 22 Myr ago inferred from loess deposits in China. *Nature*, *416*(6877), 159–163. Retrieved 2020-04-24, from http://www.nature.com/articles/416159a doi: 10.1038/416159a

Guo, Z. T., Sun, B., Zhang, Z. S., Peng, S. Z., Xiao, G. Q., Ge, J. Y., ... Liu, J. F. (2008). A major reorganization of Asian climate by the early Miocene. *Climate of the Past*, *4*(3), 153–174.

Gupta, A. K., Yuvaraja, A., Prakasam, M., Clemens, S. C., & Velu, A. (2015, November). Evolution of the South Asian monsoon wind system since the late Middle Miocene. *Palaeogeography, Palaeoclimatology, Palaeoecology*, *438*, 160–167. Retrieved 2021-09-07, from https://www.sciencedirect.com/science/article/pii/S0031018215004332 doi: 10.1016/j.palaeo.2015.08.006

Gébelin, A., Mulch, A., Teyssier, C., Jessup, M. J., Law, R. D., & Brunel, M. (2013, July). The Miocene elevation of Mount Everest. *Geology*, *41*(7), 799–802. Retrieved 2017-10-09, from http://pubs.geoscienceworld.org/geology/article/41/7/799/131318/The-Miocene-elevation-of-Mount-Everest doi: 10.1130/G34331.1

Gülyüz, E., Durak, H., Özkaptan, M., & Krijgsman, W. (2020, January). Paleomagnetic constraints on the early Miocene closure of the southern Neo-Tethys (Van region; East Anatolia): Inferences for the timing of Eurasia-Arabia collision. *Global and Planetary Change*, *185*, 103089. Retrieved 2022-03-04, from https://www.sciencedirect.com/science/article/pii/S0921818119305740 doi: 10.1016/j.gloplacha.2019.103089

Harzhauser, M., & Piller, W. E. (2007, September). Benchmark data of a changing sea

— Palaeogeography, Palaeobiogeography and events in the Central Paratethys during the Miocene. *Palaeogeography, Palaeoclimatology, Palaeoecology*, *253*(1), 8–31. Retrieved 2021-04-01, from https://www.sciencedirect.com/science/article/pii/S0031018207001927 doi: 10.1016/j.palaeo.2007.03.031

Haywood, A. M., Tindall, J. C., Dowsett, H. J., Dolan, A. M., Foley, K. M., Hunter, S. J., ... Lunt, D. J. (2020, November). The Pliocene Model Intercomparison Project Phase 2: large-scale climate features and climate sensitivity. *Climate of the Past*, *16*(6), 2095–2123. Retrieved 2021-03-09, from https://cp.copernicus.org/articles/16/2095/2020/ (Publisher: Copernicus GmbH) doi: https://doi.org/10.5194/cp-16-2095-2020

He, B. (2017, May). Influences of elevated heating effect by the Himalaya on the changes in Asian summer monsoon. *Theoretical and Applied Climatology*, *128*(3-4), 905–917. Retrieved 2017-10-09, from http://link.springer.com/10.1007/s00704-016-1746-5 doi: 10.1007/s00704-016-1746-5

Heermance, R., Pearson, J., Moe, A., Langtao, L., Jianhong, X., Chen, J., ... Bogue, S. (2018, September). Erg deposition and development of the ancestral Taklimakan Desert (western China) between 12.2 and 7.0 Ma. *Geology*, *46*. doi: 10.1130/G45085.1

Hellwig, A., Voigt, S., Mulch, A., Frisch, K., Bartenstein, A., Pross, J., ... Voigt, T. (2018). Late Oligocene to early Miocene humidity change recorded in terrestrial sequences in the Ili Basin (south-eastern Kazakhstan, Central Asia). *Sedimentology*, *65*(2), 517–539. Retrieved 2022-03-22, from http://onlinelibrary.wiley.com/doi/abs/10.1111/sed.12390 (_eprint: https://onlinelibrary.wiley.com/doi/pdf/10.1111/sed.12390) doi: 10.1111/sed.12390

Herman, A. B., Spicer, R. A., Aleksandrova, G. N., Yang, J., Kodrul, T. M., Maslova, N. P., ... Jin, J.-H. (2017, August). Eocene–early Oligocene climate and vegetation change in southern China: Evidence from the Maoming Basin. *Palaeogeography, Palaeoclimatology, Palaeoecology*, *479*, 126–137. Retrieved 2017-10-09, from http://linkinghub.elsevier.com/retrieve/pii/S0031018217300664 doi: 10.1016/j.palaeo.2017.04.023

Holbourn, A., Kuhnt, W., Clemens, S. C., & Heslop, D. (2021). A 12 Myr Miocene Record of East Asian Monsoon Variability From the South China Sea. *Paleoceanography and Paleoclimatology*, *36*(7), e2021PA004267. Retrieved 2021-09-08, from http://agupubs.onlinelibrary.wiley.com/doi/abs/10.1029/2021PA004267 (_eprint: https://onlinelibrary.wiley.com/doi/pdf/10.1029/2021PA004267) doi: 10.1029/2021PA004267

Holbourn, A. E., Kuhnt, W., Clemens, S. C., Kochhann, K. G. D., Jöhnck, J., Lübbers, J., & Andersen, N. (2018, December). Late Miocene climate cooling and intensification of southeast Asian winter monsoon. *Nature Communications*, *9*(1). Retrieved 2020-10-09, from http://www.nature.com/articles/s41467-018-03950-1 doi: 10.1038/s41467-018-03950-1

Hoorn, C., Ohja, T., & Quade, J. (2000, November). Palynological evidence for vegetation development and climatic change in the Sub-Himalayan Zone (Neogene, Central Nepal). *Palaeogeography, Palaeoclimatology, Palaeoecology*, *163*(3-4), 133–161. Retrieved 2022-06-07, from https://linkinghub.elsevier.com/retrieve/pii/S0031018200001498 doi: 10.1016/S0031-0182(00)00149-8

Hoorn, C., Straathof, J., Abels, H. A., Xu, Y., Utescher, T., & Dupont-Nivet, G. (2012, August). A late Eocene palynological record of climate change and Tibetan Plateau uplift (Xining Basin, China). *Palaeogeography, Palaeoclimatology, Palaeoecology*, *344-345*, 16–38. Retrieved 2017-10-09, from http://linkinghub.elsevier.com/retrieve/pii/S0031018212002775 doi: 10.1016/j.palaeo.2012.05.011

Hourdin, F., Foujols, M.-A., Codron, F., Guemas, V., Dufresne, J.-L., Bony, S., ... Bopp, L. (2013, May). Impact of the LMDZ atmospheric grid configuration on the climate and sensitivity of the IPSL-CM5A coupled model. *Climate Dynamics*, *40*(9-10), 2167–2192. Retrieved 2018-06-05, from http://link.springer.com/10.1007/s00382-012-1411-3 doi: 10.1007/s00382-012-1411-3

Huang, C., & Hinnov, L. (2019, December). Astronomically forced climate evolution in a

saline lake record of the middle Eocene to Oligocene, Jianghan Basin, China. *Earth and Planetary Science Letters*, *528*, 115846. Retrieved 2020-09-07, from https://linkinghub.elsevier.com/retrieve/pii/S0012821X19305382 doi: 10.1016/j.epsl.2019.115846

Huang, H., Pérez-Pinedo, D., Morley, R. J., Dupont-Nivet, G., Philip, A., Win, Z., ... Hoorn, C. (2021, August). At a crossroads: The late Eocene flora of central Myanmar owes its composition to plate collision and tropical climate. *Review of Palaeobotany and Palynology*, *291*, 104441. Retrieved 2022-06-22, from https://www.sciencedirect.com/science/article/pii/S0034666721000658 doi: 10.1016/j.revpalbo.2021.104441

Huang, J., Spicer, R. A., Li, S.-F., Liu, J., Do, T. V., Nguyen, H. B., ... Su, T. (2022, May). Long-term floristic and climatic stability of northern Indochina: Evidence from the Oligocene Ha Long flora, Vietnam. *Palaeogeography, Palaeoclimatology, Palaeoecology*, *593*, 110930. Retrieved 2022-03-22, from https://www.sciencedirect.com/science/article/pii/S0031018222001006 doi: 10.1016/j.palaeo.2022.110930

Huang, W., Dupont-Nivet, G., Lippert, P. C., van Hinsbergen, D. J. J., Dekkers, M. J., Waldrip, R., ... Kapp, P. (2015, March). What was the Paleogene latitude of the Lhasa terrane? A reassessment of the geochronology and paleomagnetism of Linzizong volcanic rocks (Linzhou basin, Tibet). *Tectonics*, *34*(3), 594–622. Retrieved 2017-10-09, from http://doi.wiley.com/10.1002/2014TC003787 doi: 10.1002/2014TC003787

Huang, Y., Clemens, S., Liu, W., Wang, Y., & Prell, W. (2007, June). Large-scale hydrological change drove the late Miocene C4 plant expansion in the Himalayan foreland and Arabian Peninsula. *Geology*, *35*. doi: 10.1130/G23666A.1

Huber, M. (2003, February). Eocene El Nino: Evidence for Robust Tropical Dynamics in the "Hothouse". *Science*, *299*(5608), 877–881. Retrieved 2020-04-15, from https://www.sciencemag.org/lookup/doi/10.1126/science.1078766 doi: 10.1126/science.1078766

Huber, M., & Goldner, A. (2012, January). Eocene monsoons. *Journal of Asian Earth Sciences*, *44*, 3–23. Retrieved 2017-10-09, from http://linkinghub.elsevier.com/retrieve/pii/S1367912011003725 doi: 10.1016/j.jseaes.2011.09.014

Hui, Z., Zhou, X., Chevalier, M., Wei, X., Pan, Y., & Chen, Y. (2021, August). Miocene East Asia summer monsoon precipitation variability and its possible driving forces. *Palaeogeography, Palaeoclimatology, Palaeoecology*, 110609. Retrieved 2021-09-22, from https://www.sciencedirect.com/science/article/pii/S0031018221003941 doi: 10.1016/j.palaeo.2021.110609

Ingalls, M., Rowley, D. B., Currie, B., & Colman, A. S. (2016, November). Large-scale subduction of continental crust implied by India–Asia mass-balance calculation. *Nature Geoscience*, *9*(11), 848–853. Retrieved 2020-10-16, from http://www.nature.com/articles/ngeo2806 (Number: 11 Publisher: Nature Publishing Group) doi: 10.1038/ngeo2806

Jacques, F. M., Guo, S.-X., Su, T., Xing, Y.-W., Huang, Y.-J., Liu, Y.-S. C., ... Zhou, Z.-K. (2011, May). Quantitative reconstruction of the Late Miocene monsoon climates of southwest China: A case study of the Lincang flora from Yunnan Province. *Palaeogeography, Palaeoclimatology, Palaeoecology*, *304*(3-4), 318–327. Retrieved 2022-05-03, from https://linkinghub.elsevier.com/retrieve/pii/S0031018210002233 doi: 10.1016/j.palaeo.2010.04.014

Jacques, F. M., Su, T., Spicer, R. A., Xing, Y., Huang, Y., Wang, W., & Zhou, Z. (2011, March). Leaf physiognomy and climate: Are monsoon systems different? *Global and Planetary Change*, *76*(1-2), 56–62. Retrieved 2022-05-06, from https://linkinghub.elsevier.com/retrieve/pii/S0921818110002560 doi: 10.1016/j.gloplacha.2010.11.009

Jagoutz, O., Royden, L., Holt, A. F., & Becker, T. W. (2015, June). Anomalously fast convergence of India and Eurasia caused by double subduction. *Nature Geoscience*, *8*(6), 475–478. Retrieved 2019-11-22, from http://www.nature.com/articles/ngeo2418

doi: 10.1038/ngeo2418

Jeong, J.-H., Ou, T., Linderholm, H. W., Kim, B.-M., Kim, S.-J., Kug, J.-S., & Chen, D. (2011, December). Recent recovery of the Siberian High intensity: RECOVERY OF THE SIBERIAN HIGH INTENSITY. *Journal of Geophysical Research: Atmospheres*, *116*(D23), n/a–n/a. Retrieved 2020-06-20, from http://doi.wiley.com/10.1029/2011JD015904 doi: 10.1029/2011JD015904

Jhun, J.-G., & Lee, E.-J. (2004, February). A New East Asian Winter Monsoon Index and Associated Characteristics of the Winter Monsoon. *Journal of Climate*, *17*(4), 711–726. Retrieved 2021-11-10, from https://journals.ametsoc.org/view/journals/clim/17/4/1520-0442_2004_017_0711_aneawm_2.0.co_2.xml (Publisher: American Meteorological Society Section: Journal of Climate) doi: 10.1175/1520-0442(2004)017⟨0711:ANEAWM⟩2.0.CO;2

Jia, G., Peng, P., Zhao, Q., & Jian, Z. (2003, December). Changes in terrestrial ecosystem since 30 Ma in East Asia: Stable isotope evidence from black carbon in the South China Sea. *Geology*, *31*(12), 1093–1096. Retrieved 2022-05-02, from https://doi.org/10.1130/G19992.1 doi: 10.1130/G19992.1

Jiang, H., & Ding, Z. (2008, July). A 20 Ma pollen record of East-Asian summer monsoon evolution from Guyuan, Ningxia, China. *Palaeogeography, Palaeoclimatology, Palaeoecology*, *265*(1-2), 30–38. Retrieved 2022-06-14, from https://linkinghub.elsevier.com/retrieve/pii/S0031018208002629 doi: 10.1016/j.palaeo.2008.04.016

Jiang, H., Wan, S., Ma, X., Zhong, N., & Zhao, D. (2017, October). End-member modeling of the grain-size record of Sikouzi fine sediments in Ningxia (China) and implications for temperature control of Neogene evolution of East Asian winter monsoon. *PLOS ONE*, *12*(10), e0186153. Retrieved 2022-06-14, from https://dx.plos.org/10.1371/journal.pone.0186153 doi: 10.1371/journal.pone.0186153

Jolivet, M., Dominguez, S., Charreau, J., Chen, Y., Li, Y., & Wang, Q. (2010). Mesozoic and Cenozoic tectonic history of the central Chinese Tian Shan: Reactivated tectonic structures and active deformation. *Tectonics*, *29*(6). Retrieved 2021-03-29, from http://agupubs.onlinelibrary.wiley.com/doi/abs/10.1029/2010TC002712 (_eprint: https://onlinelibrary.wiley.com/doi/pdf/10.1029/2010TC002712) doi: https://doi.org/10.1029/2010TC002712

Jolivet, M., Ritz, J.-F., Vassallo, R., Larroque, C., Braucher, R., Todbileg, M., ... Arzhanikov, S. (2007, October). Mongolian summits: An uplifted, flat, old but still preserved erosion surface. *Geology*, *35*(10), 871–874. Retrieved 2021-03-29, from http://pubs.geoscienceworld.org/gsa/geology/article/35/10/871/129664/Mongolian-summits-An-uplifted-flat-old-but-still (Publisher: GeoScienceWorld) doi: 10.1130/G23758A.1

Kaakinen, A., Sonninen, E., & Lunkka, J. P. (2006, August). Stable isotope record in paleosol carbonates from the Chinese Loess Plateau: Implications for late Neogene paleoclimate and paleovegetation. *Palaeogeography, Palaeoclimatology, Palaeoecology*, *237*(2-4), 359–369. Retrieved 2022-06-16, from https://linkinghub.elsevier.com/retrieve/pii/S0031018205007315 doi: 10.1016/j.palaeo.2005.12.011

Kapp, P., & DeCelles, P. G. (2019, March). Mesozoic–Cenozoic geological evolution of the Himalayan-Tibetan orogen and working tectonic hypotheses. *American Journal of Science*, *319*(3), 159–254. Retrieved 2019-11-15, from http://www.ajsonline.org/lookup/doi/10.2475/03.2019.01 doi: 10.2475/03.2019.01

Karaoğlan, F., Parlak, O., Hejl, E., Neubauer, F., & Klötzli, U. (2016, May). The temporal evolution of the active margin along the Southeast Anatolian Orogenic Belt (SE Turkey): Evidence from U–Pb, Ar–Ar and fission track chronology. *Gondwana Research*, *33*, 190–208. Retrieved 2022-03-04, from https://www.sciencedirect.com/science/article/pii/S1342937X16000599 doi: 10.1016/j.gr.2015.12.011

Kaya, M. Y., Dupont-Nivet, G., Proust, J., Roperch, P., Bougeois, L., Meijer, N., ... Zhaojie, G. (2019, June). Paleogene evolution and demise of the proto-Paratethys Sea in Central Asia (Tarim and Tajik basins): Role of intensified tectonic activity at ca. 41 Ma. *Basin Research*, *31*(3), 461–486. Retrieved 2019-11-22, from https://

onlinelibrary.wiley.com/doi/abs/10.1111/bre.12330 doi: 10.1111/bre.12330

Kent-Corson, M. L., Ritts, B. D., Zhuang, G., Bovet, P. M., Graham, S. A., & Page Chamberlain, C. (2009, May). Stable isotopic constraints on the tectonic, topographic, and climatic evolution of the northern margin of the Tibetan Plateau. *Earth and Planetary Science Letters*, *282*(1-4), 158–166. Retrieved 2017-10-09, from http://linkinghub.elsevier.com/retrieve/pii/S0012821X0900154X doi: 10.1016/j.epsl.2009.03.011

Khan, M. A., Spicer, R. A., Bera, S., Ghosh, R., Yang, J., Spicer, T. E. V., ... Grote, P. J. (2014, February). Miocene to Pleistocene floras and climate of the Eastern Himalayan Siwaliks, and new palaeoelevation estimates for the Namling–Oiyug Basin, Tibet. *Global and Planetary Change*, *113*, 1–10. Retrieved 2022-05-02, from https://www.sciencedirect.com/science/article/pii/S0921818113002749 doi: 10.1016/j.gloplacha.2013.12.003

Kong, W., Swenson, L. M., & Chiang, J. C. H. (2017, May). Seasonal Transitions and the Westerly Jet in the Holocene East Asian Summer Monsoon. *Journal of Climate*, *30*(9), 3343–3365. Retrieved 2020-03-04, from http://journals.ametsoc.org/doi/10.1175/JCLI-D-16-0087.1 doi: 10.1175/JCLI-D-16-0087.1

Krijgsman, W., Palcu, D. V., Andreetto, F., Stoica, M., & Mandic, O. (2020, November). Changing seas in the late Miocene Northern Aegean: A Paratethyan approach to Mediterranean basin evolution. *Earth-Science Reviews*, *210*, 103386. Retrieved 2022-02-04, from https://linkinghub.elsevier.com/retrieve/pii/S0012825220304323 doi: 10.1016/j.earscirev.2020.103386

Krinner, G., Viovy, N., de Noblet-Ducoudré, N., Ogée, J., Polcher, J., Friedlingstein, P., ... Prentice, I. C. (2005, March). A dynamic global vegetation model for studies of the coupled atmosphere-biosphere system: DVGM FOR COUPLED CLIMATE STUDIES. *Global Biogeochemical Cycles*, *19*(1). Retrieved 2018-10-22, from http://doi.wiley.com/10.1029/2003GB002199 doi: 10.1029/2003GB002199

Kroon, D., Steens, T., & Troelstra, S. R. (1991). Onset of monsoonal related upwelling in the western Arabian sea as revealed by planktonic foraminifers. In *Proceedings of the ocean drilling program, scientific results* (Vol. 11).

Kuhnt, W., Holbourn, A., Hall, R., Zuvela, M., & Käse, R. (2004). Neogene history of the Indonesian Throughflow. In P. Clift, W. Kuhnt, P. Wang, & D. Hayes (Eds.), *Geophysical Monograph Series* (Vol. 149, pp. 299–320). Washington, D. C.: American Geophysical Union. Retrieved 2021-09-02, from https://onlinelibrary.wiley.com/doi/10.1029/149GM16 doi: 10.1029/149GM16

Kutzbach, J. E., Prell, W. L., & Ruddiman, W. F. (1993, March). Sensitivity of Eurasian Climate to Surface Uplift of the Tibetan Plateau. *The Journal of Geology*, *101*(2), 177–190. Retrieved 2020-05-11, from https://www.journals.uchicago.edu/doi/10.1086/648215 doi: 10.1086/648215

Käßner, A., Ratschbacher, L., Jonckheere, R., Enkelmann, E., Khan, J., Sonntag, B.-L., ... Oimahmadov, I. (2016). Cenozoic intracontinental deformation and exhumation at the northwestern tip of the India-Asia collision—southwestern Tian Shan, Tajikistan, and Kyrgyzstan. *Tectonics*, *35*(9), 2171–2194. Retrieved 2021-03-26, from http://agupubs.onlinelibrary.wiley.com/doi/abs/10.1002/2015TC003897 (_eprint: https://onlinelibrary.wiley.com/doi/pdf/10.1002/2015TC003897) doi: https://doi.org/10.1002/2015TC003897

Ladant, J.-B., Donnadieu, Y., Lefebvre, V., & Dumas, C. (2014, August). The respective role of atmospheric carbon dioxide and orbital parameters on ice sheet evolution at the Eocene-Oligocene transition: Ice sheet evolution at the EOT. *Paleoceanography*, *29*(8), 810–823. Retrieved 2019-05-10, from http://doi.wiley.com/10.1002/2013PA002593 doi: 10.1002/2013PA002593

Laugié, M., Donnadieu, Y., Ladant, J.-B., Green, J. A. M., Bopp, L., & Raisson, F. (2020, June). Stripping back the modern to reveal the Cenomanian–Turonian climate and temperature gradient underneath. *Climate of the Past*, *16*(3), 953–971. Retrieved 2021-03-09, from https://cp.copernicus.org/articles/16/953/2020/

(Publisher: Copernicus GmbH) doi: https://doi.org/10.5194/cp-16-953-2020

Lee, J., Kim, S., Lee, J. I., Cho, H. G., Phillips, S. C., & Khim, B.-K. (2020, January). Monsoon-influenced variation of clay mineral compositions and detrital Nd-Sr isotopes in the western Andaman Sea (IODP Site U1447) since the late Miocene. *Palaeogeography, Palaeoclimatology, Palaeoecology*, *538*, 109339. Retrieved 2022-06-02, from https://linkinghub.elsevier.com/retrieve/pii/S0031018219303773 doi: 10.1016/j.palaeo.2019.109339

Lee, J.-Y., Wang, B., Seo, K.-H., Ha, K.-J., Kitoh, A., & Liu, J. (2015, August). Effects of mountain uplift on global monsoon precipitation. *Asia-Pacific Journal of Atmospheric Sciences*, *51*(3), 275–290. Retrieved 2017-10-09, from http://link.springer.com/10.1007/s13143-015-0077-2 doi: 10.1007/s13143-015-0077-2

Li, B., Sun, D., Wang, X., Zhang, Y., Hu, W., Wang, F., ... Liang, B. (2016, August). 18O and 13C records from a Cenozoic sedimentary sequence in the Lanzhou Basin, Northwestern China: Implications for palaeoenvironmental and palaeoecological changes. *Journal of Asian Earth Sciences*, *125*, 22–36. Retrieved 2022-05-12, from https://linkinghub.elsevier.com/retrieve/pii/S1367912016301249 doi: 10.1016/j.jseaes.2016.05.010

Li, F., Rousseau, D.-D., Wu, N., Hao, Q., & Pei, Y. (2008, October). Late Neogene evolution of the East Asian monsoon revealed by terrestrial mollusk record in Western Chinese Loess Plateau: From winter to summer dominated sub-regime. *Earth and Planetary Science Letters*, *274*(3-4), 439–447. Retrieved 2022-06-16, from https://linkinghub.elsevier.com/retrieve/pii/S0012821X08004986 doi: 10.1016/j.epsl.2008.07.038

Li, J. X., Yue, L. P., Roberts, A. P., Hirt, A. M., Pan, F., Guo, L., ... Liu, Q. S. (2018, August). Global cooling and enhanced Eocene Asian mid-latitude interior aridity. *Nature Communications*, *9*(1), 3026. Retrieved 2022-03-21, from http://www.nature.com/articles/s41467-018-05415-x (Number: 1 Publisher: Nature Publishing Group) doi: 10.1038/s41467-018-05415-x

Li, L., Dupont-Nivet, G., Najman, Y., Kaya, M., Meijer, N., Poujol, M., & Aminov, J. (2021). Middle to late Miocene growth of the North Pamir. *Basin Research*, *n/a*(n/a). Retrieved 2021-11-09, from http://onlinelibrary.wiley.com/doi/abs/10.1111/bre.12629 (_eprint: https://onlinelibrary.wiley.com/doi/pdf/10.1111/bre.12629) doi: 10.1111/bre.12629

Li, S., Xing, Y., Valdes, P. J., Huang, Y., Su, T., Farnsworth, A., ... Zhou, Z. (2018, September). Oligocene climate signals and forcings in Eurasia revealed by plant macrofossil and modelling results. *Gondwana Research*, *61*, 115–127. Retrieved 2019-10-18, from https://linkinghub.elsevier.com/retrieve/pii/S1342937X18301473 doi: 10.1016/j.gr.2018.04.015

Li, X., Zhang, R., Zhang, Z., & Yan, Q. (2017, October). What enhanced the aridity in Eocene Asian inland: Global cooling or early Tibetan Plateau uplift? *Palaeogeography, Palaeoclimatology, Palaeoecology*. Retrieved 2018-01-16, from http://linkinghub.elsevier.com/retrieve/pii/S0031018217306922 doi: 10.1016/j.palaeo.2017.10.029

Li, X., Zhang, R., Zhang, Z., & Yan, Q. (2018, January). Do climate simulations support the existence of East Asian monsoon climate in the Late Eocene? *Palaeogeography, Palaeoclimatology, Palaeoecology*. Retrieved 2018-06-12, from http://linkinghub.elsevier.com/retrieve/pii/S0031018217313123 doi: 10.1016/j.palaeo.2017.12.037

Licht, A., Dupont-Nivet, G., Win, Z., Swe, H. H., Kaythi, M., Roperch, P., ... Sein, K. (2018, November). Paleogene evolution of the Burmese forearc basin and implications for the history of India-Asia convergence. *GSA Bulletin*, *131*(5-6), 730–748. Retrieved 2021-03-29, from https://doi.org/10.1130/B35002.1 doi: 10.1130/B35002.1

Licht, A., van Cappelle, M., Abels, H. A., Ladant, J.-B., Trabucho-Alexandre, J., France-Lanord, C., ... Jaeger, J.-J. (2014, September). Asian monsoons in a late Eocene greenhouse world. *Nature*, *513*(7519), 501–506. Retrieved 2017-10-09, from http://

www.nature.com/doifinder/10.1038/nature13704 doi: 10.1038/nature13704

Ling, C.-C., Ma, F.-J., Dong, J.-L., Zhou, G.-H., Wang, Q.-J., & Sun, B.-N. (2021, October). A mid-altitude area in southwestern China experienced a humid subtropical climate with subtle monsoon signatures during the early Oligocene: Evidence from the Ningming flora of Guangxi. *Palaeogeography, Palaeoclimatology, Palaeoecology*, *579*, 110601. Retrieved 2022-05-03, from https://linkinghub.elsevier.com/retrieve/pii/S0031018221003862 doi: 10.1016/j.palaeo.2021.110601

Lippert, P. C., Van Hinsbergen, D. J., & Dupont-Nivet, G. (2014). Early Cretaceous to present latitude of the central proto-Tibetan Plateau: A paleomagnetic synthesis with implications for Cenozoic tectonics, paleogeography, and climate of Asia. *Geological Society of America Special Papers*, *507*, 1–21.

Liu, D., Li, H., Sun, Z., Cao, Y., Wang, L., Pan, J., ... Ye, X. (2017, August). Cenozoic episodic uplift and kinematic evolution between the Pamir and Southwestern Tien Shan. *Tectonophysics*, *712-713*, 438–454. Retrieved 2021-03-26, from https://www.sciencedirect.com/science/article/pii/S004019511730255X doi: 10.1016/j.tecto.2017.06.009

Liu, J., Li, J., Song, C., Yu, H., Peng, T., Hui, Z., & Ye, X. (2016, July). Palynological evidence for late Miocene stepwise aridification on the northeastern Tibetan Plateau. *Climate of the Past*, *12*, 1473–1484. doi: 10.5194/cp-12-1473-2016

Liu, W., Liu, Z., An, Z., Sun, J., Chang, H., Wang, N., ... Wang, H. (2014, November). Late Miocene episodic lakes in the arid Tarim Basin, western China. *Proceedings of the National Academy of Sciences*, *111*(46), 16292–16296. Retrieved 2022-06-17, from https://www.pnas.org/doi/full/10.1073/pnas.1410890111 (Publisher: Proceedings of the National Academy of Sciences) doi: 10.1073/pnas.1410890111

Liu, X., Guo, Q., Guo, Z., Yin, J., Dong, B., & Smith, R. (2015, October). Where were the monsoon regions and arid zones in Asia prior to the Tibetan Plateau uplift? *National Science Review*, *2*, nwv068. doi: 10.1093/nsr/nwv068

Liu, X., Sun, H., Miao, Y., Dong, B., & Yin, Z.-Y. (2015, May). Impacts of uplift of northern Tibetan Plateau and formation of Asian inland deserts on regional climate and environment. *Quaternary Science Reviews*, *116*, 1–14. Retrieved 2022-06-22, from https://linkinghub.elsevier.com/retrieve/pii/S0277379115001171 doi: 10.1016/j.quascirev.2015.03.010

Liu, X., & Yin, Z.-Y. (2002, July). Sensitivity of East Asian monsoon climate to the uplift of the Tibetan Plateau. *Palaeogeography, Palaeoclimatology, Palaeoecology*, *183*(3), 223–245. Retrieved 2021-04-14, from https://www.sciencedirect.com/science/article/pii/S0031018201004886 doi: 10.1016/S0031-0182(01)00488-6

Liu, Z., Zhang, K., Sun, Y., Liu, W., Liu, Y. C., & Quan, C. (2014). Cenozoic Environmental Changes in the Northern Qaidam Basin Inferred from n-alkane Records. *Acta Geologica Sinica - English Edition*, *88*(5), 1547–1555. Retrieved 2022-06-17, from http://onlinelibrary.wiley.com/doi/abs/10.1111/1755-6724.12317 (_eprint: https://onlinelibrary.wiley.com/doi/pdf/10.1111/1755-6724.12317) doi: 10.1111/1755-6724.12317

Lu, H., & Guo, Z. (2014, January). Evolution of the monsoon and dry climate in East Asia during late Cenozoic: A review. *Science China Earth Sciences*, *57*(1), 70–79. Retrieved 2017-10-09, from http://link.springer.com/10.1007/s11430-013-4790-3 doi: 10.1007/s11430-013-4790-3

Lu, H., Wang, X., & li, l. (2010, August). Aeolian sediment evidence that global cooling has driven late Cenozoic stepwise aridification in Central Asia. *Geological Society London Special Publications*, *342*, 29–44. doi: 10.1144/SP342.4

Lévy, M., Shankar, D., André, J.-M., Shenoi, S. S. C., Durand, F., & de Boyer Montégut, C. (2007, December). Basin-wide seasonal evolution of the Indian Ocean's phytoplankton blooms. *Journal of Geophysical Research*, *112*(C12). Retrieved 2020-07-30, from http://doi.wiley.com/10.1029/2007JC004090 doi: 10.1029/2007JC004090

Ma, T., & Chen, W. (2021). Climate variability of the East Asian winter monsoon and associated extratropical–tropical interaction: a review. *Annals of*

the New York Academy of Sciences, *1504*(1), 44–62. Retrieved 2022-03-25, from http://onlinelibrary.wiley.com/doi/abs/10.1111/nyas.14620 (_eprint: https://nyaspubs.onlinelibrary.wiley.com/doi/pdf/10.1111/nyas.14620) doi: 10.1111/nyas.14620

Ma, X., & Jiang, H. (2015, June). Combined tectonics and climate forcing for the widespread aeolian dust accumulation in the Chinese Loess Plateau since the early late Miocene. *International Geology Review*, *57*, 1861–1876. doi: 10.1080/00206814.2015.1027305

Ma, X., Jiang, H., Cheng, J., & Xu, H. (2012, September). Spatiotemporal evolution of Paleogene palynoflora in China and its implication for development of the extensional basins in East China. *Review of Palaeobotany and Palynology*, *184*, 24–35. Retrieved 2019-02-10, from https://linkinghub.elsevier.com/retrieve/pii/S0034666712001935 doi: 10.1016/j.revpalbo.2012.07.013

Ma, Y., Fang, X., Li, J., Wu, F., & Zhang, J. (2005, May). The vegetation and climate change during Neocene and Early Quaternary in Jiuxi Basin, China. *Science in China Series D: Earth Sciences*, *48*(5), 676. Retrieved 2022-06-16, from http://link.springer.com/10.1360/03yd0110 doi: 10.1360/03yd0110

Macaulay, E. A., Sobel, E. R., Mikolaichuk, A., Kohn, B., & Stuart, F. M. (2014). Cenozoic deformation and exhumation history of the Central Kyrgyz Tien Shan. *Tectonics*, *33*(2), 135–165. Retrieved 2022-03-22, from http://onlinelibrary.wiley.com/doi/abs/10.1002/2013TC003376 (_eprint: https://agupubs.onlinelibrary.wiley.com/doi/pdf/10.1002/2013TC003376) doi: 10.1002/2013TC003376

Macaulay, E. A., Sobel, E. R., Mikolaichuk, A., Wack, M., Gilder, S. A., Mulch, A., ... Apayarov, F. (2016). The sedimentary record of the Issyk Kul basin, Kyrgyzstan: climatic and tectonic inferences. *Basin Research*, *28*(1), 57–80. Retrieved 2022-03-22, from http://onlinelibrary.wiley.com/doi/abs/10.1111/bre.12098 (_eprint: https://onlinelibrary.wiley.com/doi/pdf/10.1111/bre.12098) doi: 10.1111/bre.12098

Madec, G. (2016). NEMO ocean engine. *Note du P\ ˆole de modélisation de l'Institut Pierre-Simon Laplace*(27), 396.

Madec, G., & Imbard, M. (1996, May). A global ocean mesh to overcome the North Pole singularity. *Climate Dynamics*, *12*(6), 381–388. Retrieved 2021-03-09, from https://doi.org/10.1007/BF00211684 doi: 10.1007/BF00211684

Maurin, T., & Rangin, C. (2009). Structure and kinematics of the Indo-Burmese Wedge: Recent and fast growth of the outer wedge. *Tectonics*, *28*(2). Retrieved 2021-03-29, from http://agupubs.onlinelibrary.wiley.com/doi/abs/10.1029/2008TC002276 (_eprint: https://onlinelibrary.wiley.com/doi/pdf/10.1029/2008TC002276) doi: https://doi.org/10.1029/2008TC002276

McQuarrie, N., & Hinsbergen, D. J. J. v. (2013, March). Retrodeforming the Arabia-Eurasia collision zone: Age of collision versus magnitude of continental subduction. *Geology*, *41*(3), 315–318. Retrieved 2021-04-06, from http://pubs.geoscienceworld.org/gsa/geology/article-abstract/41/3/315/131120/Retrodeforming-the-Arabia-Eurasia-collision-zone (Publisher: GeoScienceWorld) doi: 10.1130/G33591.1

Meijer, N., Dupont-Nivet, G., Abels, H. A., Kaya, M. Y., Licht, A., Xiao, M., ... Guo, Z. (2019, March). Central Asian moisture modulated by proto-Paratethys Sea incursions since the early Eocene. *Earth and Planetary Science Letters*, *510*, 73–84. Retrieved 2019-04-25, from https://linkinghub.elsevier.com/retrieve/pii/S0012821X19300019 doi: 10.1016/j.epsl.2018.12.031

Meijer, N., Dupont-Nivet, G., Barbolini, N., Woutersen, A., Rohrmann, A., Yang, Z., ... Nowaczyk, N. (2021, February). Loess-Like Dust Appearance at 40 Ma in Central China. *Paleoceanography and Paleoclimatology*, *36*. doi: 10.1029/2020PA003993

Meng, Q.-t., Bruch, A. A., Sun, G., Liu, Z.-j., Hu, F., & Sun, P.-c. (2018, December). Quantitative reconstruction of Middle and Late Eocene paleoclimate based on palynological records from the Huadian Basin, northeastern China: Evidence for monsoonal influence on oil shale formation. *Palaeogeography, Palaeoclimatology, Palaeoecology*, *510*,

63–77. Retrieved 2020-07-10, from https://linkinghub.elsevier.com/retrieve/pii/S0031018217304741 doi: 10.1016/j.palaeo.2017.11.036

Merlis, T. M., Schneider, T., Bordoni, S., & Eisenman, I. (2013, February). Hadley Circulation Response to Orbital Precession. Part II: Subtropical Continent. *Journal of Climate*, *26*(3), 754–771. Retrieved 2020-09-07, from https://journals.ametsoc.org/jcli/article/26/3/754/33493/Hadley-Circulation-Response-to-Orbital-Precession (Publisher: American Meteorological Society) doi: 10.1175/JCLI-D-12-00149.1

Metcalfe, I. (2013, April). Gondwana dispersion and Asian accretion: Tectonic and palaeogeographic evolution of eastern Tethys. *Journal of Asian Earth Sciences*, *66*, 1–33. Retrieved 2020-10-14, from https://linkinghub.elsevier.com/retrieve/pii/S1367912012005779 doi: 10.1016/j.jseaes.2012.12.020

Meulenkamp, J. E., & Sissingh, W. (2003, July). Tertiary palaeogeography and tectonostratigraphic evolution of the Northern and Southern Peri-Tethys platforms and the intermediate domains of the African–Eurasian convergent plate boundary zone. *Palaeogeography, Palaeoclimatology, Palaeoecology*, *196*(1), 209–228. Retrieved 2021-04-06, from https://www.sciencedirect.com/science/article/pii/S0031018203003195 doi: 10.1016/S0031-0182(03)00319-5

Miao, Y. (2013, August). Late Cenozoic continuous aridification in the western Qaidam Basin: evidence from sporopollen records.

Miao, Y., Fang, X., Herrmann, M., Wu, F., Zhang, Y., & Liu, D. (2011, January). Miocene pollen record of KC-1 core in the Qaidam Basin, NE Tibetan Plateau and implications for evolution of the East Asian monsoon. *Palaeogeography, Palaeoclimatology, Palaeoecology*, *299*(1-2), 30–38. Retrieved 2022-05-04, from https://linkinghub.elsevier.com/retrieve/pii/S0031018210006425 doi: 10.1016/j.palaeo.2010.10.026

Miao, Y., Herrmann, M., Wu, F., Yan, X., & Yang, S. (2012, May). What controlled Mid–Late Miocene long-term aridification in Central Asia? — Global cooling or Tibetan Plateau uplift: A review. *Earth-Science Reviews*, *112*(3), 155–172. Retrieved 2022-03-22, from https://www.sciencedirect.com/science/article/pii/S0012825212000141 doi: 10.1016/j.earscirev.2012.02.003

Miao, Y., Song, C., Fang, X., Meng, Q., Zhang, P., Wu, F., & Yan, X. (2016, January). Late Cenozoic genus Fupingopollenites development and its implications for the Asian summer monsoon evolution. *Gondwana Research*, *29*(1), 320–333. Retrieved 2017-10-09, from http://linkinghub.elsevier.com/retrieve/pii/S1342937X15000040 doi: 10.1016/j.gr.2014.12.007

Miao, Y., Wu, F., Chang, H., Fang, X., Deng, T., Sun, J., & Jin, C. (2016, March). A Late-Eocene palynological record from the Hoh Xil Basin, northern Tibetan Plateau, and its implications for stratigraphic age, paleoclimate and paleoelevation. *Gondwana Research*, *31*, 241–252. Retrieved 2017-10-09, from http://linkinghub.elsevier.com/retrieve/pii/S1342937X15000374 doi: 10.1016/j.gr.2015.01.007

Miller, K. G., Browning, J. V., Schmelz, W. J., Kopp, R. E., Mountain, G. S., & Wright, J. D. (2020, May). Cenozoic sea-level and cryospheric evolution from deep-sea geochemical and continental margin records. *Science Advances*, *6*(20), eaaz1346. Retrieved 2021-03-09, from https://advances.sciencemag.org/content/6/20/eaaz1346 (Publisher: American Association for the Advancement of Science Section: Review) doi: 10.1126/sciadv.aaz1346

Molnar, P., Boos, W. R., & Battisti, D. S. (2010, April). Orographic Controls on Climate and Paleoclimate of Asia: Thermal and Mechanical Roles for the Tibetan Plateau. *Annual Review of Earth and Planetary Sciences*, *38*(1), 77–102. Retrieved 2018-03-09, from http://www.annualreviews.org/doi/10.1146/annurev-earth-040809-152456 doi: 10.1146/annurev-earth-040809-152456

Molnar, P., England, P., & Martinod, J. (1993). Mantle dynamics, uplift of the Tibetan Plateau, and the Indian Monsoon. *Reviews of Geophysics*, *31*(4), 357. Retrieved 2020-07-27, from http://doi.wiley.com/10.1029/93RG02030 doi: 10.1029/93RG02030

Morley, R. J. (2018, July). Assembly and division of the South and South-East Asian

flora in relation to tectonics and climate change. *Journal of Tropical Ecology*, *34*(4), 209–234. Retrieved 2022-06-23, from https://www.cambridge.org/core/product/identifier/S0266467418000202/type/journal_article doi: 10.1017/S0266467418000202

Moucha, R., & Forte, A. M. (2011, October). Changes in African topography driven by mantle convection. *Nature Geoscience*, *4*(10), 707–712. Retrieved 2021-04-07, from http://www.nature.com/articles/ngeo1235 (Number: 10 Publisher: Nature Publishing Group) doi: 10.1038/ngeo1235

Mouthereau, F. (2011, November). Timing of uplift in the Zagros belt/Iranian plateau and accommodation of late Cenozoic Arabia–Eurasia convergence. *Geological Magazine*, *148*(5-6), 726–738. Retrieved 2020-06-22, from https://www.cambridge.org/core/product/identifier/S0016756811000306/type/journal_article doi: 10.1017/S0016756811000306

Mouthereau, F., Lacombe, O., & Vergés, J. (2012, April). Building the Zagros collisional orogen: Timing, strain distribution and the dynamics of Arabia/Eurasia plate convergence. *Tectonophysics*, *532-535*, 27–60. Retrieved 2021-09-15, from https://www.sciencedirect.com/science/article/pii/S0040195112000509 doi: 10.1016/j.tecto.2012.01.022

Najman, Y., Sobel, E. R., Millar, I., Stockli, D. F., Govin, G., Lisker, F., ... Kahn, A. (2020, January). The exhumation of the Indo-Burman Ranges, Myanmar. *Earth and Planetary Science Letters*, *530*, 115948. Retrieved 2021-03-29, from https://www.sciencedirect.com/science/article/pii/S0012821X19306405 doi: 10.1016/j.epsl.2019.115948

Neupane, P. C., Gani, M. R., Gani, N. D., & Huang, Y. (2020). Neogene vegetation shift in the Nepalese Siwalik, Himalayas: A compound-specific isotopic study of lipid biomarkers. *The Depositional Record*, *6*(1), 192–202. Retrieved 2022-06-07, from http://onlinelibrary.wiley.com/doi/abs/10.1002/dep2.91 (_eprint: https://onlinelibrary.wiley.com/doi/pdf/10.1002/dep2.91) doi: 10.1002/dep2.91

Okay, A. I., Zattin, M., & Cavazza, W. (2010, January). Apatite fission-track data for the Miocene Arabia-Eurasia collision. *Geology*, *38*(1), 35–38. Retrieved 2022-03-04, from https://doi.org/10.1130/G30234.1 doi: 10.1130/G30234.1

Otero, O., & Gayet, M. (2001, January). Palaeoichthyofaunas from the Lower Oligocene and Miocene of the Arabian Plate: palaeoecological and palaeobiogeographical implications. *Palaeogeography, Palaeoclimatology, Palaeoecology*, *165*(1), 141–169. Retrieved 2021-04-06, from https://www.sciencedirect.com/science/article/pii/S0031018200001589 doi: 10.1016/S0031-0182(00)00158-9

Ozsvárt, P., Kocsis, L., Nyerges, A., Győri, O., & Pálfy, J. (2016, October). The Eocene-Oligocene climate transition in the Central Paratethys. *Palaeogeography, Palaeoclimatology, Palaeoecology*, *459*, 471–487. Retrieved 2021-04-01, from https://www.sciencedirect.com/science/article/pii/S0031018216302899 doi: 10.1016/j.palaeo.2016.07.034

Page, M., Licht, A., Dupont-Nivet, G., Meijer, N., Barbolini, N., Hoorn, C., ... Guo, Z. (2019, March). Synchronous cooling and decline in monsoonal rainfall in northeastern Tibet during the fall into the Oligocene icehouse. *Geology*, *47*(3), 203–206. Retrieved 2020-01-21, from https://pubs.geoscienceworld.org/gsa/geology/article/47/3/203/568396/Synchronous-cooling-and-decline-in-monsoonal doi: 10.1130/G45480.1

Peng, T., Li, J., Song, C., Guo, B., Liu, J., Zhao, Z., & Zhang, J. (2016, April). An integrated biomarker perspective on Neogene–Quaternary climatic evolution in NE Tibetan Plateau: Implications for the Asian aridification. *Quaternary International*, *399*, 174–182. Retrieved 2022-06-09, from https://www.sciencedirect.com/science/article/pii/S104061821500422X doi: 10.1016/j.quaint.2015.04.020

Pettke, T., Halliday, A. N., & Rea, D. K. (2002). Cenozoic evolution of Asian climate and sources of Pacific seawater Pb and Nd derived from eolian dust of sediment core LL44-GPC3. *Paleoceanography*, *17*(3), 3–1–3–13. Retrieved 2022-03-25, from

http://onlinelibrary.wiley.com/doi/abs/10.1029/2001PA000673 (_eprint: https://agupubs.onlinelibrary.wiley.com/doi/pdf/10.1029/2001PA000673) doi: 10.1029/2001PA000673

Pirouz, M., Avouac, J.-P., Hassanzadeh, J., Kirschvink, J. L., & Bahroudi, A. (2017, November). Early Neogene foreland of the Zagros, implications for the initial closure of the Neo-Tethys and kinematics of crustal shortening. *Earth and Planetary Science Letters*, *477*, 168–182. Retrieved 2020-10-20, from https://linkinghub.elsevier.com/retrieve/pii/S0012821X17304302 doi: 10.1016/j.epsl.2017.07.046

Poblete, F., Dupont-Nivet, G., Licht, A., van Hinsbergen, D. J. J., Roperch, P., Mihalynuk, M. G., ... Baatsen, M. L. J. (2021, March). Towards interactive global paleogeographic maps, new reconstructions at 60, 40 and 20Ma. *Earth-Science Reviews*, *214*, 103508. Retrieved 2021-04-07, from https://www.sciencedirect.com/science/article/pii/S0012825221000076 doi: 10.1016/j.earscirev.2021.103508

Polissar, P. J., Uno, K. T., Phelps, S. R., Karp, A. T., Freeman, K. H., & Pensky, J. L. (2021). Hydrologic Changes Drove the Late Miocene Expansion of C4 Grasslands on the Northern Indian Subcontinent. *Paleoceanography and Paleoclimatology*, *36*(4), e2020PA004108. Retrieved 2022-06-07, from http://onlinelibrary.wiley.com/doi/abs/10.1029/2020PA004108 (_eprint: https://agupubs.onlinelibrary.wiley.com/doi/pdf/10.1029/2020PA004108) doi: 10.1029/2020PA004108

Poulsen, C. J., & Jeffery, M. L. (2011, June). Climate change imprinting on stable isotopic compositions of high-elevation meteoric water cloaks past surface elevations of major orogens. *Geology*, *39*(6), 595–598. Retrieved 2022-04-11, from http://pubs.geoscienceworld.org/geology/article/39/6/595/130636/Climate-change-imprinting-on-stable-isotopic doi: 10.1130/G32052.1

Pound, M. J., & Salzmann, U. (2017, February). Heterogeneity in global vegetation and terrestrial climate change during the late Eocene to early Oligocene transition. *Scientific Reports*, *7*, 43386. Retrieved 2017-11-23, from http://www.nature.com/articles/srep43386 doi: 10.1038/srep43386

Prell, W. L., & Kutzbach, J. E. (1992). Sensitivity of the Indian monsoon to forcing parameters and implications for its evolution. *Nature*, *360*(6405), 647–652.

Qiang, X., An, Z., Song, Y., Chang, H., Sun, Y., Liu, W., ... Ai, L. (2011, January). New eolian red clay sequence on the western Chinese Loess Plateau linked to onset of Asian desertification about 25 Ma ago. *Science China Earth Sciences*, *54*(1), 136–144. Retrieved 2017-10-09, from http://link.springer.com/10.1007/s11430-010-4126-5 doi: 10.1007/s11430-010-4126-5

Quade, J., Cater, J. M., Ojha, T. P., Adam, J., & Mark Harrison, T. (1995, December). Late Miocene environmental change in Nepal and the northern Indian subcontinent: Stable isotopic evidence from paleosols. *Geological Society of America Bulletin*, *107*(12), 1381–1397. Retrieved 2022-05-30, from https://pubs.geoscienceworld.org/gsabulletin/article/107/12/1381-1397/182993 doi: 10.1130/0016-7606(1995)107⟨1381:LMECIN⟩2.3.CO;2

Quade, J., & Cerling, T. E. (1995, May). Expansion of C4 grasses in the Late Miocene of Northern Pakistan: evidence from stable isotopes in paleosols. *Palaeogeography, Palaeoclimatology, Palaeoecology*, *115*(1-4), 91–116. Retrieved 2022-05-30, from https://linkinghub.elsevier.com/retrieve/pii/003101829400108K doi: 10.1016/0031-0182(94)00108-K

Rae, J. W., Zhang, Y. G., Liu, X., Foster, G. L., Stoll, H. M., & Whiteford, R. D. (2021, May). Atmospheric CO_2 over the Past 66 Million Years from Marine Archives. *Annual Review of Earth and Planetary Sciences*, *49*(1), 609–641. Retrieved 2021-06-01, from https://www.annualreviews.org/doi/10.1146/annurev-earth-082420-063026 doi: 10.1146/annurev-earth-082420-063026

Ramstein, G., Fluteau, F., Besse, J., & Joussaume, S. (1997, April). Effect of orogeny, plate motion and land–sea distribution on Eurasian climate change over the past

30 million years. *Nature*, *386*(6627), 788–795. Retrieved 2017-12-05, from http://www.nature.com/doifinder/10.1038/386788a0 doi: 10.1038/386788a0

Rea, D., Leinen, M., & Janecek, T. (1985, March). Geologic Approach to the Long-Term History of Atmospheric Circulation. *Science (New York, N.Y.)*, *227*, 721–5. doi: 10.1126/science.227.4688.721

Rea, D. K. (1994). The paleoclimatic record provided by eolian deposition in the deep sea: The geologic history of wind. *Reviews of Geophysics*, *32*(2), 159–195. Retrieved 2022-05-16, from http://onlinelibrary.wiley.com/doi/abs/10.1029/93RG03257 (_eprint: https://agupubs.onlinelibrary.wiley.com/doi/pdf/10.1029/93RG03257) doi: 10.1029/93RG03257

Ren, J., Schubert, B. A., Lukens, W. E., & Quan, C. (2021, September). Low oxygen isotope values of fossil cellulose indicate an intense monsoon in East Asia during the late Oligocene. *Palaeogeography, Palaeoclimatology, Palaeoecology*, *577*, 110556. Retrieved 2022-02-22, from https://linkinghub.elsevier.com/retrieve/pii/S0031018221003412 doi: 10.1016/j.palaeo.2021.110556

Ren, X., Nie, J., Saylor, J. E., Wang, X., Liu, F., & Horton, B. K. (2020). Temperature Control on Silicate Weathering Intensity and Evolution of the Neogene East Asian Summer Monsoon. *Geophysical Research Letters*, *47*(15), e2020GL088808. Retrieved 2022-06-09, from http://onlinelibrary.wiley.com/doi/abs/10.1029/2020GL088808 (_eprint: https://agupubs.onlinelibrary.wiley.com/doi/pdf/10.1029/2020GL088808) doi: 10.1029/2020GL088808

Roberts, E. M., Stevens, N. J., O'Connor, P. M., Dirks, P. H. G. M., Gottfried, M. D., Clyde, W. C., ... Hemming, S. (2012, April). Initiation of the western branch of the East African Rift coeval with the eastern branch. *Nature Geoscience*, *5*(4), 289–294. Retrieved 2021-04-07, from http://www.nature.com/articles/ngeo1432 (Number: 4 Publisher: Nature Publishing Group) doi: 10.1038/ngeo1432

Rodwell, M. J., & Hoskins, B. J. (1995, May). A Model of the Asian Summer Monsoon.Part II: Cross-Equatorial Flow and PV Behavior. *Journal of the Atmospheric Sciences*, *52*(9), 1341–1356. Retrieved 2019-07-05, from http://journals.ametsoc.org/doi/abs/10.1175/1520-0469%281995%29052%3C1341%3AAMOTAS%3E2.0.CO%3B2 doi: 10.1175/1520-0469(1995)052⟨1341:AMOTAS⟩2.0.CO;2

Roe, G. H., Ding, Q., Battisti, D. S., Molnar, P., Clark, M. K., & Garzione, C. N. (2016, May). A modeling study of the response of Asian summertime climate to the largest geologic forcings of the past 50 Ma: geological controls on Asian climate. *Journal of Geophysical Research: Atmospheres*, *121*(10), 5453–5470. Retrieved 2018-01-11, from http://doi.wiley.com/10.1002/2015JD024370 doi: 10.1002/2015JD024370

Rowley, D. B., & Currie, B. S. (2006, February). Palaeo-altimetry of the late Eocene to Miocene Lunpola basin, central Tibet. *Nature*, *439*(7077), 677–681. Retrieved 2020-10-17, from https://www.nature.com/articles/nature04506 (Number: 7077 Publisher: Nature Publishing Group) doi: 10.1038/nature04506

Rögl, F. (1997). Palaeogeographic Considerations for Mediterranean and Paratethys Seaways (Oligocene to Miocene). *Annalen des Naturhistorischen Museums in Wien. Serie A für Mineralogie und Petrographie, Geologie und Paläontologie, Anthropologie und Prähistorie*, *99*, 279–310. Retrieved 2021-03-09, from http://www.jstor.org/stable/41702129 (Publisher: Naturhistorisches Museum)

Rögl, F. (1999). MEDITERRANEAN AND PARATETHYS. FACTS AND HYPOTHESES OF AN OLIGOCENE TO MIOCENE PALEOGEOGRAPHY (SHORT OVERVIEW). *Geologica carpathica*, *50*(4), 339–349.

Sampe, T., & Xie, S.-P. (2010, January). Large-Scale Dynamics of the Meiyu-Baiu Rainband: Environmental Forcing by the Westerly Jet*. *Journal of Climate*, *23*(1), 113–134. Retrieved 2020-07-25, from https://journals.ametsoc.org/jcli/article/23/1/113/32279/LargeScale-Dynamics-of-the-MeiyuBaiu-Rainband doi: 10.1175/2009JCLI3128.1

Sanyal, P., Bhattacharya, S., Kumar, R., Ghosh, S., & Sangode, S. (2004, March). Mio–Pliocene monsoonal record from Himalayan foreland basin (Indian Siwalik) and

its relation to vegetational change. *Palaeogeography, Palaeoclimatology, Palaeoecology*, *205*, 23–41. doi: 10.1016/j.palaeo.2003.11.013

Sarr, A.-C., Donnadieu, Y., Bolton, C. T., Ladant, J.-B., Licht, A., Fluteau, F., ... Dupont-Nivet, G. (2022, April). Neogene South Asian monsoon rainfall and wind histories diverged due to topographic effects. *Nature Geoscience*, 1–6. Retrieved 2022-04-12, from http://www.nature.com/articles/s41561-022-00919-0 (Publisher: Nature Publishing Group) doi: 10.1038/s41561-022-00919-0

Sato, T. (2009, February). Influences of subtropical jet and Tibetan Plateau on precipitation pattern in Asia: Insights from regional climate modeling. *Quaternary International*, *194*(1-2), 148–158. Retrieved 2022-06-27, from https://linkinghub.elsevier.com/retrieve/pii/S1040618208002176 doi: 10.1016/j.quaint.2008.07.008

Saxena, R. K., & Trivedi, G. K. (2009). Palynological investigation of the Kopili Formation (Late Eocene) in North Cachar Hills, Assam, India. , 25.

Schott, F. A., & McCreary, J. P. (2001, January). The monsoon circulation of the Indian Ocean. *Progress in Oceanography*, *51*(1), 1–123. Retrieved 2020-07-23, from https://linkinghub.elsevier.com/retrieve/pii/S0079661101000830 doi: 10.1016/S0079-6611(01)00083-0

Sembroni, A., Faccenna, C., Becker, T. W., Molin, P., & Abebe, B. (2016). Long-term, deep-mantle support of the Ethiopia-Yemen Plateau. *Tectonics*, *35*(2), 469–488. Retrieved 2021-09-02, from http://agupubs.onlinelibrary.wiley.com/doi/abs/10.1002/2015TC004000 (_eprint: https://onlinelibrary.wiley.com/doi/pdf/10.1002/2015TC004000) doi: 10.1002/2015TC004000

Sepulchre, P., Caubel, A., Ladant, J.-B., Bopp, L., Boucher, O., Braconnot, P., ... Tardif, D. (2020, July). IPSL-CM5A2 – an Earth system model designed for multi-millennial climate simulations. *Geoscientific Model Development*, *13*(7), 3011–3053. Retrieved 2020-11-27, from https://gmd.copernicus.org/articles/13/3011/2020/ doi: 10.5194/gmd-13-3011-2020

Sepulchre, P., Ramstein, G., Fluteau, F., Schuster, M., Tiercelin, J.-J., & Brunet, M. (2006, September). Tectonic Uplift and Eastern Africa Aridification. *Science*, *313*(5792), 1419–1423. Retrieved 2020-06-22, from https://www.sciencemag.org/lookup/doi/10.1126/science.1129158 doi: 10.1126/science.1129158

Sha, Y., Ren, X., Shi, Z., Zhou, P., Li, X., & Liu, X. (2020, April). Influence of the Tibetan Plateau and its northern margins on the mid-latitude Westerly Jet over Central Asia in summer. *Palaeogeography, Palaeoclimatology, Palaeoecology*, *544*, 109611. Retrieved 2022-06-27, from https://linkinghub.elsevier.com/retrieve/pii/S0031018219306819 doi: 10.1016/j.palaeo.2020.109611

Sha, Y., Shi, Z., Liu, X., & An, Z. (2015). Distinct impacts of the Mongolian and Tibetan Plateaus on the evolution of the East Asian monsoon. *Journal of Geophysical Research: Atmospheres*, *120*(10), 4764–4782. Retrieved 2021-04-19, from http://agupubs.onlinelibrary.wiley.com/doi/abs/10.1002/2014JD022880 (_eprint: https://onlinelibrary.wiley.com/doi/pdf/10.1002/2014JD022880) doi: https://doi.org/10.1002/2014JD022880

Shen, X., Wan, S., France-Lanord, C., Clift, P. D., Tada, R., Révillon, S., ... Li, A. (2017, September). History of Asian eolian input to the Sea of Japan since 15 Ma: Links to Tibetan uplift or global cooling? *Earth and Planetary Science Letters*, *474*, 296–308. Retrieved 2017-10-09, from http://linkinghub.elsevier.com/retrieve/pii/S0012821X17303771 doi: 10.1016/j.epsl.2017.06.053

Shi, Z., Liu, X., Liu, Y., Sha, Y., & Xu, T. (2015). Impact of Mongolian Plateau versus Tibetan Plateau on the westerly jet over North Pacific Ocean. *Climate Dynamics*, *44*(11-12), 3067–3076. (ISBN: 0930-7575 Publisher: Springer)

Shukla, A., Mehrotra, R. C., Spicer, R. A., Spicer, T. E., & Kumar, M. (2014, October). Cool equatorial terrestrial temperatures and the South Asian monsoon in the Early Eocene: Evidence from the Gurha Mine, Rajasthan, India. *Palaeogeography, Palaeoclimatology, Palaeoecology*, *412*, 187–198. Retrieved 2017-10-09,

from http://linkinghub.elsevier.com/retrieve/pii/S003101821400399X doi: 10.1016/j.palaeo.2014.08.004

Smith, S. G., Wegmann, K. W., Ancuta, L. D., Gosse, J. C., & Hopkins, C. E. (2016, August). Paleotopography and erosion rates in the central Hangay Dome, Mongolia: Landscape evolution since the mid-Miocene. *Journal of Asian Earth Sciences*, *125*, 37–57. Retrieved 2021-03-29, from https://www.sciencedirect.com/science/article/pii/S1367912016301274 doi: 10.1016/j.jseaes.2016.05.013

Song, B., Spicer, R. A., Zhang, K., Ji, J., Farnsworth, A., Hughes, A. C., ... Shi, G. (2020, May). Qaidam Basin leaf fossils show northeastern Tibet was high, wet and cool in the early Oligocene. *Earth and Planetary Science Letters*, *537*, 116175. Retrieved 2021-05-27, from https://www.sciencedirect.com/science/article/pii/S0012821X20301187 doi: 10.1016/j.epsl.2020.116175

Sorrel, P., Eymard, I., Leloup, P.-H., Maheo, G., Olivier, N., Sterb, M., ... Replumaz, A. (2017, December). Wet tropical climate in SE Tibet during the Late Eocene. *Scientific Reports*, *7*(1). Retrieved 2018-04-03, from http://www.nature.com/articles/s41598-017-07766-9 doi: 10.1038/s41598-017-07766-9

Sosdian, S. M., & Lear, C. H. (2020). Initiation of the Western Pacific Warm Pool at the Middle Miocene Climate Transition? *Paleoceanography and Paleoclimatology*, *35*(12), e2020PA003920. Retrieved 2021-09-20, from http://onlinelibrary.wiley.com/doi/abs/10.1029/2020PA003920 (_eprint: https://onlinelibrary.wiley.com/doi/pdf/10.1029/2020PA003920) doi: 10.1029/2020PA003920

Spicer, R., Su, T., Valdes, P. J., Farnsworth, A., Wu, F.-X., Shi, G., ... Zhou, Z. (2020, May). Why 'the uplift of the Tibetan Plateau' is a myth? *National Science Review*, 19. Retrieved 2020-11-27, from https://academic.oup.com/nsr/advance-article/doi/10.1093/nsr/nwaa091/5829861 doi: 10.1093/nsr/nwaa091

Spicer, R., Yang, J., Herman, A., Kodrul, T., Aleksandrova, G., Maslova, N., ... Jin, J.-H. (2017, September). Paleogene monsoons across India and South China: Drivers of biotic change. *Gondwana Research*, *49*, 350–363. Retrieved 2022-05-03, from https://linkinghub.elsevier.com/retrieve/pii/S1342937X16304385 doi: 10.1016/j.gr.2017.06.006

Spicer, R. A., Yang, J., Herman, A. B., Kodrul, T., Maslova, N., Spicer, T. E., ... Jin, J. (2016, September). Asian Eocene monsoons as revealed by leaf architectural signatures. *Earth and Planetary Science Letters*, *449*, 61–68. Retrieved 2017-10-09, from http://linkinghub.elsevier.com/retrieve/pii/S0012821X16302618 doi: 10.1016/j.epsl.2016.05.036

Srivastava, G., Paudayal, K. N., Utescher, T., & Mehrotra, R. (2018, February). Miocene vegetation shift and climate change: Evidence from the Siwalik of Nepal. *Global and Planetary Change*, *161*, 108–120. Retrieved 2022-05-30, from https://linkinghub.elsevier.com/retrieve/pii/S092181811730317X doi: 10.1016/j.gloplacha.2017.12.001

Srivastava, G., Spicer, R. A., Spicer, T. E., Yang, J., Kumar, M., Mehrotra, R., & Mehrotra, N. (2012, July). Megaflora and palaeoclimate of a Late Oligocene tropical delta, Makum Coalfield, Assam: Evidence for the early development of the South Asia Monsoon. *Palaeogeography, Palaeoclimatology, Palaeoecology*, *342-343*, 130–142. Retrieved 2018-06-22, from http://linkinghub.elsevier.com/retrieve/pii/S0031018212002532 doi: 10.1016/j.palaeo.2012.05.002

Straume, E. O., Gaina, C., Medvedev, S., & Nisancioglu, K. H. (2020, October). Global Cenozoic Paleobathymetry with a focus on the Northern Hemisphere Oceanic Gateways. *Gondwana Research*, *86*, 126–143. Retrieved 2021-04-08, from https://www.sciencedirect.com/science/article/pii/S1342937X20301659 doi: 10.1016/j.gr.2020.05.011

Su, H., & Zhou, J. (2020, June). Timing of Arabia-Eurasia collision: Constraints from restoration of crustal-scale cross-sections. *Journal of Structural Geology*, *135*, 104041. Retrieved 2022-03-04, from https://www.sciencedirect.com/science/

article/pii/S0191814119304456 doi: 10.1016/j.jsg.2020.104041

Su, T., Farnsworth, A., Spicer, R., & Huang, J. (2019). No high Tibetan Plateau until the Neogene. *Science Advances*, 9.

Su, T., Spicer, R. A., Li, S.-H., Xu, H., Huang, J., Sherlock, S., ... Zhou, Z.-K. (2019, May). Uplift, climate and biotic changes at the Eocene–Oligocene transition in south-eastern Tibet. *National Science Review*, *6*(3), 495–504. Retrieved 2019-10-24, from https://academic.oup.com/nsr/article/6/3/495/5036537 doi: 10.1093/nsr/nwy062

Su, T., Spicer, R. A., Wu, F.-X., Farnsworth, A., Huang, J., Del Rio, C., ... Zhou, Z.-K. (2020, December). A Middle Eocene lowland humid subtropical "Shangri-La" ecosystem in central Tibet. *Proceedings of the National Academy of Sciences*, *117*(52), 32989–32995. Retrieved 2021-02-01, from http://www.pnas.org/lookup/doi/10.1073/pnas.2012647117 doi: 10.1073/pnas.2012647117

Suarez, M. B., Passey, B. H., & Kaakinen, A. (2011, December). Paleosol carbonate multiple isotopologue signature of active East Asian summer monsoons during the late Miocene and Pliocene. *Geology*, *39*(12), 1151–1154. Retrieved 2022-06-09, from http://pubs.geoscienceworld.org/geology/article/39/12/1151/130458/Paleosol-carbonate-multiple-isotopologue-signature doi: 10.1130/G32350.1

Sun, J., Liu, W., Guo, Z., Qi, L., & Zhang, Z. (2022, April). Enhanced aridification across the Eocene/Oligocene transition evidenced by geochemical record in the Tajik Basin, Central Asia. *Global and Planetary Change*, *211*, 103789. Retrieved 2022-03-22, from https://www.sciencedirect.com/science/article/pii/S092181812200056X doi: 10.1016/j.gloplacha.2022.103789

Sun, J., Ni, X., Bi, S., Wu, W., Ye, J., Meng, J., & Windley, B. F. (2015, May). Synchronous turnover of flora, fauna and climate at the Eocene–Oligocene Boundary in Asia. *Scientific Reports*, *4*(1). Retrieved 2020-02-03, from http://www.nature.com/articles/srep07463 doi: 10.1038/srep07463

Sun, J., Sheykh, M., Ahmadi, N., Cao, M., Zhang, Z., Tian, S., ... Talebian, M. (2021, February). Permanent closure of the Tethyan Seaway in the northwestern Iranian Plateau driven by cyclic sea-level fluctuations in the late Middle Miocene. *Palaeogeography, Palaeoclimatology, Palaeoecology*, *564*, 110172. Retrieved 2021-05-03, from https://www.sciencedirect.com/science/article/pii/S0031018220306209 doi: 10.1016/j.palaeo.2020.110172

Sun, J., & Windley, B. (2015, October). Onset of aridification by 34 Ma across the Eocene-Oligocene transition in Central Asia. *Geology*, *43*, G37165.1. doi: 10.1130/G37165.1

Sun, J., Ye, J., Wu, W., Ni, X., Bi, S., Zhang, Z., ... Meng, J. (2010, June). Late Oligocene–Miocene mid-latitude aridification and wind patterns in the Asian interior. *Geology*, *38*(6), 515–518. Retrieved 2022-04-06, from https://doi.org/10.1130/G30776.1 doi: 10.1130/G30776.1

Sun, J., Zhang, L., Deng, C., & Zhu, R. (2008, May). Evidence for enhanced aridity in the Tarim Basin of China since 5.3Ma. *Quaternary Science Reviews*, *27*(9-10), 1012–1023. Retrieved 2022-06-16, from https://linkinghub.elsevier.com/retrieve/pii/S0277379108000310 doi: 10.1016/j.quascirev.2008.01.011

Sun, J., & Zhang, Z. (2008, November). Palynological evidence for the Mid-Miocene Climatic Optimum recorded in Cenozoic sediments of the Tian Shan Range, northwestern China. *Global and Planetary Change*, *64*(1-2), 53–68. Retrieved 2022-05-04, from https://linkinghub.elsevier.com/retrieve/pii/S0921818108001045 doi: 10.1016/j.gloplacha.2008.09.001

Sun, J., Zhang, Z., Cao, M., Windley, B. F., Tian, S., Sha, J., ... Oimahmadov, I. (2020, May). Timing of seawater retreat from proto-Paratethys, sedimentary provenance, and tectonic rotations in the late Eocene-early Oligocene in the Tajik Basin, Central Asia. *Palaeogeography, Palaeoclimatology, Palaeoecology*, *545*, 109657. Retrieved 2020-11-02, from http://www.sciencedirect.com/science/article/pii/S0031018220301024 doi: 10.1016/j.palaeo.2020.109657

Sun, Q.-g., Collinson, M. E., Li, C.-S., Wang, Y.-f., & Beerling, D. J. (2002). Quantitative reconstruction of palaeoclimate from the Middle Miocene Shanwang flora, eastern

China. *Palaeogeography, Palaeoclimatology, Palaeoecology*, 15. doi: 10.1016/S0031-0182(01)00433-3

Sun, X., & Wang, P. (2005, July). How old is the Asian monsoon system?—Palaeobotanical records from China. *Palaeogeography, Palaeoclimatology, Palaeoecology*, *222*(3-4), 181–222. Retrieved 2017-10-09, from http://linkinghub.elsevier.com/retrieve/pii/S0031018205001203 doi: 10.1016/j.palaeo.2005.03.005

Sun, Y., Liu, J., Liang, Y., Ji, J., Liu, W., Aitchison, J. C., ... Liu, Z. (2020, September). Cenozoic moisture fluctuations on the northeastern Tibetan Plateau and association with global climatic conditions. *Journal of Asian Earth Sciences*, *200*, 104490. Retrieved 2022-05-12, from https://www.sciencedirect.com/science/article/pii/S1367912020302832 doi: 10.1016/j.jseaes.2020.104490

Tada, R., Zheng, H., & Clift, P. D. (2016, December). Evolution and variability of the Asian monsoon and its potential linkage with uplift of the Himalaya and Tibetan Plateau. *Progress in Earth and Planetary Science*, *3*(1). Retrieved 2017-10-09, from http://www.progearthplanetsci.com/content/3/1/4 doi: 10.1186/s40645-016-0080-y

Tang, H., Li, S.-F., Su, T., Spicer, R. A., Zhang, S.-T., Li, S.-H., ... Zhou, Z.-K. (2020, December). Early Oligocene vegetation and climate of southwestern China inferred from palynology. *Palaeogeography, Palaeoclimatology, Palaeoecology*, *560*, 109988. Retrieved 2022-03-11, from https://www.sciencedirect.com/science/article/pii/S0031018220304338 doi: 10.1016/j.palaeo.2020.109988

Tang, H., Micheels, A., Eronen, J. T., Ahrens, B., & Fortelius, M. (2013, March). Asynchronous responses of East Asian and Indian summer monsoons to mountain uplift shown by regional climate modelling experiments. *Climate Dynamics*, *40*(5), 1531–1549. Retrieved 2022-06-28, from https://doi.org/10.1007/s00382-012-1603-x doi: 10.1007/s00382-012-1603-x

Tang, Z.-H., & Ding, Z.-L. (2013, December). A palynological insight into the Miocene aridification in the Eurasian interior. *Palaeoworld*, *22*(3-4), 77–85. Retrieved 2022-06-23, from https://linkinghub.elsevier.com/retrieve/pii/S1871174X13000073 doi: 10.1016/j.palwor.2013.05.001

Tapponnier, P., & Molnar, P. (1979). Active faulting and cenozoic tectonics of the Tien Shan, Mongolia, and Baykal Regions. *Journal of Geophysical Research: Solid Earth*, *84*(B7), 3425–3459. Retrieved 2021-03-26, from http://agupubs.onlinelibrary.wiley.com/doi/abs/10.1029/JB084iB07p03425 (_eprint: https://onlinelibrary.wiley.com/doi/pdf/10.1029/JB084iB07p03425) doi: https://doi.org/10.1029/JB084iB07p03425

Tardif, D., Fluteau, F., Donnadieu, Y., Le Hir, G., Ladant, J.-B., Sepulchre, P., ... Dupont-Nivet, G. (2020, May). The origin of Asian monsoons: a modelling perspective. *Climate of the Past*, *16*(3), 847–865. Retrieved 2020-05-08, from https://www.clim-past.net/16/847/2020/ doi: 10.5194/cp-16-847-2020

Tardif, D., Toumoulin, A., Fluteau, F., Donnadieu, Y., Le Hir, G., Barbolini, N., ... Dupont-Nivet, G. (2021, October). Orbital variations as a major driver of climate and biome distribution during the greenhouse to icehouse transition. *Science Advances*, *7*(43), eabh2819. Retrieved 2021-10-25, from https://www.science.org/doi/10.1126/sciadv.abh2819 doi: 10.1126/sciadv.abh2819

Tauxe, L., & Feakins, S. J. (2020). A Reassessment of the Chronostratigraphy of Late Miocene C3–C4 Transitions. *Paleoceanography and Paleoclimatology*, *35*(7), e2020PA003857. Retrieved 2022-06-07, from http://onlinelibrary.wiley.com/doi/abs/10.1029/2020PA003857 (_eprint: https://agupubs.onlinelibrary.wiley.com/doi/pdf/10.1029/2020PA003857) doi: 10.1029/2020PA003857

Thomson, J. R., Holden, P. B., Anand, P., Edwards, N. R., Porchier, C. A., & Harris, N. B. W. (2021, June). Tectonic and climatic drivers of Asian monsoon evolution. *Nature Communications*, *12*(1), 4022. Retrieved 2021-10-05, from http://www.nature.com/articles/s41467-021-24244-z (Bandiera_abtest: a Cc_license_type: cc_by Cg_type: Nature Research Journals Number: 1 Primary_atype: Research Pub-

lisher: Nature Publishing Group Subject_term: Climate change;Palaeoclimate Subject_term_id: climate-change;palaeoclimate) doi: 10.1038/s41467-021-24244-z

Tong, G., Liu, Z., Zheng, M., & Wang, W. (2002, September). Primary Study on Quantitative Reconstruction of Middle Late Eocene Climate in Jianghan Basin. *Journal of Earth Science*, *13*(3). Retrieved 2020-09-07, from http://en.earth-science.net/en/article/id/128 (Publisher: Journal of Earth Science)

Toumoulin, A., Donnadieu, Y., Ladant, J., Batenburg, S. J., Poblete, F., & Dupont-Nivet, G. (2020, August). Quantifying the Effect of the Drake Passage Opening on the Eocene Ocean. *Paleoceanography and Paleoclimatology*, *35*(8). Retrieved 2020-08-13, from https://onlinelibrary.wiley.com/doi/abs/10.1029/2020PA003889 doi: 10.1029/2020PA003889

Toumoulin, A., Tardif, D., Donnadieu, Y., Licht, A., Ladant, J.-B., Kunzmann, L., & Dupont-Nivet, G. (2022, February). Evolution of continental temperature seasonality from the Eocene greenhouse to the Oligocene icehouse –a model–data comparison. *Climate of the Past*, *18*(2), 341–362. Retrieved 2022-02-28, from https://cp.copernicus.org/articles/18/341/2022/ (Publisher: Copernicus GmbH) doi: 10.5194/cp-18-341-2022

Tripathi, S., Tiwari, M., Lee, J., & Khim, B.-K. (2017, February). First evidence of denitrification vis-à-vis monsoon in the Arabian Sea since Late Miocene. *Scientific Reports*, *7*(1), 43056. Retrieved 2022-06-02, from http://www.nature.com/articles/srep43056 (Number: 1 Publisher: Nature Publishing Group) doi: 10.1038/srep43056

Valcke, S., Budich, R., Carter, M., Guilyardi, E., Lautenschlager, M., Redler, R., & Steenman-Clark, L. (2006). The PRISM software framework and the OASIS coupler. *Annual BMRC Modelling Workshop'The Australian Community Climate and Earth System Simulator (ACCESS)-challenges and opportunities'*, 10.

Valdes, P. J., Armstrong, E., Badger, M. P. S., Bradshaw, C. D., Bragg, F., Crucifix, M., ... Williams, J. H. T. (2017, October). The BRIDGE HadCM3 family of climate models: HadCM3@Bristol v1.0. *Geoscientific Model Development*, *10*(10), 3715–3743. Retrieved 2019-11-07, from https://www.geosci-model-dev.net/10/3715/2017/ doi: 10.5194/gmd-10-3715-2017

van Hinsbergen, D. J., Lippert, P. C., Li, S., Huang, W., Advokaat, E. L., & Spakman, W. (2019, June). Reconstructing Greater India: Paleogeographic, kinematic, and geodynamic perspectives. *Tectonophysics*, *760*, 69–94. Retrieved 2020-10-15, from https://linkinghub.elsevier.com/retrieve/pii/S0040195118301331 doi: 10.1016/j.tecto.2018.04.006

van Hinsbergen, D. J. J., Lippert, P. C., Dupont-Nivet, G., McQuarrie, N., Doubrovine, P. V., Spakman, W., & Torsvik, T. H. (2012, May). Greater India Basin hypothesis and a two-stage Cenozoic collision between India and Asia. *Proceedings of the National Academy of Sciences*, *109*(20), 7659–7664. Retrieved from http://www.pnas.org/content/109/20/7659.abstract doi: 10.1073/pnas.1117262109

Vassallo, R., Jolivet, M., Ritz, J. F., Braucher, R., Larroque, C., Sue, C., ... Javkhlanbold, D. (2007, July). Uplift age and rates of the Gurvan Bogd system (Gobi-Altay) by apatite fission track analysis. *Earth and Planetary Science Letters*, *259*(3), 333–346. Retrieved 2021-04-20, from https://www.sciencedirect.com/science/article/pii/S0012821X07002853 doi: 10.1016/j.epsl.2007.04.047

Vicente de Gouveia, S., Besse, J., Frizon de Lamotte, D., Greff-Lefftz, M., Lescanne, M., Gueydan, F., & Leparmentier, F. (2018, April). Evidence of hotspot paths below Arabia and the Horn of Africa and consequences on the Red Sea opening. *Earth and Planetary Science Letters*, *487*, 210–220. Retrieved 2021-10-13, from https://www.sciencedirect.com/science/article/pii/S0012821X18300487 doi: 10.1016/j.epsl.2018.01.030

Vornlocher, J., Lukens, W., Schubert, B., & Quan, C. (2021, April). Late Oligocene Precipitation Seasonality in East Asia Based on 13 C Profiles in Fossil Wood. *Paleoceanography and Paleoclimatology*, *36*. doi: 10.1029/2021PA004229

Vögeli, N., Najman, Y., van der Beek, P., Huyghe, P., Wynn, P. M., Govin, G., ... Sachse, D. (2017, August). Lateral variations in vegetation in the Himalaya since the Miocene and implications for climate evolution. *Earth and Planetary Science Letters*, *471*, 1–9. Retrieved 2022-05-02, from https://www.sciencedirect.com/science/article/pii/S0012821X17302315 doi: 10.1016/j.epsl.2017.04.037

Wan, S., Clift, P., Li, A., Li, T., & Yin, X. (2010, August). Geochemical records in the South China Sea: Implications for East Asian summer monsoon evolution over the last 20 Ma. *Geological Society, London, Special Publications*, *342*. doi: 10.1144/SP342.14

Wan, S., Li, A., Clift, P. D., & Stuut, J.-B. W. (2007, October). Development of the East Asian monsoon: Mineralogical and sedimentologic records in the northern South China Sea since 20 Ma. *Palaeogeography, Palaeoclimatology, Palaeoecology*, *254*(3-4), 561–582. Retrieved 2022-05-03, from https://linkinghub.elsevier.com/retrieve/pii/S0031018207003963 doi: 10.1016/j.palaeo.2007.07.009

Wang, B., & Ding, Q. (2008, March). Global monsoon: Dominant mode of annual variation in the tropics. *Dynamics of Atmospheres and Oceans*, *44*(3-4), 165–183. Retrieved 2019-05-16, from https://linkinghub.elsevier.com/retrieve/pii/S0377026508000055 doi: 10.1016/j.dynatmoce.2007.05.002

Wang, B., Shi, G., Xu, C., Spicer, R. A., Perrichot, V., Schmidt, A. R., ... Engel, M. S. (2021). The mid-Miocene Zhangpu biota reveals an outstandingly rich rainforest biome in East Asia. *Science Advances*, *7*(18), eabg0625. Retrieved 2022-05-03, from https://www.science.org/doi/full/10.1126/sciadv.abg0625 (Publisher: American Association for the Advancement of Science) doi: 10.1126/sciadv.abg0625

Wang, C., Dai, J., Zhao, X., Li, Y., Graham, S. A., He, D., ... Meng, J. (2014, May). Outward-growth of the Tibetan Plateau during the Cenozoic: A review. *Tectonophysics*, *621*, 1–43. Retrieved 2017-10-09, from http://linkinghub.elsevier.com/retrieve/pii/S0040195114000729 doi: 10.1016/j.tecto.2014.01.036

Wang, D., Lu, S., Han, S., Sun, X., & Quan, C. (2013, January). Eocene prevalence of monsoon-like climate over eastern China reflected by hydrological dynamics. *Journal of Asian Earth Sciences*, *62*, 776–787. Retrieved 2022-05-04, from https://linkinghub.elsevier.com/retrieve/pii/S1367912012005184 doi: 10.1016/j.jseaes.2012.11.032

Wang, H., Lu, H., Zhao, L., Zhang, H., Lei, F., & Wang, Y. (2019, November). Asian monsoon rainfall variation during the Pliocene forced by global temperature change. *Nature Communications*, *10*(1), 5272. Retrieved 2022-06-09, from https://www.nature.com/articles/s41467-019-13338-4 (Number: 1 Publisher: Nature Publishing Group) doi: 10.1038/s41467-019-13338-4

Wang, L., & Chen, W. (2014, March). An Intensity Index for the East Asian Winter Monsoon. *Journal of Climate*, *27*(6), 2361–2374. Retrieved 2021-10-13, from https://journals.ametsoc.org/view/journals/clim/27/6/jcli-d-13-00086.1.xml (Publisher: American Meteorological Society Section: Journal of Climate) doi: 10.1175/JCLI-D-13-00086.1

Wang, P., Clemens, S., Beaufort, L., Braconnot, P., Ganssen, G., Jian, Z., ... Sarnthein, M. (2005, March). Evolution and variability of the Asian monsoon system: state of the art and outstanding issues. *Quaternary Science Reviews*, *24*(5-6), 595–629. Retrieved 2020-10-11, from https://linkinghub.elsevier.com/retrieve/pii/S0277379104002975 doi: 10.1016/j.quascirev.2004.10.002

Wang, Q., Li, Y., Ferguson, D. K., Mo, W.-B., & Yang, N. (2021, July). An equable subtropical climate throughout China in the Miocene based on palaeofloral evidence. *Earth-Science Reviews*, *218*, 103649. Retrieved 2022-05-03, from https://www.sciencedirect.com/science/article/pii/S0012825221001501 doi: 10.1016/j.earscirev.2021.103649

Wang, X., Carrapa, B., Sun, Y., Dettman, D. L., Chapman, J. B., Caves Rugenstein, J. K., ... Chen, F. (2020, July). The role of the westerlies and orography in Asian hydroclimate since the late Oligocene. *Geology*, *48*(7), 728–732. Retrieved 2020-10-11, from https://pubs.geoscienceworld.org/gsa/geology/article/48/

7/728/584578/The-role-of-the-westerlies-and-orography-in-Asian doi: 10.1130/G47400.1

Wang, Y., & Deng, T. (2005, July). A 25 m.y. isotopic record of paleodiet and environmental change from fossil mammals and paleosols from the NE margin of the Tibetan Plateau. *Earth and Planetary Science Letters*, *236*(1-2), 322–338. Retrieved 2022-06-16, from https://linkinghub.elsevier.com/retrieve/pii/S0012821X0500316X doi: 10.1016/j.epsl.2005.05.006

Wasiljeff, J., Salminen, J. M., Stenman, J., Zhang, Z., & Kaakinen, A. (2022, April). Oligocene moisture variations as evidenced by an aeolian dust sequence in Inner Mongolia, China. *Scientific Reports*, *12*. doi: 10.1038/s41598-022-09362-y

Webb, A. A. G., Guo, H., Clift, P. D., Husson, L., Müller, T., Costantino, D., ... Wang, Q. (2017, April). The Himalaya in 3D: Slab dynamics controlled mountain building and monsoon intensification. *Lithosphere*, *9*(4), 637–651. Retrieved 2022-06-07, from https://doi.org/10.1130/L636.1 doi: 10.1130/L636.1

Webster, P. J., Magaña, V. O., Palmer, T. N., Shukla, J., Tomas, R. A., Yanai, M., & Yasunari, T. (1998, June). Monsoons: Processes, predictability, and the prospects for prediction. *Journal of Geophysical Research: Oceans*, *103*(C7), 14451–14510. Retrieved 2020-06-19, from http://doi.wiley.com/10.1029/97JC02719 doi: 10.1029/97JC02719

Webster, P. J., & Yang, S. (1992, July). Monsoon and Enso: Selectively Interactive Systems. *Quarterly Journal of the Royal Meteorological Society*, *118*(507), 877–926. Retrieved 2019-07-05, from http://doi.wiley.com/10.1002/qj.49711850705 doi: 10.1002/qj.49711850705

Wei, G., Li, X.-H., Liu, Y., Shao, L., & Liang, X. (2006). Geochemical record of chemical weathering and monsoon climate change since the early Miocene in the South China Sea. *Paleoceanography*, *21*(4). Retrieved 2022-05-03, from https://onlinelibrary.wiley.com/doi/abs/10.1029/2006PA001300 (_eprint: https://onlinelibrary.wiley.com/doi/pdf/10.1029/2006PA001300) doi: 10.1029/2006PA001300

Wei, H.-H., & Bordoni, S. (2016, August). On the Role of the African Topography in the South Asian Monsoon. *Journal of the Atmospheric Sciences*, *73*(8), 3197–3212. Retrieved 2019-11-15, from http://journals.ametsoc.org/doi/10.1175/JAS-D-15-0182.1 doi: 10.1175/JAS-D-15-0182.1

Wei, J., Wang, Y., Wang, G., Wei, Z., Wei, H., Zhang, T., ... Li, L. (2022, April). Biomarker Records From Eocene Lacustrine Sequence in the Eastern Tibet Plateau and Its Implication for Organic Matter Sources. *Frontiers in Earth Science*, *10*, 849041. doi: 10.3389/feart.2022.849041

Westerweel, J., Licht, A., Cogné, N., Roperch, P., Dupont-Nivet, G., Thi, M. K., ... Aung, D. W. (2020). Burma Terrane Collision and Northward Indentation in the Eastern Himalayas Recorded in the Eocene-Miocene Chindwin Basin (Myanmar). *Tectonics*, *39*(10), e2020TC006413. Retrieved 2021-03-29, from http://agupubs.onlinelibrary.wiley.com/doi/abs/10.1029/2020TC006413 (_eprint: https://onlinelibrary.wiley.com/doi/pdf/10.1029/2020TC006413) doi: https://doi.org/10.1029/2020TC006413

Westerweel, J., Roperch, P., Licht, A., Dupont-Nivet, G., Win, Z., Poblete, F., ... Aung, D. W. (2019, October). Burma Terrane part of the Trans-Tethyan arc during collision with India according to palaeomagnetic data. *Nature Geoscience*, *12*(10), 863–868. Retrieved 2019-10-17, from http://www.nature.com/articles/s41561-019-0443-2 doi: 10.1038/s41561-019-0443-2

White, R. H., Battisti, D. S., & Roe, G. H. (2017). Mongolian Mountains Matter Most: Impacts of the Latitude and Height of Asian Orography on Pacific Wintertime Atmospheric Circulation. *JOURNAL OF CLIMATE*, *30*, 18.

Wichura, H., Jacobs, L. L., Lin, A., Polcyn, M. J., Manthi, F. K., Winkler, D. A., ... Clemens, M. (2015, March). A 17-My-old whale constrains onset of uplift and climate change in east Africa. *Proceedings of the National Academy of Sciences*,

112(13), 3910–3915. Retrieved 2021-04-07, from http://www.pnas.org/content/112/13/3910 (Publisher: National Academy of Sciences Section: Physical Sciences) doi: 10.1073/pnas.1421502112

Wolfe, J. (1993). A method of obtaining climatic parameters from leaf assemblages. *US Government Printing Office.*(2040-2041).

Wu, M., Zhuang, G., Hou, M., & Liu, Z. (2021, July). Expanded lacustrine sedimentation in the Qaidam Basin on the northern Tibetan Plateau: Manifestation of climatic wetting during the Oligocene icehouse. *Earth and Planetary Science Letters*, *565*, 116935. Retrieved 2022-05-04, from https://linkinghub.elsevier.com/retrieve/pii/S0012821X21001941 doi: 10.1016/j.epsl.2021.116935

Xia, K., Su, T., Liu, Y.-S. C., Xing, Y.-W., Jacques, F. M., & Zhou, Z.-K. (2009, May). Quantitative climate reconstructions of the late Miocene Xiaolongtan megaflora from Yunnan, southwest China. *Palaeogeography, Palaeoclimatology, Palaeoecology*, *276*(1-4), 80–86. Retrieved 2022-03-22, from https://linkinghub.elsevier.com/retrieve/pii/S0031018209000819 doi: 10.1016/j.palaeo.2009.02.024

Xiao, G. Q., Abels, H. A., Yao, Z. Q., Dupont-Nivet, G., & Hilgen, F. J. (2010, July). Asian aridification linked to the first step of the Eocene-Oligocene climate Transition (EOT) in obliquity-dominated terrestrial records (Xining Basin, China). *Climate of the Past*, *6*(4), 501–513. Retrieved 2017-10-09, from http://www.clim-past.net/6/501/2010/ doi: 10.5194/cp-6-501-2010

Xing, Y., Utescher, T., Jacques, F. M., Su, T., Liu, Y. C., Huang, Y., & Zhou, Z. (2012, November). Paleoclimatic estimation reveals a weak winter monsoon in southwestern China during the late Miocene: Evidence from plant macrofossils. *Palaeogeography, Palaeoclimatology, Palaeoecology*, *358-360*, 19–26. Retrieved 2022-05-04, from https://linkinghub.elsevier.com/retrieve/pii/S0031018212004129 doi: 10.1016/j.palaeo.2012.07.011

Xiong, Z., Ding, L., Spicer, R. A., Farnsworth, A., Wang, X., Valdes, P. J., ... Yue, Y. (2020, August). The early Eocene rise of the Gonjo Basin, SE Tibet: From low desert to high forest. *Earth and Planetary Science Letters*, *543*, 116312. Retrieved 2020-10-12, from https://linkinghub.elsevier.com/retrieve/pii/S0012821X20302569 doi: 10.1016/j.epsl.2020.116312

Xiong, Z., Liu, X., Ding, L., Farnsworth, A., Spicer, R. A., Xu, Q., ... Yue, Y. (2022). The rise and demise of the Paleogene Central Tibetan Valley. *Science Advances*, *8*(6), eabj0944. Retrieved 2022-02-10, from http://www.science.org/doi/10.1126/sciadv.abj0944 (Publisher: American Association for the Advancement of Science) doi: 10.1126/sciadv.abj0944

Xu, Q., Ding, L., Spicer, R. A., Liu, X., Li, S., & Wang, H. (2018, February). Stable isotopes reveal southward growth of the Himalayan-Tibetan Plateau since the Paleocene. *Gondwana Research*, *54*, 50–61. Retrieved 2020-10-20, from https://linkinghub.elsevier.com/retrieve/pii/S1342937X17303295 doi: 10.1016/j.gr.2017.10.005

Xu, Q., Ding, L., Zhang, L., Cai, F., Lai, Q., Yang, D., & Liu-Zeng, J. (2013, January). Paleogene high elevations in the Qiangtang Terrane, central Tibetan Plateau. *Earth and Planetary Science Letters*, *362*, 31–42. Retrieved 2020-10-17, from http://www.sciencedirect.com/science/article/pii/S0012821X1200684X doi: 10.1016/j.epsl.2012.11.058

Yang, C., Dang, H., Zhou, X., Zhang, H., Wang, X., Wang, Y., ... Jian, Z. (2021, April). Upper ocean hydrographic changes in response to the evolution of the East Asian monsoon in the northern South China Sea during the middle to late Miocene. *Global and Planetary Change*, *201*, 103478. doi: 10.1016/j.gloplacha.2021.103478

Yang, W., Zuo, R., Wang, X., Song, Y., Jiang, Z., Luo, Q., ... Zhang, Z. (2019, January). Sensitivity of lacustrine stromatolites to Cenozoic tectonic and climatic forcing in the southern Junggar Basin, NW China: New insights from mineralogical, stable and clumped isotope compositions. *Palaeogeography, Palaeoclimatology, Palaeoecology*, *514*, 109–123. Retrieved 2022-06-17, from https://linkinghub.elsevier.com/retrieve/pii/S0031018218303985 doi: 10.1016/j.palaeo.2018.10.011

Yang, X., Groeneveld, J., Jian, Z., Steinke, S., & Giosan, L. (2020). Middle Miocene Intensification of South Asian Monsoonal Rainfall. *Paleoceanography and Paleoclimatology*, *35*(12), e2020PA003853. Retrieved 2021-03-17, from http://agupubs.onlinelibrary.wiley.com/doi/abs/10.1029/2020PA003853 (_eprint: https://onlinelibrary.wiley.com/doi/pdf/10.1029/2020PA003853) doi: https://doi.org/10.1029/2020PA003853

Yao, Y.-F., Bruch, A. A., Mosbrugger, V., & Li, C.-S. (2011, May). Quantitative reconstruction of Miocene climate patterns and evolution in Southern China based on plant fossils. *Palaeogeography, Palaeoclimatology, Palaeoecology*, *304*(3-4), 291–307. Retrieved 2022-05-06, from https://linkinghub.elsevier.com/retrieve/pii/S003101821000221X doi: 10.1016/j.palaeo.2010.04.012

Yarmolyuk, V. V., Kudryashova, E. A., Kozlovsky, A. M., & Lebedev, V. A. (2008, October). Late Cenozoic volcanism of Khangai (Central Mongolia): Evidence for recent orogeny in Central Asia. *Doklady Earth Sciences*, *422*(1), 1032–1036. Retrieved 2021-03-29, from http://link.springer.com/10.1134/S1028334X08070064 doi: 10.1134/S1028334X08070064

Yu, E., Zhang, R., Jiang, D., Ramstein, G., Zhang, Z., & Sun, J. (2018, October). High-resolution simulation of Asian monsoon response to regional uplift of the Tibetan Plateau with regional climate model nested with global climate model. *Global and Planetary Change*, *169*, 34–47. Retrieved 2021-09-24, from https://linkinghub.elsevier.com/retrieve/pii/S0921818118300407 doi: 10.1016/j.gloplacha.2018.07.002

Yuan, Q., Barbolini, N., Ashworth, L., Rydin, C., Gao, D.-L., Shan, F.-S., ... Vajda, V. (2021, July). Palaeoenvironmental changes in Eocene Tibetan lake systems traced by geochemistry, sedimentology and palynofacies. *Journal of Asian Earth Sciences*, *214*, 104778. Retrieved 2022-05-04, from https://linkinghub.elsevier.com/retrieve/pii/S1367912021001164 doi: 10.1016/j.jseaes.2021.104778

Yuan, Q., Barbolini, N., Rydin, C., Gao, D.-L., Wei, H.-C., Fan, Q.-S., ... Vajda, V. (2020, November). Aridification signatures from fossil pollen indicate a drying climate in east-central Tibet during the late Eocene. *Climate of the Past*, *16*(6), 2255–2273. Retrieved 2022-05-04, from https://cp.copernicus.org/articles/16/2255/2020/ doi: 10.5194/cp-16-2255-2020

Yuan, W., Carter, A., Dong, J., Bao, Z., An, Y., & Guo, Z. (2006, January). Mesozoic–Tertiary exhumation history of the Altai Mountains, northern Xinjiang, China: New constraints from apatite fission track data. *Tectonophysics*, *412*(3), 183–193. Retrieved 2021-03-26, from https://www.sciencedirect.com/science/article/pii/S004019510500449X doi: 10.1016/j.tecto.2005.09.007

Zhang, R., Jiang, D., Liu, X., & Tian, Z. (2012, December). Modeling the climate effects of different subregional uplifts within the Himalaya-Tibetan Plateau on Asian summer monsoon evolution. *Chinese Science Bulletin*, *57*(35), 4617–4626. Retrieved 2017-10-09, from http://link.springer.com/10.1007/s11434-012-5284-y doi: 10.1007/s11434-012-5284-y

Zhang, R., Jiang, D., Ramstein, G., Zhang, Z., Lippert, P. C., & Yu, E. (2018, February). Changes in Tibetan Plateau latitude as an important factor for understanding East Asian climate since the Eocene: A modeling study. *Earth and Planetary Science Letters*, *484*, 295–308. Retrieved 2018-01-16, from http://linkinghub.elsevier.com/retrieve/pii/S0012821X1730746X doi: 10.1016/j.epsl.2017.12.034

Zhang, R., Jiang, D., & Zhang, Z. (2017, December). Effects of the uplifts of the main and marginal Tibetan Plateau on the Asian climate under modern and ˜30 Ma boundary conditions. *Palaeogeography, Palaeoclimatology, Palaeoecology*. Retrieved 2018-01-16, from http://linkinghub.elsevier.com/retrieve/pii/S0031018217308866 doi: 10.1016/j.palaeo.2017.12.022

Zhang, R., Jiang, D., Zhang, Z., & Zhang, C. (2021). Effects of Tibetan Plateau Growth, Paratethys Sea Retreat and Global Cooling on the East Asian Climate by the Early Miocene. *Geochemistry, Geo-*

physics, Geosystems, *22*(6), e2021GC009655. Retrieved 2021-09-24, from http://onlinelibrary.wiley.com/doi/abs/10.1029/2021GC009655 (_eprint: https://agupubs.onlinelibrary.wiley.com/doi/pdf/10.1029/2021GC009655) doi: 10.1029/2021GC009655

Zhang, Z., Flatøy, F., Wang, H., Bethke, I., Bentsen, M., & Guo, Z. (2012, January). Early Eocene Asian climate dominated by desert and steppe with limited monsoons. *Journal of Asian Earth Sciences*, *44*, 24–35. Retrieved 2017-10-09, from http://linkinghub.elsevier.com/retrieve/pii/S1367912011002148 doi: 10.1016/j.jseaes.2011.05.013

Zhang, Z., Ramstein, G., Schuster, M., Li, C., Contoux, C., & Yan, Q. (2014, September). Aridification of the Sahara desert caused by Tethys Sea shrinkage during the Late Miocene. *Nature*, *513*(7518), 401–404. Retrieved 2019-09-06, from http://www.nature.com/articles/nature13705 doi: 10.1038/nature13705

Zhang, Z., & Sun, J. (2011, January). Palynological evidence for Neogene environmental change in the foreland basin of the southern Tianshan range, northwestern China. *Global and Planetary Change*, *75*(1-2), 56–66. Retrieved 2022-05-04, from https://linkinghub.elsevier.com/retrieve/pii/S0921818110002304 doi: 10.1016/j.gloplacha.2010.10.006

Zhang, Z., Wang, H., Guo, Z., & Jiang, D. (2007, March). What triggers the transition of palaeoenvironmental patterns in China, the Tibetan Plateau uplift or the Paratethys Sea retreat? *Palaeogeography, Palaeoclimatology, Palaeoecology*, *245*(3-4), 317–331. Retrieved 2017-10-09, from http://linkinghub.elsevier.com/retrieve/pii/S0031018206004469 doi: 10.1016/j.palaeo.2006.08.003

Zhang, Z., Xiao, W., Majidifard, M. R., Zhu, R., Wan, B., Ao, S., ... Esmaeili, R. (2017, June). Detrital zircon provenance analysis in the Zagros Orogen, SW Iran: implications for the amalgamation history of the Neo-Tethys. *International Journal of Earth Sciences*, *106*(4), 1223–1238. Retrieved 2022-03-04, from https://doi.org/10.1007/s00531-016-1314-3 doi: 10.1007/s00531-016-1314-3

Zhao, H., Qiang, X., Xu, X., & Sun, Y. (2020, April). Iron oxide characteristics of the Chinese loess-red clay sequences and their implications for the evolution of the East Asian summer monsoon since the Late Oligocene. *Palaeogeography, Palaeoclimatology, Palaeoecology*, *543*, 109604. Retrieved 2022-06-09, from https://linkinghub.elsevier.com/retrieve/pii/S0031018219308995 doi: 10.1016/j.palaeo.2020.109604

Zhao, L., Lu, H., Wang, H., Meadows, M., Ma, C., Tang, L., ... Zhang, H. (2020, October). Vegetation dynamics in response to evolution of the Asian Monsoon in a warm world: Pollen evidence from the Weihe Basin, central China. *Global and Planetary Change*, *193*, 103269. Retrieved 2022-06-09, from https://linkinghub.elsevier.com/retrieve/pii/S0921818120301600 doi: 10.1016/j.gloplacha.2020.103269

Zheng, H., Wei, X., Tada, R., Clift, P. D., Wang, B., Jourdan, F., ... He, M. (2015, June). Late Oligocene–early Miocene birth of the Taklimakan Desert. *Proceedings of the National Academy of Sciences*, *112*(25), 7662–7667. Retrieved 2022-02-11, from http://www.pnas.org/lookup/doi/10.1073/pnas.1424487112 doi: 10.1073/pnas.1424487112

Zheng, H., Yang, Q., Cao, S., Clift, P. D., He, M., Kano, A., ... Jourdan, F. (2022, December). From desert to monsoon: irreversible climatic transition at ˜ 36 Ma in southeastern Tibetan Plateau. *Progress in Earth and Planetary Science*, *9*(1), 12. Retrieved 2022-05-02, from https://progearthplanetsci.springeropen.com/articles/10.1186/s40645-022-00470-x doi: 10.1186/s40645-022-00470-x

Zhisheng, A., Guoxiong, W., Jianping, L., Youbin, S., Yimin, L., Weijian, Z., ... Juan, F. (2015, May). Global Monsoon Dynamics and Climate Change. *Annual Review of Earth and Planetary Sciences*, *43*(1), 29–77. Retrieved 2017-10-09, from http://www.annualreviews.org/doi/10.1146/annurev-earth-060313-054623 doi: 10.1146/annurev-earth-060313-054623

Zhisheng, A., Kutzbach, J. E., Prell, W. L., & Porter, S. C. (2001, May). Evolution of Asian

monsoons and phased uplift of the Himalaya–Tibetan plateau since Late Miocene times. *Nature*, *411*(6833), 62–66. Retrieved 2021-09-16, from http://www.nature.com/articles/35075035 (Bandiera_abtest: a Cg_type: Nature Research Journals Number: 6833 Primary_atype: Research Publisher: Nature Publishing Group) doi: 10.1038/35075035

Zhuang, G., Pagani, M., & Zhang, Y. G. (2017, July). Monsoonal upwelling in the western Arabian Sea since the middle Miocene. *Geology*, *45*(7), 655–658. Retrieved 2022-05-02, from https://doi.org/10.1130/G39013.1 doi: 10.1130/G39013.1

Ziegler, C. L., Murray, R. W., Hovan, S. A., & Rea, D. K. (2007, February). Resolving eolian, volcanogenic, and authigenic components in pelagic sediment from the Pacific Ocean. *Earth and Planetary Science Letters*, *254*(3), 416–432. Retrieved 2022-03-25, from https://www.sciencedirect.com/science/article/pii/S0012821X06008661 doi: 10.1016/j.epsl.2006.11.049

Zoura, D., Hill, D., Dolan, A., Hunter, S., Tang, Z., & Haywood, A. (2019, August). Atmospheric carbon dioxide, ice sheet and topographic constraints on palaeo moisture availability in Asia. *Earth and Planetary Science Letters*, *519*, 12–27. Retrieved 2019-09-12, from https://linkinghub.elsevier.com/retrieve/pii/S0012821X19302390 doi: 10.1016/j.epsl.2019.04.035

3330 # 9 Supplementary

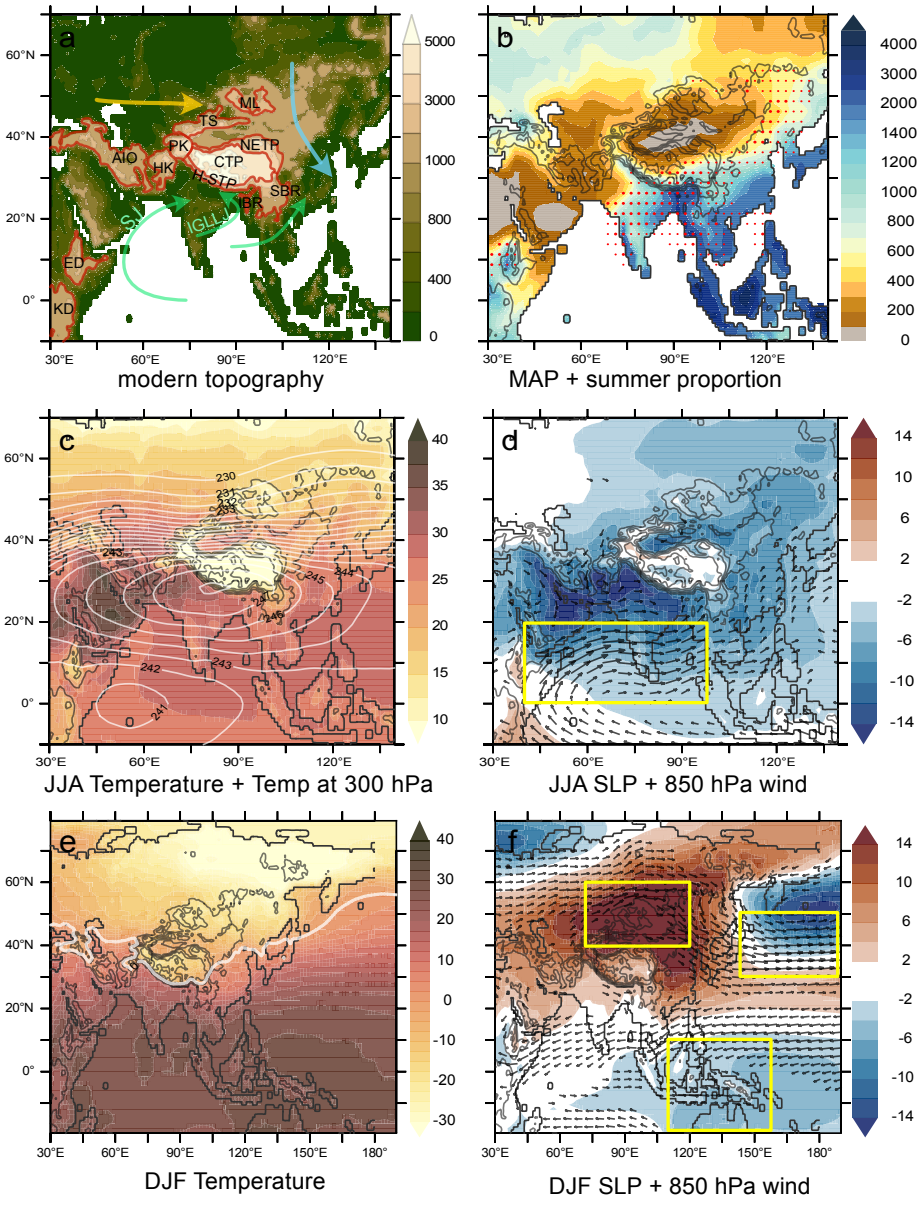

Figure 14. South Asian orography and main seasonal characteristics of South and East Asian Monsoons subsystems from observations an reanalysis. **(a)** Modern geography and topography (in m), with main seasonal winds: Westerlies (yellow arrow), Winter monsoon (blue arrow) and Summer monsoon (green arrows) ; Somali Jet (SJ), Indo-Gangetic-Low Level Jet (IGLLJ) and main geographic units mentioned in Section 4 highlighted: KD - Kenyan Dome, ED - Ethiopian Dome, AIO - Anatolian and Iranian orogens, PK - Pamir-Karakoram, HK - Hindu Kush, CTP - Central Tibetan Plateau, H-STP - Himalayas and Southern Tibetan Plateau, NETP - North-eastern TP, TS - Tian Shan, IBR - Indo Burman Ranges, SBR - Sino Burman Ranges, ML - Mongolian Landforms.; **(b)** Mean Annual Precipitation (shading, mm/yr), and regions where the Monsoon Precipitation Index is over 0.5 (thin red dots) and 0.75 (thick red dots). The Monsoon Precipitation Index is defined in the Monsoon Metrics section 5.3 ; **(c)** JJA mean 2m temperature (shading, Celsius) and 300 hPa atmospheric temperature (white contour, Kelvin) ; **(d)** JJA normalized Sea Level Pressure anomalies (shading, hPa) and 850 hPa winds (vectors over 4m/s). Yellow box highlight the region of calculation of the Webster-Yang Index, defined in the Monsoon Metrics section 5.3 ; **(e)** DJF mean 2m temperature (shading, Celsius) ; **(f)** DJF normalized Sea Level Pressure anomalies (shading, hPa) and 850 hPa winds (vectors over 4m/s). Yellow boxes highlight the regions of calculation of the Eastern Asian Monsoon Index, defined in the Monsoon Metrics section. In all captions, topography (each 1000 m) is in gray contour. Precipitation for 1979-2021 from the Global Precipitation Climatology Project (GPCP) (Pendergrass, Angeline, Wang, Jian-Jian National Center for Atmospheric Research Staff (Eds). Last modified 06 Nov 2020. "The Climate Data Guide: GPCP (Monthly): Global Precipitation Climatology Project." Retrieved from https://climatedataguide.ucar.edu/climate-data/gpcp-

	Reference
1	(Averyanova et al., 2021)
2	(Hellwig et al., 2018)
3	(Macaulay et al., 2016)
4	(Caves Rugenstein et al., 2017)
5	(Carrapa et al., 2015)
6	(J. Sun et al., 2022)
7	(J. Sun et al., 2010)
8	(J. Sun & Windley, 2015)
9	(Baldermann et al., 2021)
10	(Caves Rugenstein et al., 2014)
11	(Kent-Corson et al., 2009)
12	(Zheng et al., 2015)
13	(Meijer et al., 2021)
14	(Licht et al., 2014)
15	(Wasiljeff et al., 2022)
16	(Hoorn et al., 2012)
17	(X. Ma & Jiang, 2015)
18	(Guo et al., 2002)
19	(Guo et al., 2008)
20	(Q. Yuan et al., 2020)
21	(Ao et al., 2016)
22	(Ao et al., 2021)
23	(Shen et al., 2017)
24	(S. Li et al., 2018)
25	(C. Huang & Hinnov, 2019)
26	(Ling et al., 2021)
27	(R. Spicer et al., 2017)
28	(Herman et al., 2017)
29	(Vornlocher et al., 2021)
30	(J. Ren et al., 2021)
31	(Q. Wang et al., 2021)
32	(Fang et al., 2021)
33	(Zheng et al., 2022)
34	(Sorrel et al., 2017)
35	(Jacques, Guo, et al., 2011)
36	(Xia et al., 2009)
37	(Xing et al., 2012)
38	(Wan et al., 2007)
39	(Jia et al., 2003)
40	(P. Clift et al., 2008)
41	(P. D. Clift, 2020)
42	(Z. Ding et al., 2021)
43	(Srivastava et al., 2012)
44	(Bhatia, Khan, et al., 2021)
45	(Shukla et al., 2014)
46	(Khan et al., 2014)
47	(Vögeli et al., 2017)
48	(Bhatia et al., 2022)
49	(Bhatia, Srivastava, et al., 2021)
50	(Srivastava et al., 2018)
51	(Sanyal et al., 2004)
52	(S. Ali et al., 2021)
53	(Betzler et al., 2016)
54	(Betzler et al., 2018)
55	(Beasley et al., 2021)
56	(Zhuang et al., 2017)
57	(Page et al., 2019)
58	(Q. Yuan et al., 2021)
59	(Meng et al., 2018)

Table 2. List of references used in Figure 2 for paleoclimate indicators compilation

	Reference (suite)
60	(Miao, 2013)
61	(Z. Zhang & Sun, 2011)
62	(J. Sun & Zhang, 2008)
63	(Q.-g. Sun et al., 2002)
64	(J. Sun et al., 2020)
65	(T. Su, Spicer, et al., 2019)
66	(Wu et al., 2021)
67	(Song et al., 2020)
68	(Miao, Wu, et al., 2016)
69	(D. Rea et al., 1985)
70	(Pettke et al., 2002)
71	(Ziegler et al., 2007)
72	(B. Li et al., 2016)
73	(Garzione et al., 2005)
74	(Qiang et al., 2011)
75	(Bougeois et al., 2018)
76	(W. Yang et al., 2019)
77	(J. Lee et al., 2020)
78	(Bolton et al., 2022)
79	(Hui et al., 2021)
80	(Miao, Song, et al., 2016)
81	(H. Zhao et al., 2020)
82	(C. Yang et al., 2021)
83	(L. Zhao et al., 2020)
84	(Heermance et al., 2018)
85	(J. Liu et al., 2016)
86	(Jiang & Ding, 2008)
87	(Peng et al., 2016)
88	(Suarez et al., 2011)
89	(Barbolini et al., 2020)
90	(Y. Ma et al., 2005)
91	(H. Wang et al., 2019)
92	(Jiang et al., 2017)
93	(W. Liu et al., 2014)
94	(Kaakinen et al., 2006)
95	(Y. Wang & Deng, 2005)
96	(F. Li et al., 2008)
97	(Z. Liu et al., 2014)
98	(Miao et al., 2011)
99	(Charreau et al., 2012)
100	(A. E. Holbourn et al., 2018)
101	(G. Wei et al., 2006)
102	(Y. Huang et al., 2007)
103	(Gupta et al., 2015)
104	(X. Yang et al., 2020)
105	(Bialik et al., 2020)
106	(H. Tang et al., 2020)
107	(H. Huang et al., 2021)
108	(Hoorn et al., 2000)
109	(Polissar et al., 2021)

Table 3. (suite) List of references used in Figure 2 for paleoclimate indicators compilation

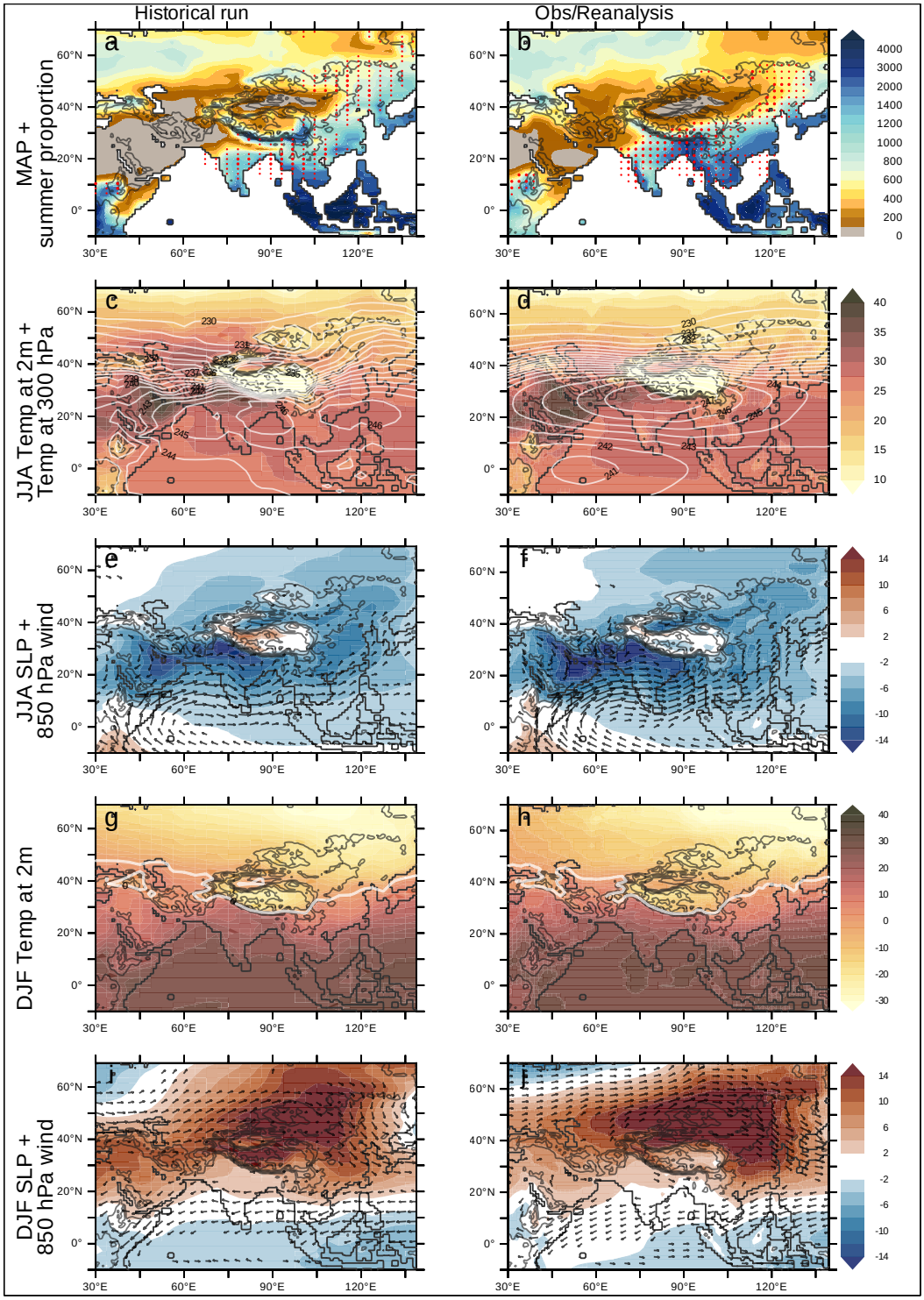

Figure 15. Comparison of monsoon diagnostics obtained in our control historical simulation (**Left column**) with modern observations and reanalysis (**Right column**). **(a,b)** Mean Annual Precipitations (shading, mm/yr), and regions where the Monsoon Precipitation Index is over 0.5 (thin red dots) and 0.75 (thick red dots) ; **(c,d)** JJA mean 2m temperature (shading, Celsius) and 300 hPa atmospheric temperature (white contour, Kelvin) ; **(e,f)** JJA normalized Sea Level Pressure anomalies (shading, hPa) and 850 hPa winds (vectors over 4m/s); **(g,h)** DJF mean 2m temperature (shading, Celsius) ; **(i,j)** DJF normalized Sea Level Pressure anomalies (shading, hPa) and 850 hPa winds (vectors over 4m/s). In all captions, topography in gray contour, each 1000 m. On the right column, precipitation are from GPCP, pressure and 300hPa temperature from ERAINT, 850hPa winds and surface temperature from ERA40.

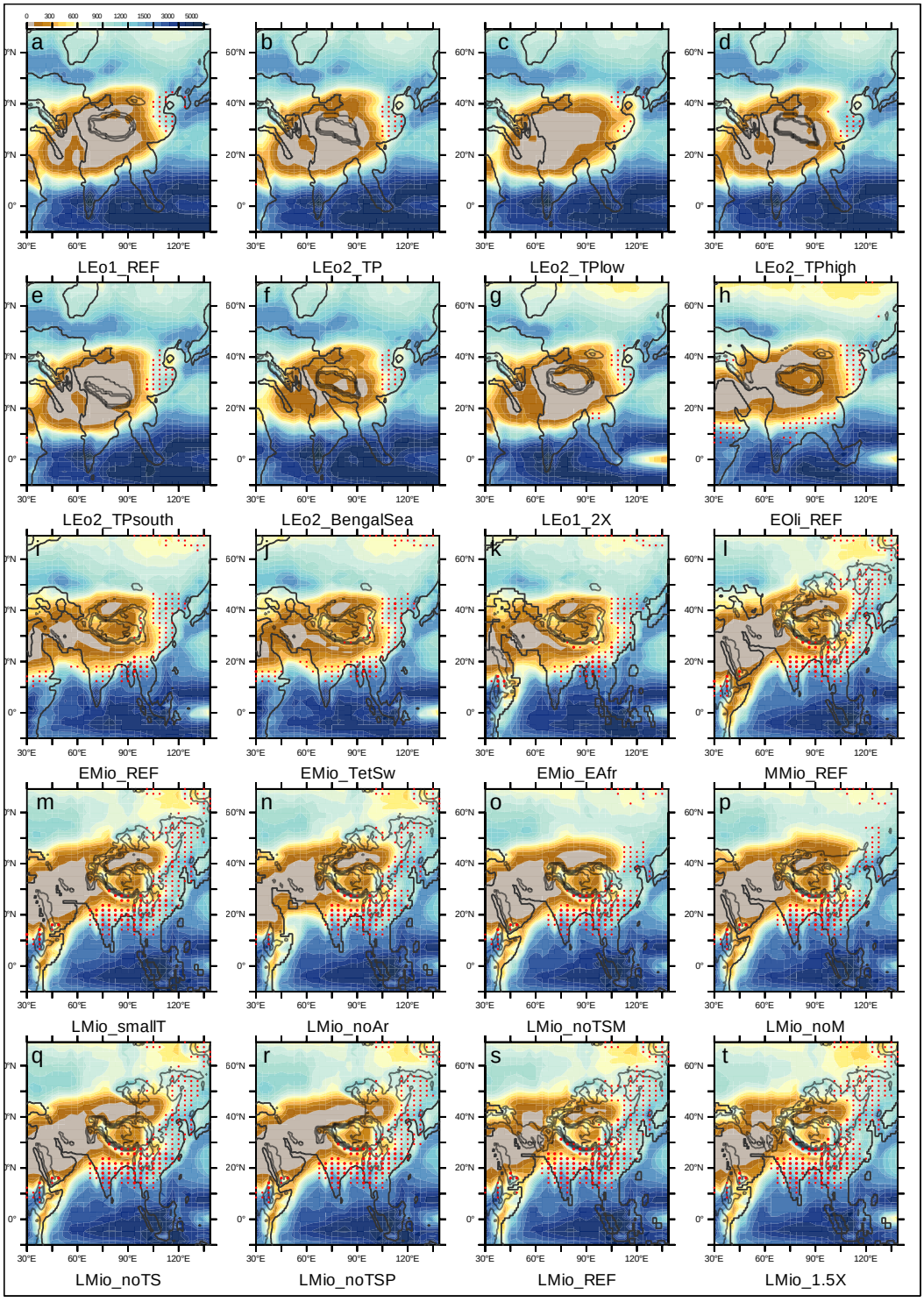

Figure 16. Mean Annual Precipitation (shading, mm/yr), overlain with regions where the Monsoon Precipitation Index (B. Wang & Ding, 2008) is over 0.5 (thin red dots) and 0.75 (thick red dots), for all reference and sensitivity experiments.

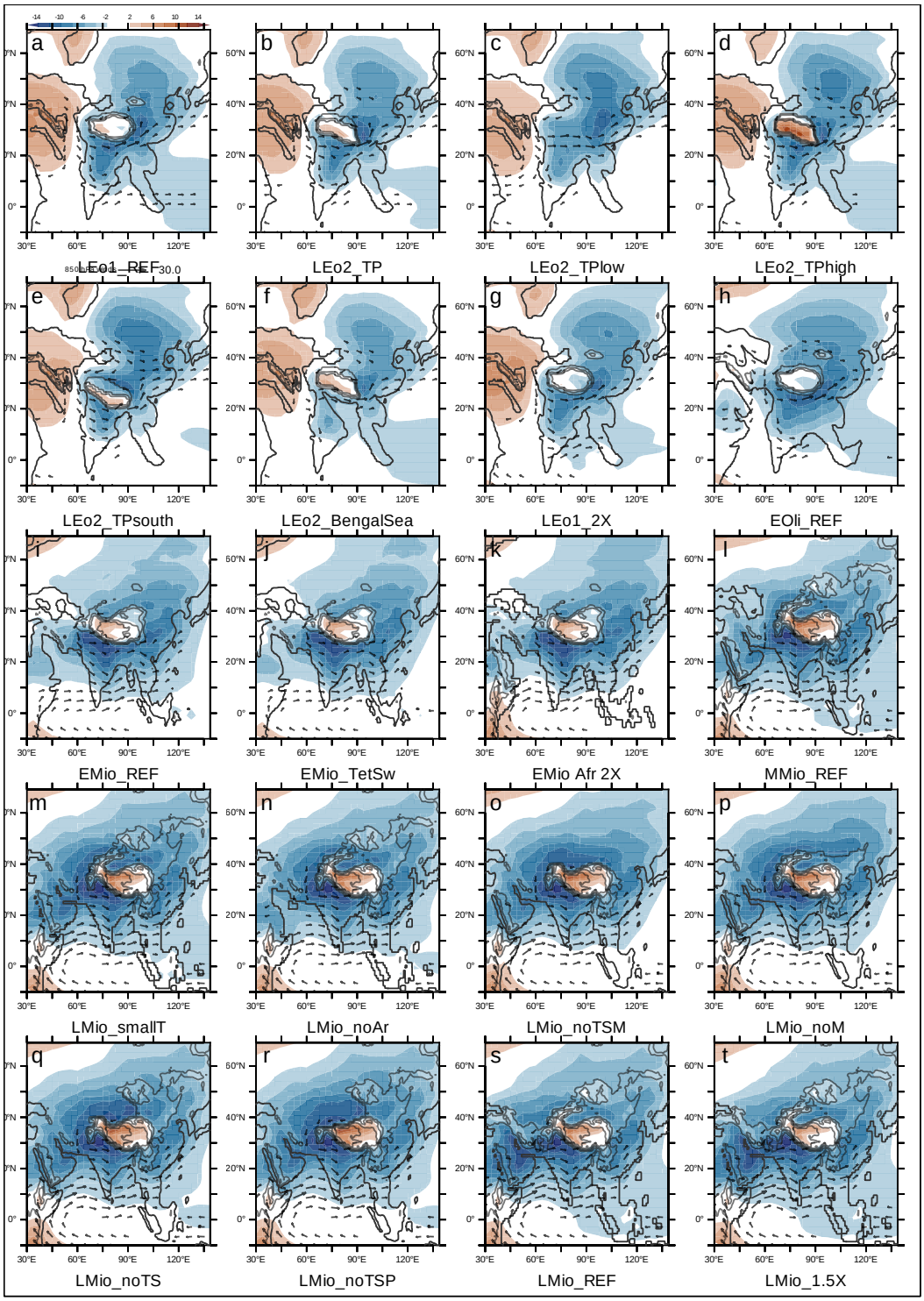

Figure 17. June-August (JJA) normalized Sea Level Pressure anomalies (shading, hPa) and 850 hPa winds over 4 m/s (vectors), for all reference and sensitivity experiments.

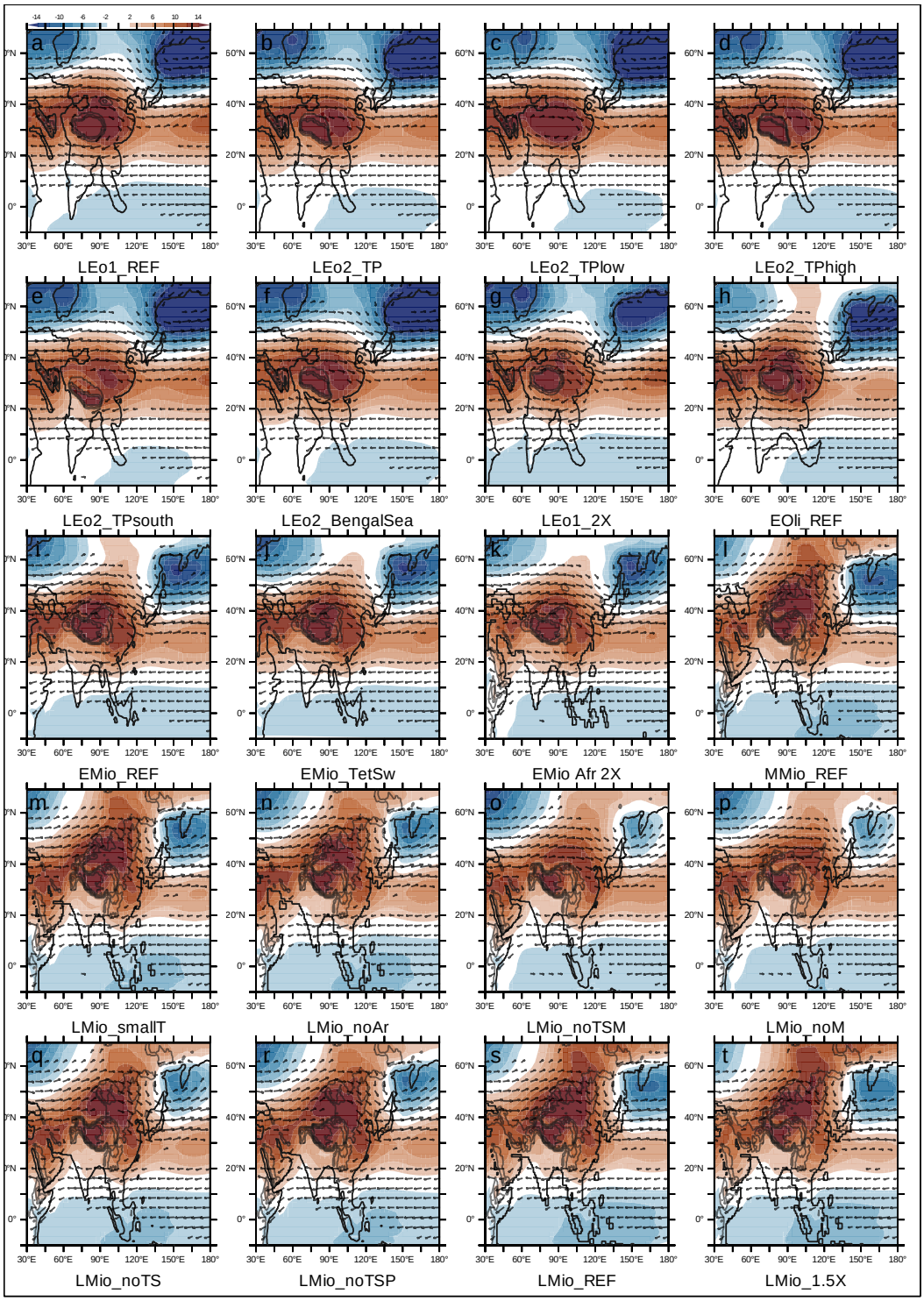

Figure 18. December-February (DJF) normalized Sea Level Pressure anomalies (shading, hPa) and 850 hPa winds over 4 m/s (vectors), for all reference and sensitivity experiments.

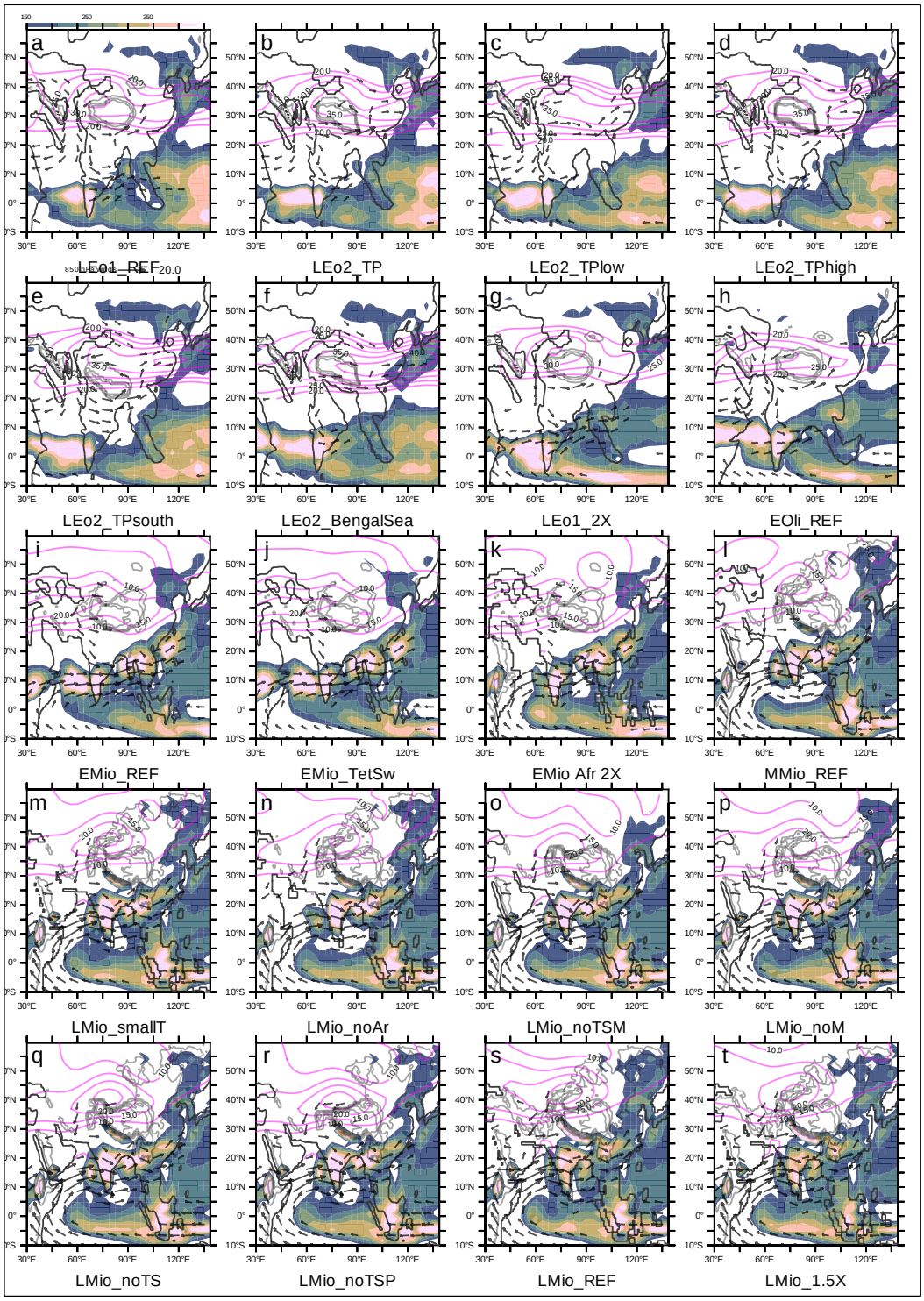

Figure 19. Jet Stream velocity and localization over Asia in August (purple outline), for all sensitivity experiments and precipitation for the month of August (shading, mm/month).

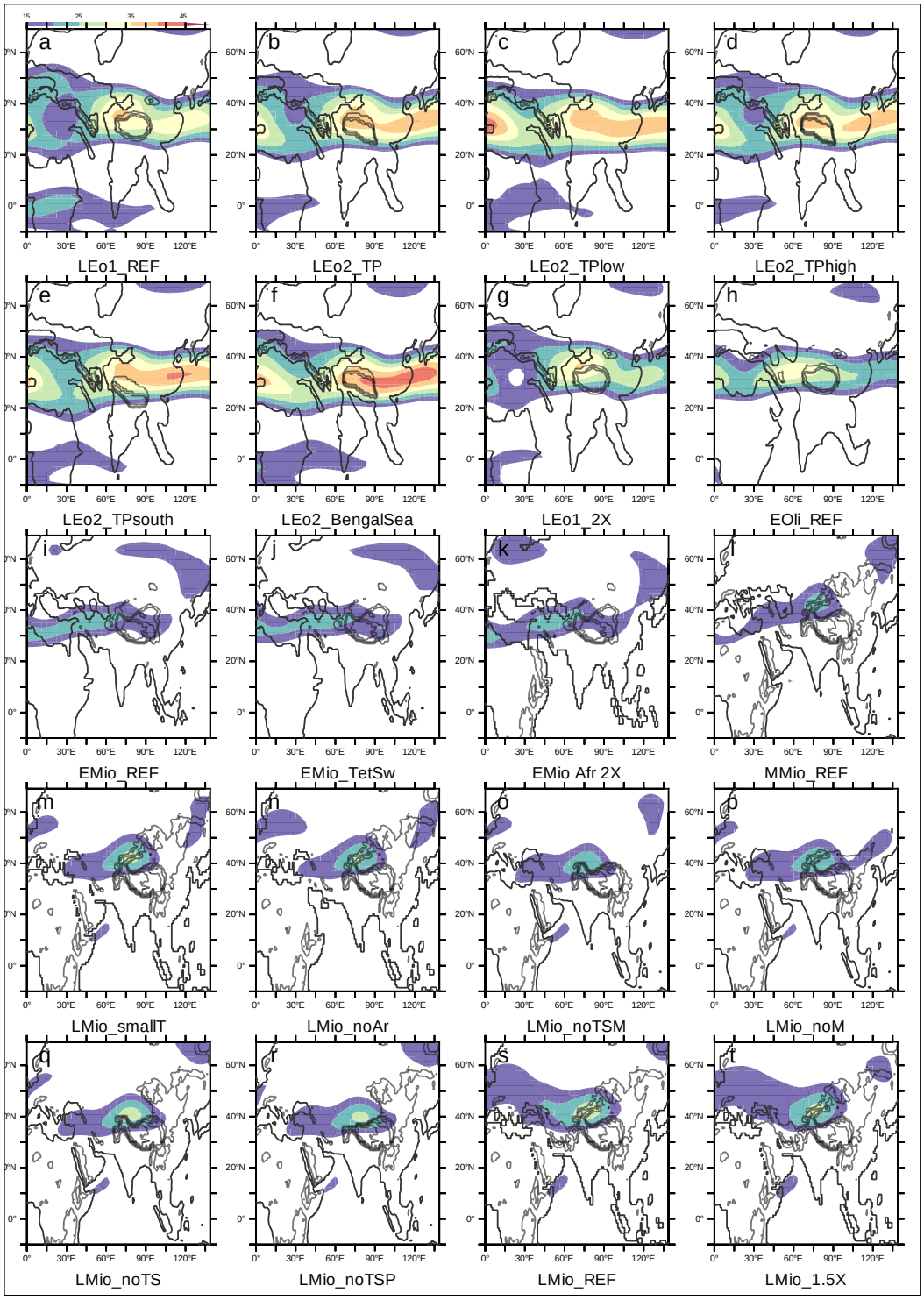

Figure 20. Jet Stream August velocity and localization over Asia, for all sensitivity experiments.

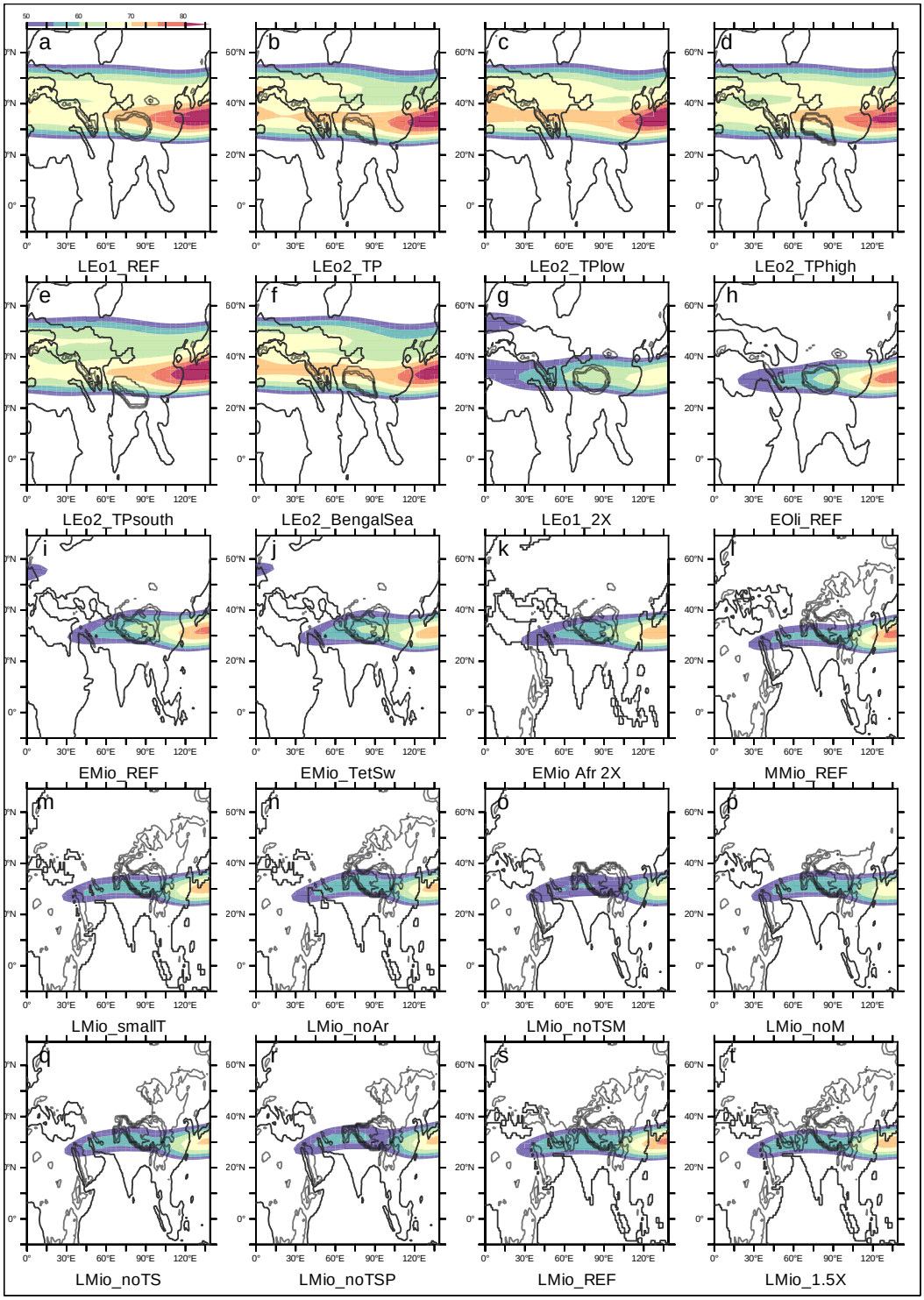

Figure 21. Jet Stream April velocity and localization over Asia, for all sensitivity experiments.